Dissertation

submitted to the

combined Faculties for the Natural Sciences and for Mathematics

of the Ruperto-Carola University of Heidelberg, Germany

for the degree of

Doctor of Natural Sciences

Presented by

Natalie K. Horvat, M.Sc.

Born in: Edmonton, Canada

Oral Examination: 27.09.21

Polarization of tumor-associated macrophages (TAMs) by super-paramagnetic iron oxide nanoparticles (SPIONs) as a candidate for adjuvant lung cancer therapy

Referees:

Prof. Dr. Marc Freichel

Dr. Jan Korbel

Prof. Dr. Ursula Klingmüller

Dr. Martin Jechlinger

Summary

Tumor-Associated Macrophages (TAMs) play an important role in shaping the tumor microenvironment (TME) and in promoting tumor metastasis. When applied to the TME, Superparamagnetic Iron Oxide Nanoparticles (SPIONs) specifically activate TAMs and induce an anti-tumor (pro-inflammatory) phenotype, indicating a potential window for therapeutic development. We have developed and tested a novel type of nanoparticle with or without an iron core. These nanoparticles are taken up specifically by murine bone marrow-derived macrophages (BMDMs) and human macrophages. Importantly, our nanoparticles containing an iron core induce TAM polarization to an anti-tumor phenotype significantly more than nanoparticles lacking the iron core. In both human and mouse systems, the nanoparticle-induced phenotype is characterized by increased mRNA expression of cytokines and chemokines such as TNF, IL1β, IL6 and iNOS, as well as cell surface proteins such as CD80, CD86 and MHC II, suggesting that SPIONs may be a tool for clinical application. This SPION induced phenotype was mediated by a combination of iron stimulation and TLR4 signaling pathways. In co-cultures of macrophages and Lewis lung carcinoma (LLC) cells, SPIONs reduce tumor cell division and trigger an increase in tumor cell death compared to control nanoparticles. The increased cancer cell death was mediated by the secretion of toxic molecules from SPION activated macrophages that induced oxidative stress in LLC cells, suggesting a mechanism of cytotoxic action. Preliminary data indicate that SPIONs, when administered in mice instilled with LLC cells are primarily taken up by macrophages and lead to the recruitment of more myeloid cells to the lungs compared to the control nanoparticles. Based on these data, targeting TAMs in the TME with SPIONs may render lung tumors susceptible to treatment, laying the foundation for a novel avenue of adjuvant drug development.

Zusammenfassung

Tumorassoziierte Makrophagen (TAMs) spielen eine wichtige Rolle bei der Gestaltung der Tumormikroumgebung (TME) und bei der Förderung der Tumormetastasierung. Wenn sie in die TME eingebracht werden, aktivieren superparamagnetische Eisenoxid-Nanopartikel (SPIONs) spezifisch TAMs und induzieren einen Anti-Tumor-(pro-inflammatorischen) Phänotyp, welcher für eine mögliche therapeutische Entwicklung von Vorteil sein könnte. Wir haben einen neuartigen Typ von Nanopartikeln mit oder ohne Eisenkern entwickelt und getestet. Diese Nanopartikel werden spezifisch von aus dem Knochenmark stammenden Makrophagen (BMDMs) der Maus sowie menschlichen Makrophagen aufgenommen. Wichtig ist, dass diejenigen Nanopartikel, die einen Eisenkern enthalten, die TAM-Polarisierung zu einem Anti-Tumor-Phänotyp signifikant stärker induzieren als Nanopartikel ohne Eisenkern. Sowohl im menschlichen, als auch im Maussystem ist der Nanopartikel-induzierte Phänotyp durch eine erhöhte mRNA-Expression von Zytokinen und Chemokinen wie TNF, IL1β, IL6 und iNOS sowie von Zelloberflächenproteinen wie CD80, CD86 und MHC II gekennzeichnet, was darauf hindeutet, dass SPIONs von Interesse für die klinische Anwendung sein könnten. Der SPION-induzierte Phänotyp wird durch eine Kombination von Eisen stimulierten Effekten und TLR4-Signalwegen vermittelt. In Ko-Kulturen von Makrophagen und Lewis-Lungenkarzinom (LLC)-Zellen reduzieren die SPIONs die Teilung der Tumorzellen und lösen im Vergleich zu Kontroll-Nanopartikeln einen erhöhten Tumorzelltod aus. Der erhöhte Krebszelltod wurde durch die Sekretion von toxischen Molekülen aus SPION-aktivierten Makrophagen vermittelt, die oxidativen Stress in LLC-Zellen induzierten, was auf einen Mechanismus der zytotoxischen Wirkung hinweist. Vorläufige Daten deuten darauf hin, dass SPIONs, wenn sie mit LLC-Zellen infiltrierten Mäusen verabreicht werden bevorzugt in TAMs aufgenommen werden und zurRekrutierung von mehr myeloischen Zellen in der Lunge führen. Diese Ergebnisse legen die Grundlage für weiterführende Untersuchungen, in der ein verbessertes Ansprechen von Lungentumoren auf Standardtherapien durch die Anwendung einer adjuvanten Tumortherapie mittels SPIONs getestet werden wird.

Acknowledgements

Table of Contents

List of Tables

List of Figures

Abbreviations

%	per cent
μ	micro
°C	celsius
7AAD	7-aminoactinomycin D
ALK	anaplastic lymphoma kinase gene
AM	alveolar macrophage
AT1	alveolar epithelial type 1 cells
AT2	alveolar epithelial type 2 cells
BMDM	bone marrow-derived macrophages
CCPMs	core cross-linked polypept(o)ide
CD	cluster of differentiation
cDNA	complementary DNA
CLI	CLI-095
Ct	threshold cycles
CFSE	carboxyfluorescein succinimidyl ester
DAMP	damage-associated molecular pattern
DFI	deferiprone
DMEM	dulbecco's modified Eagle's medium
DMSO	dimethyl sulfoxide
DMT1	divalent metal transporter 1
dNTP	deoxynucleotide triphosphate
EDTA	ethylenediaminetetraacetic acid
EML4	echinoderm microtubule-associated protein-like 4
FCS	fetal calf serum
Fpn1	ferroportin
g	gram
GEMM	genetically modified mouse model
h	hour
H_2O	water
HAMP	hepcidin antimicrobial peptide
HIF	hypoxia inducible factor
HO-1	heme oxygenase 1
iNOS	inducible nitric oxide synthase
IL	interleukin
IM	interstitial macrophage
IRP	iron-regulatory protein
kDa	kilo Dalton
LfR	lactoferrin
LLC	lewis lung carcinoma
l	liter
LPS	lipopolysaccharide
LUAD	lung adenocarcinoma
M	molar
m	mili
mAMs	monocytic-derived alveolar macrophages
mDMs	monocytic-derived macrophages
mDDCs	monocytic-derived dendritic cells
min	minute

mRNA ....messenger RNA
n.. nano
NaCl ....sodium chloride
Nqo1 .... NAD(P)H:quinone oxidoreductase
NFκB .... nuclear factor of kappa light polypeptide gene enhancer in B-cells
NP... nanoparticle
NO ....nitric oxide
NOS... nitric oxide species
Nrf2 ....nuclear factor (erythroid-derived 2)-like 2
NSCLC ....non-small cell lung cancer
NT..not treated
PAMP .... pathogen-associated molecular pattern
PBS .... phosphate-buffered saline
Pen/Strep ....Penicillin/Streptomycin
PS .... phosphotidylserine
qPCR .... quantitative polymerase chain reaction
rAMs.. resident alveolar macrophages
ROS ....reactive oxygen species
RNA .... ribonucleic acid
RNS .... reactive nitrogen species
rpm ....rotations per minute
RPMI-1640... Roswell Park Memorial Institute-1640
RT.. reverse transcription
RT-qPCR...real time quantitative polymerase chain reaction
SAHA ....suberoylanilide hydoxamic acid
SD... standard deviation
SEM... standard error of measurements
SLC40A1 ....solute carrier family 40 (iron-regulated transporter), member 1
SPIONs..super para-magnetic iron oxide nanoparticles
STAT3 .... signal transducer and activator of transcription 3
TAMs .... tumor-associated macrophages
Tf.. transferrin
TFR1.. transferrin receptor 1
TGFβ .... transforming growth factor-β
TLR .... toll like receptor
TME ....tumor microenvironment
TNF ....tumor necrosis factor
TRM .... tissue-resident macrophage
WT..wild type

Contributions and publications

Core cross-linked polymeric micelles for specific iron delivery: inducing sterile inflammation in macrophages

Tobias A. Bauer*, **Natalie K. Horvat***, Oriana Marques, Sara Chocarro, Christina Mertens, Silvia Colucci, Sascha Schmitt, Luca M. Carrella, Svenja Morsbach, Kaloian Koynov, Federico Fenaroli, Peter Blümler, Michaela Jung, Rocio Sotillo, Matthias W. Hentze, Martina U. Muckenthaler, and Matthias Barz.

*Contributed equally

Results, corresponding figures, or methods that were not generated by me or that which contains portions of data generated by someone else are marked appropriately throughout the text.

Schematics and/or cartoon figures were created with BioRender.com.

Chapter 1: Introduction

Macrophages are vital in host defense and tissue homeostasis. In addition to being one of the most abundant leukocyte in the body ($\sim10^{10}$ cells)[1], macrophages orchestrate and coordinate communication between different types of cells, nurture and protect cells, as well as initiate mechanisms that defend or mobilize host defenses against pathogens[2]. From the beginning stages of an embryo, macrophages play an important role in the selective clearance of cells to shape bodily structures, such as fingers and toes[3]. This role in regulating tissue structure extends throughout the life of an organism, as macrophages are an important part of organ and tissue homeostasis. Macrophages can be dedicated to specific organs, termed tissue-resident macrophages (TRMs), are phenotypically defined based on their tissue of residence, or macrophages patrol throughout the body in a more transient role. Whether they are tissue-resident or not, macrophages primarily have four main roles: surveillance of the surrounding environment; orchestrating tissue repair/healing pathways; inhibition of either pathogen infection and spread or over-activation of immune cells; and presentation of internalized epitopes that signal alerts to other immune cells[1]. Understanding these specific roles and the interplay between them is integral in comprehending the complex nature of macrophage biology within the scope of the innate immune system and the macrophage role in health and disease.

The two major types of macrophages, TRMs and the transient interstitial macrophages (IMs) engage in each of the four general macrophage functions. Tissue-resident macrophages residing in organs perform the four general macrophage functions in addition to tissue specific tasks that ensure homeostasis[3]. IMs originate from bone marrow-derived monocytes and serve as an arsenal for acute responses to tissue damage. In comparison to TRMs, IMs are typically short lived. Upon receiving a stimulus, IMs quickly differentiate from monocytes and respond to rapid fluctuations in their immediate external environment. IMs have been found to undergo major internal transcriptional and metabolic reprogramming that leads to immense variations of metabolism and morphology between individual IMs. In fact, monocyte-derived macrophages recruited to the lungs have been found to adopt up to 90% of the transcriptional profile of alveolar macrophages (AMs), lung TRMs, vastly differing from IMs that are recruited to other organs in the body[4].

The interplay between tissue-resident and interstitial macrophages, and by extension monocytes, throughout the body is tightly regulated under normal circumstances[5]. Some organs

such as the heart, pancreas, or gut have continual recruitment of IMs along with the presence of TRMs, constituting a coordinated steady state occupancy of both cell types. Other organs, such as the lung, brain, or liver, are primarily populated with TRMs, and the appearance of monocytes and IMs in these organs can be an indication of perturbed tissue homeostasis[4]. Recent evidence suggests that specific TRMs, such as AMs, have been found not only to engage in clonal expansion[6] but to also de-differentiate into monocytic-like macrophages under situations of tissue duress highlighting the power of the flexible, functional response in macrophages[7]. Alternatively, IMs that assume transcriptional programming of AMs have been found to replace lost TRMs and acquire TRMs functions when the need arises[8]. The pliable and multifaceted response of all macrophages, called plasticity, accentuates the reason why macrophages are the central focal point in host defense and tissue homeostasis[9,10].

SECTION 1.2: MACROPHAGE POLARIZATION

The ability of macrophages to respond to stimuli in a rapid and versatile manner is an important facet of homeostasis[9]. Often when macrophages are sampled from a single organ or tissue specific location, a heterogeneous population of macrophages is found, and not a homogeneous macrophage population[1]. Numerous environmental cues dictate the functional state of both IMs and TRMs. In addition to the commonly described macrophage functions (sampling, healing, inhibiting, and presenting), both IMs and TRMs have been found to engage in specific fine-tuned functions, which have been characterized as macrophages subtypes. These subtypes are based on the profiles of gene expression response after cytokine and/or microbial challenge[11]. Overall, we can categorically summarize macrophage subtypes into a dichotomy: on either end exists a stimulatory (inflammatory) and a suppressive (anti-inflammatory) subtype[1] (Figure 1.1). In between the two extremes is a cascade of different subtypes, each equally independent and similar to their respective neighboring subtype along a continuum[3,9]. These states have been loosely referred to as the macrophage polarization state and are provoked by the sampling of a macrophages' immediate external environment. Stimuli can include nutrients, microbials, cytokines, cell debris or others. The flexibility of the macrophage response is exemplified by the ability to switch between polarization states[12,13], representing a unique and powerful characteristic of plasticity in macrophage function[1].

When the idea of macrophage subtypes was being introduced, very basic nomenclature for specific subtypes was applied[1,13–17]. M1 and M2 were used to describe the distinct stimulatory/inflammatory and suppressive/anti-inflammatory macrophage subtypes, respectively. This nomenclature was based on macrophage stimulated T-helper 1 (Th1) and T-helper 2 (Th2) CD4+ T cell responses as well as the ability to express the oxidative enzyme inducible nitric oxide synthase (iNOS) or arginase (Arg1), respectively[18]. From these studies in the late 1990s, a dogma was established that laid way for a new field of macrophage biology, called macrophage polarization[1,12]. Eventually, the two subtypes became known as the pathogen-eliminating phenotype (M1) and nursing/healing phenotype (M2)[9]. The M2 subtype is thought to arise from the lack of signals required to stimulate the M1 macrophage, thereby indicating that M2 is a more basal state. Therefore, it became common to characterize these cells by what they produce rather than the received stimulation[13,19]. With experimentation under cultured settings, other subtypes that closely resemble the M2 phenotype were elucidated, labeled as M2a, M2b, and M2c[16,20–22]. Much of our knowledge about macrophage polarization comes from experiments in cultured cells, which has had many limitations and led to misunderstanding incorrectly assigned subtypes, where some have vaguely represented cells

found *in vivo*[3,15,16,23,24]. It wasn't until 2014 that many macrophage specialists collectively published a recommendation for macrophage polarization nomenclature in effort to iron out confusion and unify inconsistencies growing in the field[16]. Since that time, studies have come closer to accurately defining macrophage subtypes and their associated function due to technological advancements in immunohistochemistry, flow cytometry, single-cell and in-depth multi-omic approaches[15,25,26].

M1 macrophages are involved in inflammatory responses. Both interstitial macrophages and tissue-resident macrophages can "activate" into an M1 macrophage subtype as they encounter an increasing gradient of inflammatory stimuli. These signals are produced in response to either injury or infection, and macrophages recognize these signals with specific receptors that respond to repeating patterns called damage- or pathogen-associated molecular patterns (DAMPs or PAMPs, respectively)[27–29]. DAMPS can occur as released cellular content, such as proteins or metabolites, changes in pH, osmolarity or oxygen levels. PAMPs include specific molecules, sugars, proteins, or nucleic acids, that stem from pathogens. DAMPs and PAMPs serve as normal cellular or pathogenic functions for other cells, but for macrophages, they serve as exploits to assess environmental conditions. The M1 macrophage subtype can manifest rapidly: macrophages undergo huge metabolic shifts within minutes and output massive amounts of oxidative and inflammatory cytokines such as IL12, TNF, IL6, and IL1β, chemokines such as CXCL10, IL-8 and CCL2, as well as increasing cell surface proteins that signal inflammation, such as CD64, CD86, CD80, MHCII and CD38[1,30]. Signals produced by M1 macrophages stimulate Th-1 responses from the adaptive immune system, which may activate T cells (T lymphocytes) and their proliferation. Classically, M1 macrophages were found to secrete large amounts of nitric oxide (NO), produced by the enzyme iNOS, upon inflammatory stimulation[2]. Eventually, reactive oxygen species (ROS) were found to be highly upregulated in this phenotype, leading to an understanding of the necessity of ROS/NOS in the signaling and activation of this phenotype[15]. While some reports have found that the endpoint for the classically activated M1 macrophage is to initiate apoptosis once inflammatory situations are resolved, others report that in certain conditions, such as in atherosclerotic plaques or in chronic heart failure, M1 macrophages can retreat from the recruited site or even remain at the site, adopting near-perfect TRM-like qualities[31–33]. The fate or lifespan of M1 macrophages under other types of inflammatory conditions other than atherosclerosis and chronic heart failure remains poorly understood.

Most macrophages, including TRMs, operate in the general default state of suppressive/anti-inflammatory programming (herein referred to as M2)[1,3,4,9,17,20,21,23,34–38].

Traditionally, this state was characterized by *in vitro* experimentation where cultured macrophages were treated with the IL4 cytokine and observed to upregulate levels of markers such as IL10, CD206, as well as suppress iNOS[17]. DAMPs or cytokine signals recognized by M2 macrophages often initiate responses that favor healing and cell survival. In general, M2 macrophages increase the production of the cytokines IL4, IL10, CCL24, CCL17, the enzyme arginase-1 (Arg-1), and the mRNA transcripts *Ym1* and *Fizz1*. Three subclasses of M2 macrophages have been established to differentiate between different stimulatory situations and transcriptional programming that tend to partially overlap[39]. M2a was defined based on the macrophage response solely to IL4, M2b is used for stimulatory situations with immune complexes and toll-like receptors (TLR) ligands, and M2c mainly describes macrophages in response to glucocorticoids and IL10[13,16,23,40,41]. The function of all these subtypes is to ensure homeostasis: repairing extracellular matrices from damage, aid in replacing tissue, clearing debris, and recycling nutrients from senescent cells. Along these lines, M2 macrophages are also necessary to prevent chronic inflammation by suppressing inflammatory responses at the stage of resolution through the secretion of cytokines such as IL13, IL10 or TGFβ and the enzyme indoleamine 2,3-dioxygenase (IDO). *In vivo* it was found that these cells coordinate adaptive immune responses to CD4+ T-cells by producing Th-2 like cytokines, which, among other functions, potentiate responses to B cells[42]. Situations that overly impose the M2 state, such as the high levels of IL4 and M2-specific DAMPs, can lead to adverse disease states. This effect can be observed in lung tumors where an overabundant populace of M2 macrophages can accelerate disease progression[43,44] and are often associated with poor prognosis in cancer patients[4,45].

Like most systems in biology, regulation is critical. Each regulated step in the system depends on the preceding and subsequent step and implemented in a timely fashion to ensure smooth operation. For the macrophage, their function to ensure homeostasis requires tight regulation and coordination of communication to surrounding cells. If we consider just the two most extreme macrophage subtypes, an intricate cycle can be illustrated when a harmful threat occurs: M2 macrophages, in constant regulation of tissue (either through the absence of inflammatory signals or the flux of normal operating signals), receive DAMPs from injured tissue and amplify signals to recruit other TRMs and monocytes, in addition to other cells. Recruited macrophages activate M1/inflammatory programming while at the same time relocate to the epicenter of danger. They release inflammatory cytokines and secrete toxic oxidative species like ROS or NOS to neutralize the hazard, which once eliminated, M2 macrophages clear away debris, resolve structural tissue damages, and secrete cytokines to

suppress further inflammation. Rapid and coordinated macrophage responses are possible because of the sheer abundance of macrophages present throughout the body, their constant sampling of signals in combination with highly flexible functional capacity for each macrophage cell[19]. Therefore, the evaluation of a macrophage population at any one time does not result in a binary measurement of the macrophage polarization state but rather a ratio, linking back to the concept of the macrophage subtype continuum. The excess of one subtype beyond the normal state in the population can indicate a state of bodily dysregulation. The idea of balance with macrophages applies also to the intracellular programming that determines their subtype. M1/inflammatory macrophages express high amounts of the iNOS enzyme, whereas M2 macrophages can express high amounts of the Arg1 enzyme, but the expression of each enzyme is not exclusive to either subtype[1,46,47]. The relevance of these two enzymes is important not just in macrophage biology but also in disease conditions as macrophages participating tumorigenesis have been found to express equal levels of both enzymes[48]. The ratio of iNOS to Arg1 is a bidirectional line of macrophage metabolism since both iNOS and Arg1 use arginine as their substrate. The products of both enzymes and the triggered downstream events are vastly different, illuminating a forked road for macrophage subtype determination. The activation of one enzyme over the other, i.e., balance of expression of the two enzymes, is directed by external environmental cues. Additionally, the rapid and flexible response in macrophage function can in part be attributed to this simplified and streamlined intracellular signaling[46]. The amount of one enzyme over the other is one of the most important determinators of the macrophage subtype. As a result, with macrophages that have been found to aid or worsen disease, understanding the cyclical regulation of macrophage subtypes could aid in the development of drug targeting strategies.
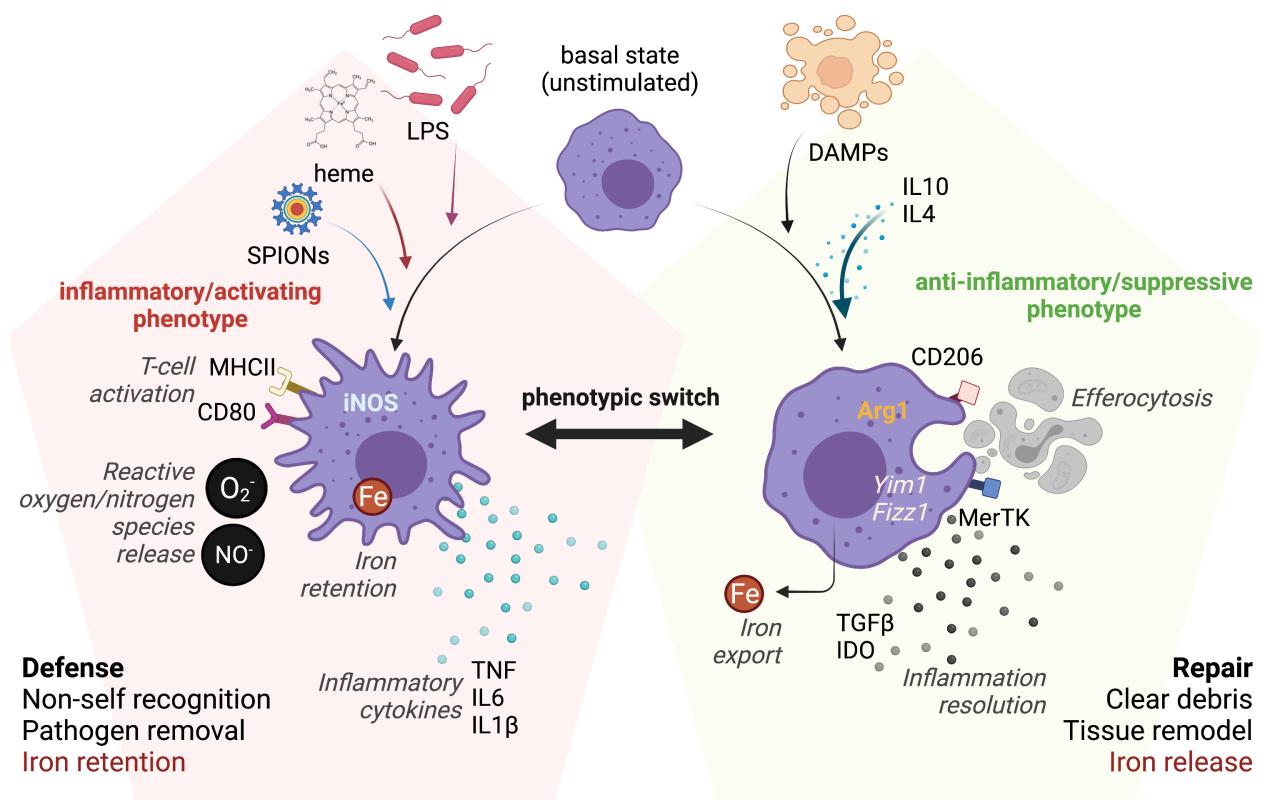
Figure 1.1. Spectrum of macrophage polarization.
Macrophages exist in a low activation profile (unstimulated) which can rapidly respond to external cues. Upon stimulation by LPS, heme, or SPIONs, macrophages adopt a stimulatory/pro-inflammatory phenotype that then engages in defense. These pro-inflammatory macrophages have higher levels of MHCII and CD80 proteins, increase production of reactive oxygen or nitrogen species (ROS/RNS), retain iron, and release inflammatory cytokines such as TNF, IL1, IL1β, and IL6. Macrophages that react to damage associated molecular patterns (DAMPS) or the cytokines IL10 and IL4 adopt a suppressive/anti-inflammatory phenotype and engage in repairing/healing functions. These macrophages have increased levels of CD206 and MerTK proteins, engage in apoptotic dead cell clearance, called efferocytosis, and release iron as well as cytokines including TGFβ and IDO. A phenotypic switch can occur between the stimulatory/pro-inflammatory phenotype and the suppressive/anti-inflammatory phenotype when external stimuli change, such as by SPIONs treatment. Figure adapted from previously published studies[366].

Iron is an essential molecule that facilitates and participates in almost all molecular reactions and the stable control of its levels requires firm regulatory mechanisms to avoid irreversible harmful consequences. In addition to their role in surveillance, healing and defense, macrophages are also important orchestrators of iron homeostasis[49–51].

Iron homeostasis involves a delicate balance between iron import, iron storage and iron export. Every day, macrophages recycle approximately 2×10^{11} red blood cells (RBCs)[9] and aid in the maturation of new ones[52,53]. The iron contained within RBCs together with the iron being recycled from RBCs by TRMs in the bone marrow and the spleen comprises the most considerable portion of iron found in the body[54]. Specialized macrophages, called erthrophagocytic macrophages, digest RBCs within the phagolysosome, releasing heme from hemoglobin into the cytosol[55]. Heme is broken down by the enzyme heme oxygenase-1 (HO-1) releasing iron into the labile iron pool in the cytosol and producing biliverdin and carbon monoxide[56,57]. HO-1 is an integral contributor in the coordination of iron inside the macrophage and the resultant anti-oxidative response that incurs. Following HO-1 mediated breakdown, the fate of iron is determined by the levels of intracellular iron present in the cell. Due to its highly reactive nature, the processing of free iron occurs quickly. Free iron in the cytosol can be shuttled to storage nanocages called ferritin (Ft) for later usage, used for cellular metabolic purposes, or shunted out of the cell by the export channel protein ferroportin-1 (Fpn1)[49,58–61]. The coordination of iron within the cell requires rapid feedback mechanisms to prevent free iron from producing toxic radicals in the cell. In addition to transcriptional regulation, post-translational mechanisms govern the levels of iron regulatory proteins within the cell. A coordination of mRNA-binding iron-regulatory proteins (IRPs) target transcripts containing cis-regulatory iron-regulatory elements (IREs) direct the binding of IRPs on mRNA transcripts of proteins such as ALAS1, ACO2, Ft, and Fpn1. Intracellular iron levels dictate IRPs binding to IREs and impact the translation of specific genes, representing an important level of iron mediated protein production.

The coordination of iron regulation is complex as it involves regulatory mechanisms at the systemic level in addition to multi-level intracellular mechanisms. For example, Fpn1 is a highly efficient protein known to be the only mechanism that cells use to export iron[57]. As the primary cells that express Fpn1, macrophages, along with hepatocytes and enterocytes, coordinate the levels and thus access of systemic iron. Hepcidin is a serum peptide hormone expressed primarily by hepatocytes in the liver and binds to Fpn1. The secretion of iron is blocked by hepcidin as it inhibits the transport of iron on the extracellular side of the plasma

membrane and triggers the degradation of Fpn1[62]. Therefore, gene expression and protein levels of Fpn1 in cells requires coordination of regulatory factors at the transcriptional, translational, post-translational and systemic level. The disruption at any level can contribute to iron dysregulation within the body and contribute to the pathology of several diseases such as anemia, neurological disorders, or cancer[63–66].

Once iron is shuttled out of the cell by Fpn1 into the blood, most iron binds to transferrin (Tf), the iron transport protein in the plasma, while only a small portion remains as non-transferrin bound iron (NTBI). Cells maintain their iron stores by acquiring iron-bound Tf, as it binds to its receptor, the transferrin receptor (TFR1, also known as CD71) and is endocytosed[67]. The level of TFR1 at the cell surface is often indicative of the cell's iron status. The amount of TFR1 is also an indicator of healthy cells; too much or too little indicates some degree of dysregulation of iron or stress. Since cells require iron to divide, fast dividing cells are often found with very high levels of TFR1, which can also serve as an indication of cancer cells[68].
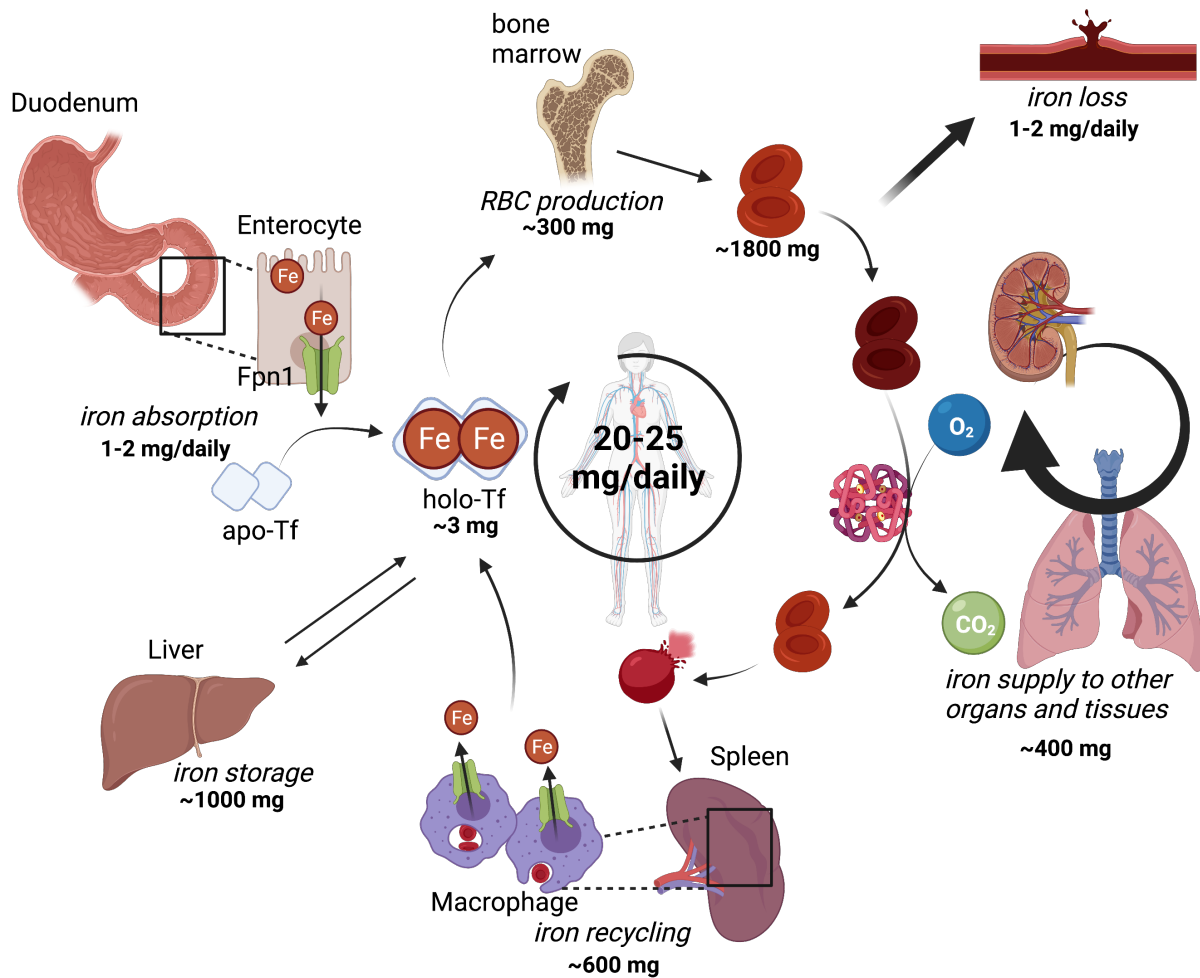
Figure 1.2. Systemic iron homeostasis.
1-2 mg of iron enters the body daily through enterocytes in the duodenum, which export iron to the systemic blood by ferroportin (Fpn1). Once exported, iron binds to apo-transferrin (Tf) in the blood; ~ 3 mg of iron is found bound to Tf. ~300 mg of iron is used to produce red blood cells (RBCs) and ~1800 mg of iron is held within RBCs which circulate throughout the body to provide oxygen to tissue. Aged or lysed RBCs are recycled by splenic macrophages, where ~ 600 mg of iron resides, which can be shuttled out by Fpn1. The primary stores of iron within the body are within the liver, which holds ~ 1000 mg. Every day 20 – 25 mg of iron is recycled throughout the body within this system. The primary method of iron loss is blood-letting or dead cell shedding, which can amount to ~1-2 mg/daily. Figure adapted from previously published studies[57]

Even though a subset of TRMs primarily function to recycle RBCs, this function can also be carried out by other non-resident macrophages that have an M2-like phenotype[69]. In line with their healing and supportive role, M2 macrophages express high levels of TFR1, high levels of ferritin and contribute to tissue homeostasis by recycling RBCs or iron debris, such as heme, hemoglobin, and hemopexin, as well as clear away dead cells[49,70]. High levels of Fpn1 coupled with functions to clear away iron debris suggests that M2 macrophages retain low levels of iron to actively distribute iron to tissue cells, thereby serving as nutritive suppliers[71,72], which is in line with other M2/healing or regulatory functions. On the other hand, macrophages found laden with iron have low levels of Fpn1 and TFR1 and high levels of ferritin. Iron-loaded macrophages express high levels of inflammatory cytokines, such as IL6, IL1β and TNF, and are essential for iron sequestration in situations where free iron can cause irreparable damage[49].

The unique way that macrophages handle iron is also a significant factor in determining their activation status and functioning as a phenotypic driver[49]. By applying iron to macrophages, in the form of non-Tf bound iron (NTBI), un-stimulated bone marrow-derived macrophages (BMDMs) can be activated to an M1-like phenotype[73,74]. The role of iron in promoting M1 polarization of macrophages was shown to be essential as macrophages lacking an iron source had attenuated M1 activation[75]. Moreover, studies have shown that applying sources of iron to M2-like macrophages can initiate a phenotypic switch towards an M1-like phenotype[74,76]. While these results produced in culture are exaggerated compared to *in vivo* situations, they nevertheless elucidate the potential of iron to influence function and the degree of activation in macrophages. In various pathophysiological conditions, the significance of iron and the macrophage phenotype is an etiological factor, such as in wound healing and cancer cell growth, where an accumulation of "iron donating" M2 macrophages worsens the disease[69]. Studies have identified that iron targeted to M2 macrophages can induce a phenotypic switch in M2 macrophages to a more M1-like phenotype, correlating with cancer cell death and anti-cancer inflammation[77]. However, the effect of iron on macrophages *in vivo*, especially in the context of cancer, is not yet fully understood[50], but nonetheless illustrates an interesting opportunity for the development of targeted iron-based therapies.

The importance of iron regulation in lung function and disease

Being an organ that is highly vascularized, the lungs are heavily perfused in blood where TFR1 on lung tissue internalizes iron-bound Tf. Control of iron levels within lung tissue is orchestrated by local tissue regulatory mechanisms as well as endocrine mechanisms from organs such as the liver. Disruption of these iron regulation mechanisms in the lung can lead to severe diseases. Excessive iron deposition in lung tissue has been found to be associated with impaired lung function, decreased total lung capacity as well as chronic tissue dysregulation diseases such as chronic obstructive pulmonary disease, idiopathic pulmonary fibrosis and cancer[78–81]. Certain cells in the lungs, like macrophages, have been found to accumulate iron more than others, suggesting a protective role[78,80,82]. Structural cells in the lungs, such as alveolar type 2 cells (AT2), can be more iron laden than others[79]. An unbalanced regulation of iron from within the body can also adversely impact lung function, immune lung function and has been linked to many diseases.

External exposure to harmful agents in the air, like iron contaminated pollution or cigarette smoke, sediments toxic metallic particulates in the tissue areas that can challenge delicate lung cells[83,84]. In these cases, tissue damage can result from iron-induced reactions that radiate toxic free radicals, a chemical reaction called the Fenton reaction[85]. In a tissue immersed in an oxidative environment, slight oxidative/reductive perturbations in the lungs can amplify oxidative stress and cytotoxicity in lung cells. The failure to protect lung cells from these harmful agents and the associated oxidative stress can lead to lung damage and chronic lung diseases[86]. Cigarette smoke is one of the most common causes of primary lung cancer. Oxidative free radicals induced by inhaled metals in cigarette smoke can damage intracellular organelles and result in oxidant-induced DNA damage or chromosomal instability. These lesions accrue over time and can be aggressive drivers for lung cancer[84,87,88]. Studies aimed at understanding the mechanisms of iron regulation in the lung are not only important for increasing our fundamental understanding of iron homeostasis in the lung but can also uncover possible avenues to prevent human diseases.

Structure of the lung

Compared to other organs, the tissue in the lungs have a very slow turnover rate (~7 years in humans)[88,89]. Yet lung tissue injury has a fast rate of regeneration involving the mobilization of many cells that possess stem cell-like properties, called alveolar type II (AT2) cells. Their function, along with the help of basal cells, in this process is to mitigate damage and replace dead cells[90,91]. AT2 cells under normal circumstances give rise to different

anatomical lung tissue compartments. The main alveolar structure, called alveolus, is formed by AT2 cells and alveolar type I (ATI) cells which is specialized for gas exchange. Throughout the lung tissue, club, and ciliated cells in conjunction with basal cells cover and line the basement membrane to form the highly flexible lung tissue of the bronchi.

Immune cells in the lung

Apart from the structural and functional cells comprising lung tissue, immune cells are found throughout the lung and are constantly in flux[92]. As an organ that has contact with the outside environment, innate immune cells constantly surveil to protect against pathogens and prevent damage. Macrophages are the most densely populated immune cells in the lungs and are generally the first to encounter any kind of challenge[92,93]. The contact that macrophages maintain with the epithelial layer is vital for reciprocal communication and lung tissue homeostasis. Macrophages have low phagocytosis activity and cytokine expression in the steady-state yet rapidly initiate inflammatory attacks in response to danger cues from the surrounding microenvironment[93–96]. As macrophages patrol, they also aid in maintaining lung surfactant, as well as perform functions of identifying, removing, or processing pathogens, harmful particulates, and noxious gases[95,97–100].

Within the cycle of macrophage recognition, initiation, and participation in an inflammatory attack, they also orchestrate the resolution of inflammation within the lungs[92]. Negative feedback loops to reduce inflammatory responses in macrophages initiate the need to clear away dead cells or debris, which goes hand in hand with driving the process of tissue remodeling and repair. CD206+ macrophages coordinate this function by secreting TGFβ, IL-13 and IL-4 and expressing resolution markers MerTK and CD163[101]. The specific timing, the intricate cocktail of environmental cues, coordination from other cells, and intracellular signaling pathways involved in macrophage switching from an inflammation-inducing response to wound healing and resolution response is still not clear[94,102–107].

Subsets of lung macrophages

Macrophages within the lungs share some general functional capacities yet are heterogeneous in origin and phenotype[3,108,109]. All types of macrophages found in the murine lung express classical "macrophage" identifiers, such as CD64, F4/80, and CD36. They also have the capacity to phagocytose, express Fc receptors and flexibly respond to micro-environmental stimuli[110]. There are two main subsets of lung macrophages, alveolar and interstitial. Alveolar macrophages (AMs) occupy the structural components of the alveoli, are densely populated in the lung, and are easily isolated, being identified using cell surface

markers such as CD45+/SiglecF+/CD11c+ and oxidative phosphorylation metabolism signatures. They can be classified further into two groups, resident AMs (rAMs), which are derived from the embryonic development stage of the body, or the monocytic (or recruited) AM (mAMs), which possess slight differences from rAMs in cell proliferation and metabolism[111]. Both types of AMs are involved in the maintenance of lung surfactant and engage in defensive roles due to their location within the alveoli.

Non-alveolar macrophages within the interstitium are labeled as interstitial macrophages (IM)[110,112]. Since their abundance is relatively low, ~8X less than AMs, isolation and identification from the lungs require tissue digestion along with a diverse combination of cell surface markers that differ from those found on AMs[113,114]. In-depth transcriptional analyses have identified five subsets of IMs under normal circumstances, IM1, IM2, IM3, IM Lyv1^{lo}MHCII^{hi}and IM Lyv1^{hi}MHCII^{low}[114]. Overall, the function of IMs is generally thought of as regulatory[110]. Each category is determined by phenotype, i.e., on the degree of marker expression found on the cell surface, as well as by the specific location found within the lungs. For example, the Lyv1^{lo}MHCII^{hi} subset possess strong antigen presentation cell (APC) function and have been found to locate at or near nerves within the bronchi. On the other hand, Lyv1^{hi}MHCII^{low} secrete cytokines that facilitate repair and have been found around vessels. IMs were initially thought to stem from a putative pool from circulating systemic monocytes, but experiments depleting blood monocytes by injecting clodronate-containing liposomes, an apoptosis-inducing compound, did not affect the population of IMs in the lung[113]. Other reports using comprehensive transcriptomic techniques suggest that the IM3 subtype is monocytic-derived, whereas the other IM subtypes are residential. The determination of IM subsets' cell of origin as well as functional capacity is currently being investigated and will likely become clear as combinatory techniques of flow cytometry with single-cell sequencing advance[111,114–118].

Iron and lung macrophages

Even with recent advances in iron and macrophage biology, the mechanisms of iron homeostasis in the lung, as well as the participation of macrophages in this process, are poorly understood. One of the prominent roles of the AMs is lung cell protection. Sequestration of iron by macrophages is an essential protective mechanism to prevent the overloading of iron in lung cells as well as a defense mechanism against invading pathogens[119]. AMs constitutively express TFR1 to promote uptake of Tf bound iron. AMs also import iron, through receptor-specific mechanisms, including lactoferrin (LfR) and the divalent metal transporter 1 (DMT1)

or scavenging/phagocytosis for the uptake of non-Tf bound sources of iron[120,121]. AMs are often found with little to no FPN1 expression, further indicating a general iron sequestration phenotype[79]. Indeed, global analysis of lung AMs shows that a proportion are iron-loaded under normal conditions and that this proportion increases under conditions of disease or iron dysregulation, such as idiopathic pulmonary fibrosis, bacterial infection and chronic obstructive pulmonary disease[122–124].

Macrophages are immune regulators in the lung

Macrophages are master regulators of innate immune responses in the lung[93,125]. In pathogenic infection or particulate accumulation, macrophages are initial responders that stimulate several pathways for defense and protection. This response is initiated by pattern recognition receptors, such as toll-like receptors (TLRs) on macrophages[126]. Scavenger receptors, such as CD36, are used to remove debris build up especially after noxious or oxidative inhalations. Phagocytosis of the invader or debris activates macrophages to secrete oxidative species, such as ROS or NOS. This mechanism is tightly regulated to block pathogenic spread while limiting host tissue damage[127–130]. Propagation of inflammatory responses by the release of cytokines, chemokines or oxidative species results in the rapid influx of other innate immune cells, like neutrophils, monocytic-derived macrophages (MDMs), eosinophils, and monocytic-derived dendritic cells (MDDCs), that aid in the defense or resolution of inflammation.

In certain lung diseases, including cancer, an inundation of immune cells in lung tissue as well as functionally exhausted resident macrophages have been found to sustain or worsen the underlying disease conditions. Studies have found that the depletion of CD206+ macrophages in the lung by clodronate-liposomes attenuated lung injury in mice[131,132]. Desensitization of macrophages due to persistent long-term exposures can result in impaired phagocytosis and reduced clearing of apoptotic cells while also chronically inducing the expression of inflammatory cytokines[129,130,133]. Alternatively, other studies found that preventing macrophage recruitment to the lung reduced the severity and progression of lung cancer[134]. These studies show that macrophages in the lung represent an important factor that influences lung disease progression and pose as potential drug targets.
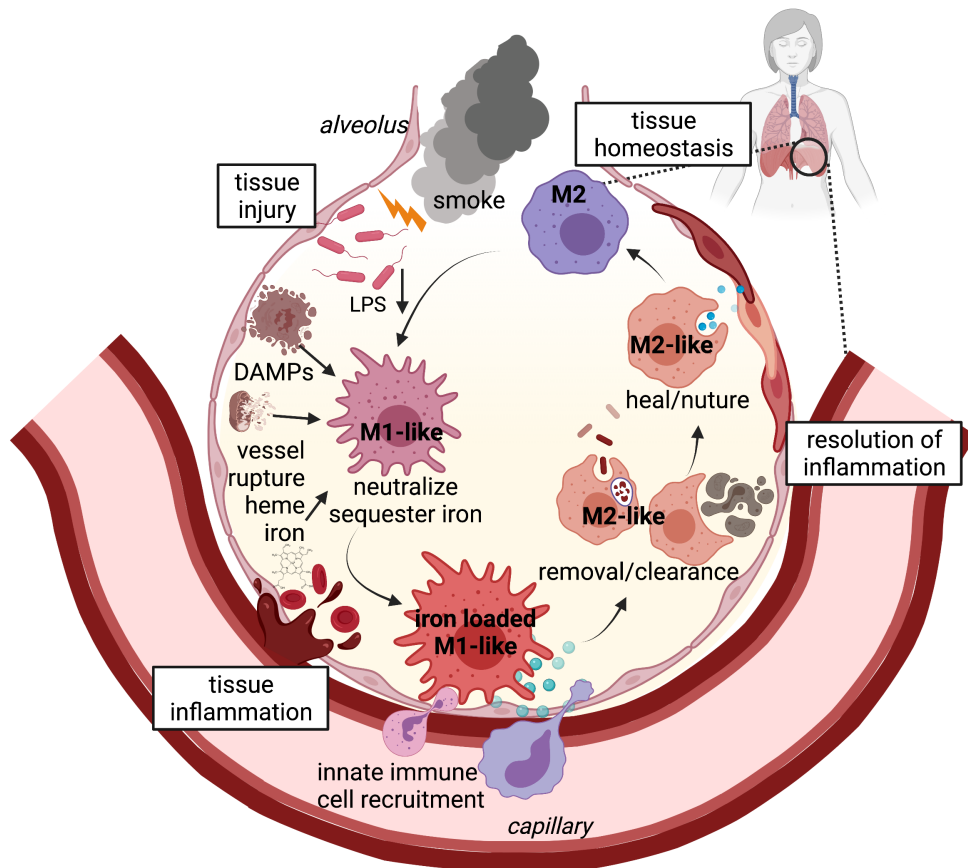
Figure 1.3. The role of macrophage polarization in defence and healing of tissue within the alveolus of the lung.

Alveolar and interstitial macrophages patrol and protect the lung tissue in order to maintain lung *tissue homeostasis*. Upon *tissue injury* to the lungs, for example by pathogenic infection or oxidative stress by inhaled smoke, damage associated molecular patterns (DAMPS) and secreted factors from injured tissue cells recruit macrophages to the site of injury. In the process, macrophages adopt an inflammatory (M1-like) phenotype, where they secrete reactive oxidative species and retain iron in order to neutralize foreign entities and prevent further tissue damage. *Tissue inflammation,* where the recruitment of monocytic-derived cells, such as monocytes and neutrophils, occurs as a response to secreted factors released by M1-like macrophages and injured tissue. The process of *resolution of inflammation* is done by macrophages that adopt an M2-like phenotype and contribute to removing dead cell debris and facilitate the healing of injured tissue. Figure adapted from previously published studies[117,180,367–373].

SECTION 1.6: LUNG CANCER

Lung cancer is the second most frequent type of cancer after breast cancer, yet the survival rate of lung cancer patients is the lowest across all cancer types[81]. One major reason being due to the difficulty in distinguishing the diagnosis of lung cancer from other lung diseases. Most patients present few to no symptoms at early stages and with the severity of the disease progressing rapidly, fatality is often quick[81]. For primary lung cancer, 60-80% of cases are either one of two types of non-small cell lung cancer (NSCLC) and 40-20% are of small-cell lung cancer (SCLC). NSCLC can be categorized into adenocarcinoma (lung adenocarcinoma (LUAD)), being the most prevalent type in adults, and squamous cell carcinoma. 75% of patients with LUAD are chronic smokers, where the activation of the oncogene *KRAS* has been characterized as one of the main drivers[135]. LUAD occurring in non-smokers has the tendency to initiate metastasis very early and has very low rates of early detection, which contributes to the high fatality rate of this disease. Non-smoker LUAD patients frequently harbor genetic aberrations, such as EGFR mutations or gene fusions involving the Anaplastic Lymphoma Kinase (ALK)[136]. LUAD is distinguished from other NSCLC types based on lung cancer cell morphology, histological staining and mutational or molecular landscapes[122–124]. With advancements in understanding the origins of LUAD as well as characterization of LUAD molecular landscapes, treatment options are starting to be derived that are more personal and effective, laying way for the possibility to use personalized medicine to treat lung cancer[125,127].

Since the initial findings that carcinogens can initiate lung cancer in the 1930s, our understanding of the origin of LUAD has progressed immensely[119]. Despite this many questions remain unanswered. The research into the pathogenesis of lung cancer has relied on the use of genetically manipulated mouse models that phenocopy gain of function or loss of function mutations in lung cancer. These models have been instrumental in identifying cell populations involved in initiating tumor formation. The origin of the different NSCLC subtypes is mainly believed to be from two different cell types: AT2 and club cells[88,137]. The stem cell like and proliferative properties of AT2 cells makes them highly sensitive cells susceptible to malignant transformation and they are therefore the focus of many LUAD studies. Despite this, more recent findings have shown that multiple lung cell types, such as club cells, contribute in combination with AT2 cells to the initiation of LUAD[125]. As a result, cell heterogeneity and molecular heterogeneity in LUAD initiation, identification and progression is prominent. Until recently, many LUAD patients were incorrectly categorized as histologically equivalent due to the lack of in-depth pathogenic knowledge of LUAD.

Mouse models of lung cancer

Mouse models provide an avenue for cancer research that was not achievable with traditional 2D culturing methods[138,139]. The interplay between cancer development and the surrounding tissue is a diverse and complex reaction. Tumor heterogeneity that arises in different cancer types is not simply due to variability in genetic composition of cancer cells but is also influenced by the intricate complexity of the surrounding microenvironment (TME) of the tumor. This includes a multitude of various types of cells, such as fibroblasts, innate and adaptive immune cells, endothelial cells, as well as matrix components and vascular structures, all of which influence progression of the disease and response to therapy[140,141]. Introduced in the early 1950s, xenograft lung cancer mouse models were integral in understanding tumor growth kinetics, progression of metastases, and aided in the development of cancer therapeutics[142,143]. Traditionally, syngeneic and xenograft mouse models were the state-of-the-art model for cancer research[144]. These models are implanted with either mouse-derived cancer cells (syngeneic) or human-derived cancer cells (xenograft) either in the organ of cancer cell origin (orthotropic) or without consideration of its origin (heterotopic). Most of these models are typically cost effective, reliable, and simple to use[138]. Orthotopic models are more representative model of cancer biology compared to heterotopic models because of the consistency in studying cancer cells in their native environment.

Where syngeneic and xenograft models fall short, genetically engineered mouse models (GEMM) have proved to be superior to study the complex drivers of lung cancer subtypes[145–148]. With these models, one can insert or delete one gene at a time or alter multiple genes simultaneously, providing a highly customizable tool to elucidate specific drivers for lung cancer initiation[138]. The most common lung cancer model is called the KP model in which a mutation is inserted in the *KRAS* gene and p53 is deleted at the same time. GEMMs for cell specific Cre drivers are developed using mainly two methods: engineered knock-in strategies or with the use of adenoviral vectors containing specific promoters for the expression of Cre drivers. Intratracheal instillation of adenoviral vectors allows for non-invasive lung specific targeting that make it possible to model the promotion of the most common NSCLC types, such as *KRAS* mutant tumors or the chromosomal rearrangement variant, *EML4-ALK*[145,149]. Other studies have used lung cancer GEMMs to undergo large scale screenings to determine genetic and other context dependent interactions involved in human lung adenocarcinomas[150]. With such fine-tuned mechanisms to elicit precise genetic alterations, the manipulation of cancers in these models has become highly reproducible and are established as indispensable tools for lung cancer research.

Model		Cells (species of origin)	Tissue implantation
Syngeneic	Orthotopic	Mouse	Lung
	Heterotopic	Mouse	Subcutaneous, intraperitoneal
Xenograft	Orthotopic	Human	Lung
	Heterotopic	Human	Subcutaneous, intraperitoneal
Transgenic (GEMM)		N/A	Lung

Table 1.1 Lung cancer mouse models

Iron and lung cancer

The dualistic function of iron, being both required for cell growth and toxic in high concentrations, plays a prevalent role in cancer biology; fast dividing cells require high levels of iron to supplement their greater metabolic needs[151–155]. Increased iron accumulation in cells can lead to the production of reactive oxygen species (ROS), which can oxidize DNA, lipids and proteins and damage cellular functions. ROS generation has been well characterized as an inducer of carcinogensis[153,155]. Elevated levels of iron import proteins, iron storage proteins and reduced iron export proteins have been found in NSCLC cells and have clinically been used as identifiers of malignant cells[140].

The role of iron in fostering cancer growth was determined early in cancer research[156,157]. The mechanism by which dysregulation of iron occurs in cancer cells and the association of iron with the risk of cancer in humans had laid way to in-depth understanding of the major role iron partakes in cancer development, progression as well as diagnosis and therapy. The general association between iron levels in the body and risk of cancer is still a controversial topic, with data heavily relied upon from epidemiological studies. In humans, high iron levels have been found to both contribute and reduce the risk of cancer[153,158–162]. On the other hand, a reduced risk of cancer was found in individuals who donate blood more often or who suffer from anemia[160]. Experimental mouse data has shown more clear parallels between increased iron and a higher risk of lung cancer[55,143–146]. Studies done in mice fed a high iron diet showed that an increase in body iron levels stimulated the development of lung tumors[147] and mice on a low iron diet correlated with reduced lung cancer incidence[163].

The association of iron and cancer has opened many opportunities to apply or manipulate iron for the benefit of the patient[164]. Iron-related proteins, like haptoglobin, transferrin, or those related to inflammation, called acute phase proteins (APPs), identified in the blood of patients are commonly associated with the indication or presence of lung cancer[149].

Manipulating iron levels through the deprivation of iron or the overloading of iron in cancer cells has generated significant focus in developing anti-lung cancer therapies[153,165,166].

Tumor-associated macrophages (TAMs) and lung cancer

The lungs contain most of the macrophages in the body. The most populated type, the alveolar macrophage (AMs), has only recently been implicated in lung cancer[167]. Macrophages of monocytic origin are the more commonly identified macrophage associated with lung cancer [168] and debate regarding the origin of tumor-associated macrophages (TAMs) in NSCLC is still ongoing. However, to date the best understood immune response associated with cancer and its role in cancer progression has been in human NSCLC[45,169,170].

The inundation of innate immune cells, mostly macrophages, is associated in almost all solid cancer types and is considered a hallmark of cancer[171,172]. When considering the cell composition of a solid lung tumor, inflammation can make up to ~ 50% of cell mass, to which TAMs constitute a significantly large portion[173–175]. The environment that surrounds the tumor, the primary location of immune cell infiltration, is composed of a milieu containing secreted factors, structural cells and tissue matrices that make up the tumor-microenvironment (TME). TAMs are central regulators within the TME, functioning to direct other immune cells, nurse cancer cells by secreting nutrients and growth factors, clear away debris, and facilitate a supportive environment for growth[176]. Under normal circumstances, these functions would be ideal for tissue homeostasis however within the context of cancer, high levels of TAMs can lead to increased tumor growth. In general, TAMs are primarily suppressive/anti-inflammatory expressing the cell surface biomarkers CD163+ and CD206+, which are used as identifiers[177]. Their function also encompasses a protective role as the presence of TAMs can interfere or mitigate the efficacy of conventional chemotherapeutics in lung cancer[178]. In human NSCLC, high TAM density within lung cancers is associated with poor prognosis and poor survival[172,179,180]. However, the detailed mechanisms of how TAMs support tumor growth and progression in lung cancer is still unclear[181].

Since the first descriptions of the tumor micro-environment and the recruitment of TAMs in cancer, macrophages have been identified as important immunotherapeutic targets[182]. The removal of TAMs from the TME by injection of clodronate encapsulated in liposomes, into a murine lung cancer mouse model reduced tumor burden and growth over time[183]. However, since eliminating macrophages from patients' is not a viable therapeutic strategy, the focus has now turned to reprogramming TAMs within the TME. It was only recently that the idea of reprogramming TAMs to kill cells and orchestrate anti-cancer responses developed as

a therapeutic strategy for cancer[182]. With the advancement in macrophage biology, polarization strategies targeting the population of TAMs have been promising therapeutics in combination with additional chemotherapeutics. Many therapeutics have been developed to either prevent TAMs from acquiring a suppressive/anti-inflammatory (M2) phenotype, to activate suppressive/inflammatory (M2) TAMs to an inflammatory (M1) phenotype, or to prevent the production of secreted factors from suppressive/anti-inflammatory TAMs[184,185]. Administering agents to polarize suppressive/anti-inflammatory TAMs to a pro-inflammatory phenotype is by far the most popular approach due to the low risk of side effects to the patient: many agents used for this strategy are short lived and are administered in a pulse-like fashion. In lung cancer, patients who have more inflammatory-like TAMs within the TME fair better in prognosis than those with an abundance of suppressive/inflammatory TAMs[179,186]. In this respect, the capability of iron to polarize TAMs to an inflammatory phenotype opens an opportunity of using iron as an anti-cancer therapeutic.

The gold standard in treating NSCLC is surgical resection and pulmonary radiotherapy[128,159]. Therapies such as tyrosine kinase inhibitors (TKI), anti-VEGF and platinum-based chemotherapies are used to target and kill malignant cells of specific tumor types[184]. However, in 10-40% of cases, chemotherapy-induced resistance causes relapse, and the resultant cancer that remains has a very low response rate to additional conventional therapies. One aspect that can contribute to this relapse or therapeutic resistance are TAMs[178]. For these difficult cancer cases, reprogramming TAMs to more inflammatory-like is a promising window of therapeutic opportunity.

Immunotherapy

Immunotherapy targets and activates cells of the immune system to attack cancer cells or limit cancer growth[187]. In a field that has rapidly expanded in the last ten years, immunotherapy has provided a chance of survival to cancer patients where previously there was none. Because of the heterogeneity in lung adenocarcinoma, immunotherapy can offer patients a broad range of treatment options and have contributed substantially to the benefit of lung cancer patients' lives[160–162]. Immunotherapy, such as immune checkpoint inhibitors (anti-CTLA and anti-PD1), work to stimulate Th1 responses in the adaptive immune system which then activate cytotoxic CD8+ T cells, the host cell killers of the adaptive immune system[184]. The other side to immunotherapy has been to target innate immune cells, like macrophages, which then coordinate responses to CD8+ T cells and direct the action of cytotoxicity against tumors. Macrophages activated to an inflammatory-like (M1) phenotype express receptors that have high antigen presentation capacity, activating Th1 stimulatory patterns. Polarizing TAMs to an inflammatory state has shown promising results in clinical settings and is done in combination with traditional chemotherapy options, immune checkpoint therapy and radiotherapy according to a patient's histological, phenotypic and genotypic classification[188].

The focus of iron within the context of cancer has garnered significant interest. Rather than being applied directly to malignant cells, the application of iron is done to cells of the TME. Iron-loaded macrophages in mouse lung cancer models have correlated with reduced cancer growth over time[189]. Iron-loaded TAMs within the TME were phenotyped as inflammatory-like, expressing proteins such as CD86 and MHCII, as well as inflammatory cytokines TNF, IL6 and IL1β. However, the direct application of elemental iron is toxic and has many deleterious effects. Therefore, a need arises for developing strategies of safe iron delivery to the TME [190].

Nanotherapy

Nanotherapy is an emerging field of medical therapies that has recently gained a lot of attention[191–199]. Manly due to the advancements in technologies, production of nanoscale materials has propelled interdisciplinary research between chemistry, biology, and medicine[200]. The production of nanoparticles is not novel as nanoparticles are routinely used for electronic or industrial applications[201]. However, new methods for nanoparticles construction produce particles with properties that are particularly suitable for use in biological systems[190,202]. In fact, the use of nanoparticles to study biological systems has proven indispensable in a multitude of biological innovations, such as advancing areas of *in vivo* imaging, *in vivo* cell tracking, disease diagnosis, or administration of vaccinations[203–219].

Due to the multitude of combinations and permutations that can be used to compose nanoparticles, the field of nanomedicine has expanded with a multitude of therapies and targets[220,221]. Nanoparticles are made up of a combination of molecules that come together to form a molecular structure, which can vary in size, surface area, shape, and volume[195,202,222,223]. They can range anywhere form 5 – 100 nm in diameter. The construction and composition of a nanoparticle dictates its functional properties, as the size and coating of a specific molecule can determine the overall charge of the nanoparticle and its distribution within the body, providing the potential for targeted approaches. The composition and properties of a nanoparticle can be designed with a specific intention in mind and functionalized with tools, such as fluorophores, that allow tracking. Super-paramagnetic iron oxide nanoparticles (SPIONs) are a type of nanoparticle composed of a polymer shell encapsulating an iron oxide core[224–226]. The coating allows for the application of iron in a non-toxic and biocompatible manner. Some SPIONs already in clinical use to treat chronic kidney disease[227]. Due to their size, SPIONs are mainly taken up by phagocytic cells rather than cancerous epithelial cells, making them an ideal immunotherapeutic delivery system. For lung cancer, preliminary pre-clinical studies show that SPIONs within the TME can reduce tumor growth over time[189,228]. In these studies, TAMs internalized SPIONs and adopted an inflammatory-like phenotype. Therefore, the development of SPIONs to target TAMs in lung cancer is a promising strategy for therapeutic development of an anti-cancer therapy.

SECTION 1.8: AIM OF THE STUDY

The aim of this study is to develop and test SPIONs as a candidate adjuvant lung cancer therapy. We have developed a new class of super-paramagnetic iron oxide nanoparticles (SPIONs) that activate macrophages to an inflammatory-like phenotype. To test the cancer killing potential of SPION activated macrophages, we performed co-culture experiments with lewis lung carcinoma (LLC) cells and SPION treated BMDMs. To validate our results, we tested SPIONs *in vivo* by intratracheally instilling SPIONs into the lungs of wildtype C57Bl/6 mice. SPIONs were then tested *in vivo* by intravenous injection in an orthotopic lung cancer mouse model, where LLC cells were intratracheally instilled in C57Bl/6 mice.

Chapter 2: Materials and Methods

2.1 M ATERIALS

Frequently used reagents and chemicals

Chemical name	Abbreviation	Product number	Supplier
β-mercaptoethanol	BME	M3148	Sigma-Aldrich
1400W dihydrochloride	1400W	1415/10	R&D Systems
(4-(2-hydroxyethyl)-1-piperazineethanesulfonic acid)	HEPES	H0887-20ML	Sigma-Aldrich
4′,6-diamidino-2-phenylindole	DAPI	422801	BioLegend
7-Aminoactinomycin D	7-AAD	420404	BioLegend
Ammonium iron (III) citrate	FAC	F5879-500g	Sigma-Aldrich
5-(and-6)-Carboxyfluorescein diacetate, succinimidyl ester	CFSE	C1157	Life Technologies
Bromophenol blue		B8026-5g	Sigma-Aldrich
CLI-095	CLI	tlrl-cli95	InvivoGen
Ethylenediaminetetraacetic acid	EDTA	1233508-200MG	Sigma-Aldrich
Ethanol		5054.1	Carl Rother
FcR Blocking Reagent, mouse	FcR Block	130-092-575	Miltenyi
Ferric chloride heme	Heme	16009-13-5	Sigma-Aldrich
Ferric hydroxide dextran complex	Iron Dextran	D8517-25ml	Sigma-Aldrich
Fetal bovine serum	FBS	10500064	Life Technologies
Formalin		HT501128-4L	Sigma-Aldrich
Glycerol		3783.1	Carl Roth
Glycine		G8790-100g	Sigma-Aldrich
Hydrogen chloride	HCl	7647-01-0	Life Technologies
Methanol		BISI: 01061152	Carl Roth
NP-40		9016-45-9	Calbiochem
Phosphate-buffered saline	PBS	D1408-6X500ML	Sigma-Aldrich
Polyoxymethylene	PFA	28906	Life Technologies
StemPro Accutase Cell Dissociation Reagent	Accutase	A1110501	Life Technologies
Sodium chloride	NaCl	3957.2	Carl Roth
Trichlormethane	Chloroform	67-66-3	Sigma-Aldrich
Sodium lauryl sulfate	SDS	CN30.2	Carl Roth

Trichloroacetic acid	TCA	8789.1	Carl Roth
Trisaminomethane	Tris	B9754-100g	Sigma-Aldrich
Triton® X-100		1.086.031.000	Merck Millipore
Tween® 20		9127.1	Carl Roth

Table 2.1 Materials and reagents

Antibodies

Antibody	Fluorophore	Clone/Catalogue number	Isotype	Manufacturer
Flow cytometry				
Anti-mouse				
CD11b	PerCP	ICRF44	N/A	Life Technologies
CD11c	PE	N418	N/A	BioLegend
CD163	Pe-Cy7	25-1631-82	Rat IgG2a, κ	Life Technologies
CD172a	PerCP-eFluor 710	46-1721-82	Rat IgG1, κ	Life Technologies
CD206	Alexa Fluor 700	MR6F3	Rat IgG2b, κ	Life Technologies
CD301	PerCP-Cy5.5	LOM-14	Rat IgG2b, κ	BioLegend
CD38	FITC	90	Rat IgG2a, κ	BioLegend
CD45	PerCP-Cy5.5	104	N/A	Life Technologies
CD64	Brilliant Violet V711	X54-5/7.1	N/A	BioLegend
CD71 (TFR1)	Brilliant Violet 510	RI7217	Rat IgG2a, κ	BioLegend
CD80	Brilliant Violet 650	16-10A1	Armenian Hamster IgG	BioLegend
CD86	Brilliant Violet 421	GL-1	Rat IgG2a, κ	BioLegend
F4/80	BV605	T45-2342	N/A	Life Technologies
Ly6C	PE-Dazzle	HK1.4	N/A	BioLegend
Ly6G	FITC	1A8	N/A	BioLegend
MerTK	BV421	108928	Rat IgG2a	Life Technologies
MHC II	PE-Cy5	M5/114.15.2	Rat IgG2b, κ	BioLegend
Siglec-F	APC-Cy7	E50-2440	N/A	Life Technologies
Anti-human				
CD80	PE	2D10	Mouse IgG1, κ	BioLegend
CD86	Alexa Fluor 488	IT2.2	Mouse IgG2b, κ	BioLegend
Antibody	**Fluorophore**	**Clone/Catalogue number**	**Species**	**Manufacturer**

Microscopy				
Iba1	N/A	NB100-1028SS	Goat	Novus Biologicals
Donkey anti-Goat IgG (H+L) Cross-adsorbed Secondary Antibody	Alexa Fluor 568	A-11057	N/A	Life Technologies
Western blot				
β-actin	N/A	A1978-200UL	Mouse	Sigma-Aldrich
FtL	N/A	Ab69090	Rabbit	Abcam
GPX4	N/A	125066	Rabbit	Abcam
HO-1	N/A	ADI-SPA-896-D	Rabbit	ENZO
TFR1	N/A	NB100-1028SS	Mouse	Novus Biologicals
Vinculin	N/A	V4505-2ML	Mouse	Sigma-Aldrich

Table 2.2 Antibodies

Buffers and solutions

All buffers and solutions used in this study are listed in Table 2.3.

Buffer	Components	Application
FACS Buffer	1 % FBS 1 mM EDTA 2.5 mM HEPES, pH 7.0	Flow cytometry
4x Laemmli Sample Buffer	250 mM Tris-HCl pH 6.8 8 % (w/v) SDS 40 % (v/v) glycerol 10 % -mercaptoethanol 0.06 % (w/v) bromophenol blue	Western blot analysis
PBS-T	PBS 0.01% Triton X-100	Microscopy
RIPA Buffer	10 mM Tris-HCl pH 8.0 150 mM NaCl 1 mM EDTA 1% NP-40 0,1% SDS	Western blot analysis
Transfer Buffer	25 mM Tris 192 mM glycine 10 % methanol	Western blot analysis
TBS-T	100 mM Tris-HCl pH 7.6 150 mM NaCl 0.5 % Tween® 20	Western blot analysis

Table 2.3 Buffers and Solutions

Kits

Table 2.4 includes the list of kits used in this study. Unless otherwise stated, manufacturer's recommendations were followed.

Name	Application	Product number	Supplier
Accustain iron stain	Perls' Prussian blue iron stain	No. HT20	Sigma-Aldrich (Germany)
Celltiter blue assay	Cell viability measurement	G8080 (BISI: 01122880)	Promega (Madison, USA)
Celltiter-glo ATP assay	Cell viability measurement	G7570 (BISI: 01087071)	Promega (Madison, USA)
Glutathione colometric assay	GSH/GSSG measurement	EIAGSHC	Life Technologies (Carslbad, USA)
CytoTox 96 cytotoxicity assay	Cell viability measurement	G1780 (BISI:01063904)	Promega (Madison, USA)
Lung dissociation kit	Tissue digestion	130-095-927	Miltenyi (Bergisch Gladbach, Germany)
Iron SFBC method	Plasma iron biochemistry	REF 800	Abliance SAS (Biolabo)
SYBR green PCR master mix	Quantitative PCR (qPCR)	A25780	Applied Biosystems (Warrington, UK)
Bio&SELL RNA-minikit	RNA extraction	BS67.311.0250	Bio&Sell (Feucht, Germany)
Pierce BCA protein assay	Protein quantification	23227	Life Technologies (Carslbad, USA)

Table 2.4 Kits

Oligonucleotides used for quantitative PCR analysis

All primers were purchased from Sigma-Aldrich Chemie GmbH (Taufkirchen, Germany).

Gene	Sequence
Mus musculus oligonucleotides	
Arg1	Forward 5' AATCTGCATGGGCAACCTGT 3'
	Reverse 5' GTCTACGTCTCGCAAGCCAA 3'
Cdo1	Forward 5' GGGCTTTGTATGCCAAATTC 3'

		Reverse 5' CCCAGCACAGAATCATCAGA 3'
Cd163	Forward 5' CGACAGATTCAGCGACTTACAG 3'	
	Reverse 5' GGAATTTTCCGAGGATTTCAGC 3'	
Cxcl10	Forward 5' ACGTGTTGAGATCATTGCCAC 3'	
	Reverse 5' GTCGCACCTCCACATAGCTT 3'	
Fth	Forward 5' TGGAACTGCACAAACTGGCTACT 3'	
	Reverse 5' ATGGATTTCACCTGTTCACTCAGATAA 3'	
Ftl	Forward 5' GCTCCTTGCCCGGGACTTA 3'	
	Reverse 5' AAAAAGAAGCCCAGAGAGAGGT 3'	
Gclc	Forward 5' AGATGATAGAACACGGGAGGAG 3'	
	Reverse 5' TGATCCTAAAGCGATTGTTCTTC 3'	
Gpx4	Forward 5' GCCTTCCCGTGTAACCAGT 3'	
	Reverse 5' GCGAACTCTTTGATCTCTTCGT 3'	
Gstm1	Forward 5' TCCGTGCAGACATTGTGGAG 3'	
	Reverse 5' CTGCTTCTCAAAGTCAGGGTTG 3'	
Hif1a	Forward 5' CATGATGGCTCCCTTTTTCA3'	
	Reverse 5' GTCACCTGGTTGCTGCAATA 3'	
Ho1	Forward 5' AGGCTAAGACCGCCTTCCT 3'	
	Reverse 5' TGTGTTCCTCTGTCAGCATCA 3'	
Il-6	Forward 5' GCTACCAAACTGGATATAATCAGGA 3'	
	Reverse 5' CCAGGTAGCTATGGTACTCCAGAA 3'	
Il-1β	Forward 5' GCAACTGTTCCTGAACTCAACT 3'	
	Reverse 5' ATCTTTTGGGGTCCGTCAACT 3'	
Ireg1	Forward 5' TGTCAGCCTGCTGTTTGCAGGA 3'	
	Reverse 5' TCTTGCAGCAACTGTGTCACCG 3'	
Irf5	Forward 5' CCCTGTCCCAGACCCAAATC 3'	
	Reverse 5' AGGTCCGTCAAAGGCAACAT 3'	
Lcn2	Forward 5' CCATCTATGAGCTACAAGAGAACAAT 3'	
	Reverse 5' TCTGATCCAGTAGCGACAGC 3'	
Nos2	Forward 5' TGGAGACTGTCCCAGCAATG 3'	
	Reverse 5' CAAGGCCAAACACAGCATACC 3'	
Nqo1	Forward 5' AGCGTTCGGTATTACGATCC 3'	
	Reverse 5' AGTACAATCAGGGCTCTTCTCG 3'	
Rpl19	Forward 5' AGGCATATGGGCATAGGGAAGAG 3'	
	Reverse 5' TTGACCTTCAGGTACAGGCTGTG 3'	
Slc7a11	Forward 5' TCCACAAGCACACTCCTCTG 3'	
	Reverse 5' CGTCAGAGGATGCAAAACAA 3'	
Spi-C	Forward 5' AAAGGGAGGAAGAGGCAGGAGAAA 3'	
	Reverse 5' AAGTCTTTGGAGAACAGCCTCGCT 3'	
Socs3	Forward 5' CCTTTGACAAGCGGACTCTC 3'	
	Reverse 5' GCCAGCATAAAAACCCTTCA 3'	
Stab1	Forward 5' ACTGGAGCTCCTACGGAACA 3'	
	Reverse 5' AGCATGTGGCACAAAGACAG 3'	
Stat1	Forward 5' GTCATCCCGCAGAGAGAACG 3'	
	Reverse 5' GCAGAGCTGAAACGACCTAGA 3'	
Tfrc	Forward 5' CCCATGACGTTGAATTGAACCT 3'	
	Reverse 5' GTAGTCTCCACGAGCGGAATA 3'	
Tnf	Forward 5' TGCCTATGTCTCAGCCTCTTC 3'	

	Reverse 5' GAGGCCATTTGGGAACTTCT 3'	
Ym1	Forward 5' CCAGCAGAAGCTCTCCAGAAGCA 3'	
	Reverse 5' GGCCTGTCCTTAGCCCAACTGGT 3'	
Homo sapien oligonucleotides		
Il-6	Forward 5' AAATTCGGTACATCCTCGACGGA 3'	
	Reverse 5' GGAAGGTTCAGGTTGTTTTCTGC 3'	
Il-1β	Forward 5' CTCGCCAGTGAAATGATGGCT 3'	
	Reverse 5' GTCGGAGATTCGTAGCTGGAT 3'	
Rpl19	Forward 5' TCGCCTCTAGTGTGTCCTCCG 3'	
	Reverse 5' GCGGCCCAAGGTGTTTTTC 3'	
Tnf	Forward 5' ATGAGCACTGAAAGCATGATCC 3'	
	Reverse 5' GAGGGCTGATTAGAGAGAGGTC 3'	

Table 2.5 Oligonucleotides sequences

2.2 CELL CULTURE METHODOLOGIES

Cell lines and primary cells

Immortalized cells lines used in this study are listed in Table 2.6. Each line was regularly tested for mycoplasma contamination and authenticated by visual observations of cell morphology. Cells were cultured in Roswell Park Memorial Institute Medium (RPMI, Life Technologies) containing 10 % FBS and 1 % penicillin/streptomycin.

Immortalized cell line	Abbreviation	Morphology	Tissue	Species
Lewis lung carcinoma	LLC	Epithelial	Lung	Mus musculus
B16 melanoma	B16	Spindle- and epithelial-like	Skin	Mus musculus
NCI-H838 adenocarcinoma	H838	Epithelial	Lung	Homo sapiens
Human Embryonic kidney 293	HEK-293	Epithelial	Embryonic kidney	Homo sapiens

Table 2.6 Immortalized cell lines.

Preparation of bone marrow-derived macrophages (BMDMs)

The procedure conducted follows previously established protocol.[61] Briefly, bone marrow cells were flushed from the tibia and femurs of C57BL/6N wild-type mice (8-10 weeks of age) using ice cold PBS, filtered through a 70 μm filter cell strainer and plated at a density of 3.5 x 10^5 cells/ml. Cells were differentiated for one-week using RPMI medium supplemented with 10 ng/ml M-CSF (M9170, Sigma-Aldrich), 10 % fetal bovine serum (FBS)

and 1 % penicillin/streptomycin (Gibco). For each independent experiment, BMDMs were prepared from three different mice. Cells were then prepared for analysis of cell surface protein levels by flow cytometry measurement (antibodies in Table 2.2) or differential mRNA expression by qPCR (primers in Table 2.5).

Preparation of human macrophages

Human monocytes were isolated from commercially available buffy coats (DRK-Blutspendedienst Baden-Württemberg-Hessen, Frankfurt, Germany) using Ficoll-Hypaque gradients (LSM-1077; PAA Laboratories). Monocytes were differentiated into primary human macrophages with RPMI 1640 containing 5% AB-positive human serum (DRK-Blutspendedienst) for 7 days and achieved approximately 80% confluence. 24 h prior to stimulation, cells were serum starved. Cells were then prepared for analysis of cell surface protein levels by flow cytometry measurement (antibodies in Table 2.2) or differential mRNA expression by qPCR (primers in Table 2.5).

2.3 MOLECULAR BIOLOGY METHODOLOGIES

Cellular cytotoxicity measurement

BMDM viability was quantified using CytoTox96 LDH release kit (Promega), Celltiter Blue as well as CytoTox96 kit (Promega). For all assays, cells were plated in a black side/black bottom 96 well plate at a concentration of 10,000 cells in 100 μl/well for 24 h. Viability was calculated by subtracting the media blank from experimental values and normalized to the non-treated condition (NT).

For LDH release, after treatment, supernatant was collected by centrifuging the plate at 500 G for 10 mins to sediment cells and 100 μl was transferred to a new 96 well plate. 50 ul of substrate was added to 50 ul of supernatant and incubated for 30 minutes at room temperature in the dark. After 30 minutes, 20 μl stop solution was added to each well and signal at 490 nm was measured on a spectrofluorometer (SpectraMax, Molecular Devices). To measure redox capacity, after treatments, 10 μl of Celltiter Blue was added to each well and plate was incubated at 37°C for 4 h. Absorbance was then measured at 520 nm and all values were subtracted from the media blank control and normalized to the NT condition. To measure ATP levels using the Cell-titerglo-ATP kit (Promega), after treatments cells were washed twice with cold PBS. Reagent was mixed with lysis buffer in a 1:1 ratio and added to cells. Cell lysates were shaken for 2 minutes on an orbital shaker and measured as per manufacturer's protocol.

DAB-enhanced Perls' staining

BMDMs (3.5×10^5) were plated on a 13 mm (Life Technologies #A1048301) glass slip. After treatment, cells were washed three times with PBS and fixed with 4% paraformaldehyde at room temperature for ten minutes. Cells were then washed three times with PBS. For tissue sections, tissues were fixed for 24 h at 4°C by immersion in a solution of 10% neutral buffered formalin (Sigma), dehydrated and then paraffin embedded. Tissues were sectioned at 3 μm and mounted on polysine slides (Thermo Scientific). Tissue sections were rehydrated and stained for 15 min with a potassium ferrocyanide/HCl solution (Accustain Iron Stain No. HT20 (Sigma-Aldrich)) following manufacturer's instructions. After washing with distilled water, tissues were treated with 3,3-diaminobenzidinetetrahydrochloride (DAB) (Sigma Aldrich), washed with distilled water and counterstained Fast Red (Sigma Aldrich). Samples were mounted using the VectaMount (H5501, Biozol). Images were digitally acquired with a Nikon Ni-E microscope, using the Nikon NIS-Elements Viewer software, and assembled into figures using Adobe Photoshop and Illustrator software packages.

Flow cytometry

For preparation of tissue, mouse lungs were resected and washed in PBS. Single-cell suspensions (200 μL) were generated by applying chemical and mechanical digestion using the Miltenyi Lung Dissociation Kit and pelleted by centrifugation for 5 mins at 300G. For preparation of cultured cells, BMDMs or immortalized cells lines were washed twice with ice cold PBS and detached by incubation with StemPro Accutase enzyme solution (Life Technologies).

Collected cells were then washed with FACS buffer (1% fetal bovine serum, 2.5 mM 1M HEPES, 1 mM EDTA). Single-cell suspensions from either cultured cells or from dissociated tissue were incubated with Fc-γ receptor blocking solution (Miltenyi) for 10 minutes and followed by 30 minutes of staining with antibodies listed in Table 2.2. Data were acquired using a FACS Fortessa (BD, Biosciences) or Cytotek Aurora flow cytometer at the EMBL Flow Cytometry Core Facility and analysis was performed using the FlowJo Software (Tree Star Inc). The expression of surface markers on BMDMs was calculated by subtracting the geometric median fluorescence intensity (MFI) of cells stained with the isotype-matched antibody from the MFI of those stained with the specific antibody and is shown as fold-change compared to the non-treated (NT) control.

Glutathione measurement

Cells were plated in a clear 96 well plate to a total cell concentration of 10,000 cells in 100 µl/well for 24 h. For co-culturing of BMDMs with Lewis lung carcinoma cells, a ratio of 5:2 was used per well. Samples were then prepared and analysed according to manufacturer's protocol.

Isolation of CD45+ cells from co-cultures

After culturing and treatments, attached cells were lifted after incubation with StemPro Accutase enzyme solution (Life Technologies) at 37℃ for 10 minutes. All cells were collected and washed with FACS buffer. CD45+ cells were magnetically separated from single-cell suspensions using MicroBeads (MACS) according to manufacturer's instruction and lyzed for differential mRNA expression by qPCR (primers in Table 2.5).

Immunofluorescence microscopy

BMDMs were plated on 13 mm collagen-coated (Life Technologies #A1048301) glass cover slips in a density of 1.0×10^5 cells/slip. After treatment, cells were washed three times with phosphate-buffered saline (PBS) and fixed with 4% paraformaldehyde for 15 minutes at room temperature. Cells were then washed three times with PBS and blocked with 2.5% milk in PBS-T (0.1% Tween) solution for 30 minutes on an orbital shaker. Slips were then washed three times with 0.1% PBS-T and incubated with primary antibody Iba1 (NB100-1028SS, Bio Techne) overnight at 4℃ or 1 hour at room temperature. After washing with PBS-T, samples were incubated with secondary antibody (A-11057, Donkey anti-Goat IgG (H+L) Cross-adsorbed Secondary Antibody Alexa Fluor 568, Life Technologies) for 1 hour at room temperature. Slips were then washed with PBS and mounted using Prolong Gold Antifade Mountant with DAPI (P36931, Life Technologies). Samples were acquired at the University of Heidelberg Nikon Imaging Centre using a Ni-E confocal microscope. Images were analysed using Fiji (National Institute for Health) using a written macro for intracellular quantification of the Cy5+ signal. Images were compiled into figures using Adobe Photoshop and Illustrator.

Measurement of ROS accumulation

Accumulation of ROS in BMDM cells was assessed by using the oxidant-sensitive fluorescent dye CELLROX™ Green and CELLROX™ Orange (Life Technologies). Upon cellular uptake, the non-fluorescent CELLROX™ probe undergoes deacetylation by intracellular esterases producing a fluorescent green signal following oxidation by intracellular ROS. BMDMs were maintained untreated or were treated for up to 36 h with 20 µM SPION-CCPMs, CCPMs, 100 ng/mL lipopolysaccharide (LPS) or interferon-ɣ, 20 µM ferric

ammonium citrate (FAC), or 20 μM heme. The amount of SPION-CCPMs added to cells was calculated to 20 μM iron from within the core. The amount of CCPMs added to cells was calculated to match the mass of CCPMs contained within added SPION-CCPMs. 2.5 mM of CELLROX™ Green or Orange was added to cells and incubated for 30 minutes at 37 °C under 5% CO_2 atmosphere. Cells were washed twice with Hanks' Balanced Salt Solution (HBSS) and fluorescence intensity was measured using Cytotek Aurora flow cytometer. Fluorescence intensity is represented as fold change compared to the non-treated condition (NT).

Plasma biochemistry and tissue iron quantification

Plasma iron concentration and unsaturated iron binding capacity were assessed using the SFBC and UIBC kits (Biolabo, Maizy, France). Transferrin saturation was calculated using the formula, SFBC/(SFBC+UIBC) X 100. Tissue non-heme iron content was measured using the bathopenanthroline method and calculated against dry tissue weight[229].

Total RNA extraction and reverse transcription

Total RNA extraction from tissue was performed using Trizol (Life technologies) according to manufacturer's instruction. The concentration and purity of RNA was determined by Nanodrop2000 (Thermo Scientific). 1 (or 0.5) μg of total RNA was used for reverse transcription (RT). RNA and 1 μl of random primers (0.2 μg/μl) were denatured at 70°C for 10 minutes then cooled on ice for 2 minutes. The reverse transcription reaction mixture contained a total volume of 25 μl consisting of RT buffer (Fermentas), 0.4 mM dNTPs, 100 units of RevertAid H minus M-MuLV Reverse Transcriptase (Fermentas), 1 μl random primers (0.2 μg/μl) and 1 (or 0.5) μg of denatured total RNA. The mix was incubated at 42°C for 90 minutes, then at 70°C for 10 minutes. The resultant cDNA samples were then diluted for the subsequent qPCR analysis by adding 175 μl of H_2O to cDNA obtained from cells or 475 μl of H_2O cDNA from tissues.

Quantitative PCR

The reaction of quantitative PCR followed the standard RNA extraction/cDNA synthesis protocol. The reaction mixture (20μl) contained 10 μl SYBR Green PCR Master Mix, 0.5 μM of the forward and reverse primers and 5 μl cDNA. The qPCR mixture was run on StepOnePlus™ Real-Time PCR System (4376600, Applied Biosystems™) following amplification conditions: 50°C 2 minutes, 95 °C 10 minutes, then 40 cycles of 95°C 15s and 60°C 15 s. Intron-spanning primers were designed to specifically amplify human or murine transcripts. Sequences of primers are shown in Table 2.5. Threshold cycles (C_t) were defined as the fractional cycle number at which the fluorescence passed the fixed threshold. C_t values

were extracted and calculations for normalization and further analysis were done in Excel software (Microsoft Office). The mRNA/cDNA abundance of each gene was calculated relative to the expression of the housekeeping gene *Rpl19* encoding the 60S ribosomal protein L19 and data were analyzed by apply the $\Delta\Delta C_t$ method[230,231].

Western blot analysis

Tissues were lysed by homogenization in radioimmunoprecipitation assay (RIPA) buffer supplemented 1X Complete Mini Protease Inhibitor Mixture (04693116001, Roche Applied Science) and phosSTOP phosphatase inhibitors cocktail (04906845001, Roche Applied Science). After 30 minutes of incubation on ice, samples were centrifuged at 10,000 rpm for 10 minutes at 4°C and supernatants were collected. Protein concentration was determined using the BSA Assay (Thermo Scientific). A total of 50 μg of protein were mixed with 4X Laemmli buffer and denatured by heating at 95 °C for 5 minutes. The samples were subjected to 12% SDS-PAGE and the proteins were transferred to a PVDF membrane using wet transfer method. The membrane was blocked with 5 % milk in TBS containing 0.1 % Tween-20 (TBS/T) for 1 h at room temperature. Primary antibodies indicated in 2.2 were incubated for 1 h at room temperature or over-night. Membranes were then washed with TBS/T and incubated with anti-rabbit or anti-mouse IgG secondary antibody (Sigma-Aldrich). After washing, the immune complexes formed on the blot were visualized by ECL-Plus (Amersham Biosciences), quantified with Vilber Lourmat (Eberhardzell, Germany) Fusion-FX Chemiluminescence system and normalized to β-actin or vinculin.

2.4 MICE

C57Bl/6 mice, aged 6-8 weeks, used for cancer experiments were purchased Javier Laboratories. Mice were housed at the DKFZ (Deutsches Krebsforschungszentrum) animal facility under constant a light-dark cycle and maintained on a standard diet with ad libitum access to food and water. Experimentation was performed at the DKFZ animal facilities, in accordance with institutional guidelines, and were approved by the Regierungspräsidium Karlsruhe, Germany, under permit number G214/19. Mice were anaesthetized by intraperitoneal injection of 100 μg g^{-1} ketamine and 14 μg g^{-1} xylazine and intratracheally instilled or intravenously injected with SPION-CCPM (10 mg/kg of iron to body weight), CCPMs, or PBS in a final volume of 50 μl. Mice were then kept on a warm pad until conscious. For intravenous injection, mice were restrained and a maximum of 50 μl was injected into the tail vein.

In vivo imaging

For imaging using the IVIS optical imaging system (PerkinElmer), mice were anesthetized using 4% isoflurane in a gas chamber and kept under 4% isoflurane on a heat pad during imaging.

2.5 STATISTICAL ANALYSIS

For the analysis of data, Graphpad (Prism) was used to calculate statistics. At least 3 independent experiments were represented for each experiment and represented as mean plus or minus standard error (SEM). Two tailed, Student's t-test or one way ANOVA was used for estimation to the non-treated condition (NT) unless otherwise indicated: * $p < 0.01$, ** $p < 0.001$, *** $p < 0.0001$.

Chapter 3: Characterization of the SPION stimulated macrophage response

SECTION 3.1: SYNTHESIS OF SUPER-PARAMAGNETIC IRON OXIDE NANOPARTICLES (SPIONS)

Previous work in our group used an iron oxide nanoparticle, called cross-linked iron oxide nanoparticle (CLIO)[209], to evaluate iron-loaded-nanoparticle effects on macrophage activation. However, CLIO production was discontinued, and the published synthesis protocol was difficult to reproduce, prompting a search for alternative nanoparticle sources. In cooperation with a chemistry research group, we developed SPIONs that were customized for our experimental purposes. The design, construction, and synthesis of the SPIONs was done exclusively by Tobias Bauer, a doctoral student in the research group of Matthias Barz and built on a protocol previously developed by this research group[232]. This section contains a brief description of the particle synthesis (Figure 3.1).

The SPION is coated in a composition of polysacrosine-*block*-poly-(S-ethylsulfonyl-L-cysteine) (pSar-*b*-pCys(SO$_2$Et) polymers, which hold specific properties that enable steric shielding and cross-linking in downstream applications (Figure 3.1A). The construction of SPIONs involves a co-self-assembly process (Figure 3.1B): ɣ-maghemite iron oxide nanoparticles (Fe$_2$O$_3$) were solubilized in (pSar-*b*-pCys(SO$_2$Et) polymers and then cross-linked with lipoic acid. The cross-linking done by lipoic acid establishes a bridge between nanoparticle and polymer, resulting in a stable encapsulation of the iron nanoparticles. To enable tracking of SPIONs, a Cy5-NHS ester was attached to the polymers. Empty nanoparticles lacking the iron core, called cross-linked polymeric micelles (CCPMs), were prepared to serve as a control using (pSar-*b*-pCys(SO$_2$Et) polymers in a synthesis procedure previously published[232]. The chemical and morphological characterization of SPIONs presented spherical structures with a hydrodynamic diameter (Dh) of 82 nm. SPIONs remained intact after being challenged with human plasma and 10 μM glutathione, indicating strong colloidal stability in biological solutions. The synthesis of SPIONs, along with a brief characterization of SPION-triggered macrophage activation has been published[233]. SPIONs and CCPMs were used for all experiments in this study, and experiments conducted in cultured cells and in mice were done by me.
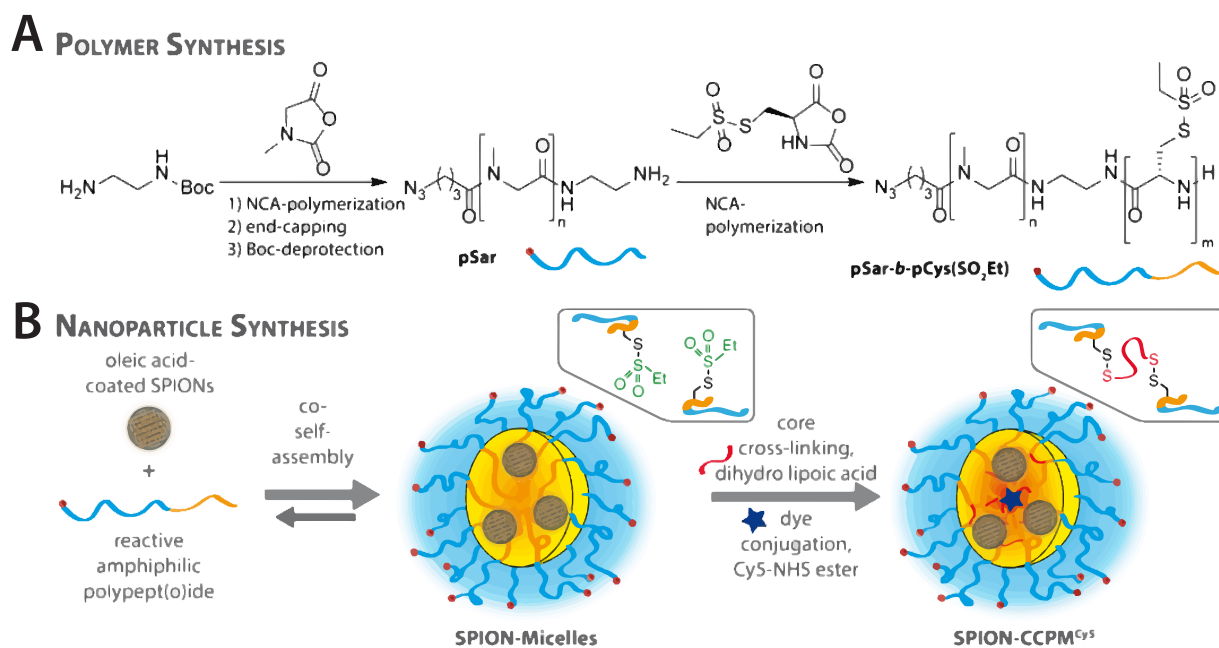
Figure 3.1. Synthesis of polymers and SPIONs. A. Schematic of chemical process used to construct polypept(o)ide polymers[232]. **B**. Illustrated synthesis of nanoparticles with polypept(o)ide polymers. ***Figure adapted from published manuscript: Bauer, T. A. et al. Core Cross-Linked Polymeric Micelles for Specific Iron Delivery: Inducing Sterile Inflammation in Macrophages. Adv Healthc Mater 2100385 (2021) doi:10.1002/adhm.202100385.*

SECTION 3.2: SPIONS AND CCPMS ARE TAKEN UP BY MACROPHAGES

To characterize the biological response to nanoparticle (NP) treatment in cultured cells, the levels of up-take by macrophages and the impact on macrophage activation were both evaluated. The uptake of the iron-containing NP (SPIONs) or the control NP (CCPMs) was tested on primary murine bone marrow-derived macrophages (BMDMs) with different concentrations of SPIONs or CCPMs after 24 h of treatment. The amount of SPIONs added to cells was calculated based on the concentration of iron contained in the core. A range of 1, 4, 20 and 100 µM iron was used, which was derived from previously published work[74]. The amount of control NP added to cells was calculated to match the mass of shell in SPIONs at each concentration. Since a Cy5-NHS ester was integrated into the NP, quantification of up-take and cellular distribution was done by detecting fluorescence signal. Internalization of NP was measured by intracellular fluorescent intensity using flow cytometry. At concentrations of 1 and 100 µM, NP were taken up by a similar number of macrophages (Figure 3.2A, left), indicating a threshold of minimal and maximal NP incorporation at the lower and higher concentrations. At 4 and 20 µM, a higher number of cells with SPION fluorescence signal above background compared to cells treated with CCPMs. Moreover, the fluorescence intensity per cell was also higher in SPION treated cells compared to CCPM treated cells at the 20 and 100 µM concentrations (Figure 3.2A, right). To rule out the possibility that NP were bound to the extracellular surface of BMDMs and therefore not internalized, confocal fluorescence microscopy was used to visualize NP distribution after 24 h of incubation. Fluorescent signal pertaining to NP was observed primarily within the cytosol of treated cells and did not accumulate at the periphery of cells, which was determined by staining for the cell surface marker Iba1 (Figure 3.2B). Quantification of fluorescence intensity within each cell correlated with results obtained by flow cytometry (Figure 3C). At all concentrations, cell morphology of macrophages did not change by the treatment with NP. Additionally, flow cytometry-based analysis using the 7AAD viability dye indicated that neither NP had significant effects on cell viability (Figure 3.2D).
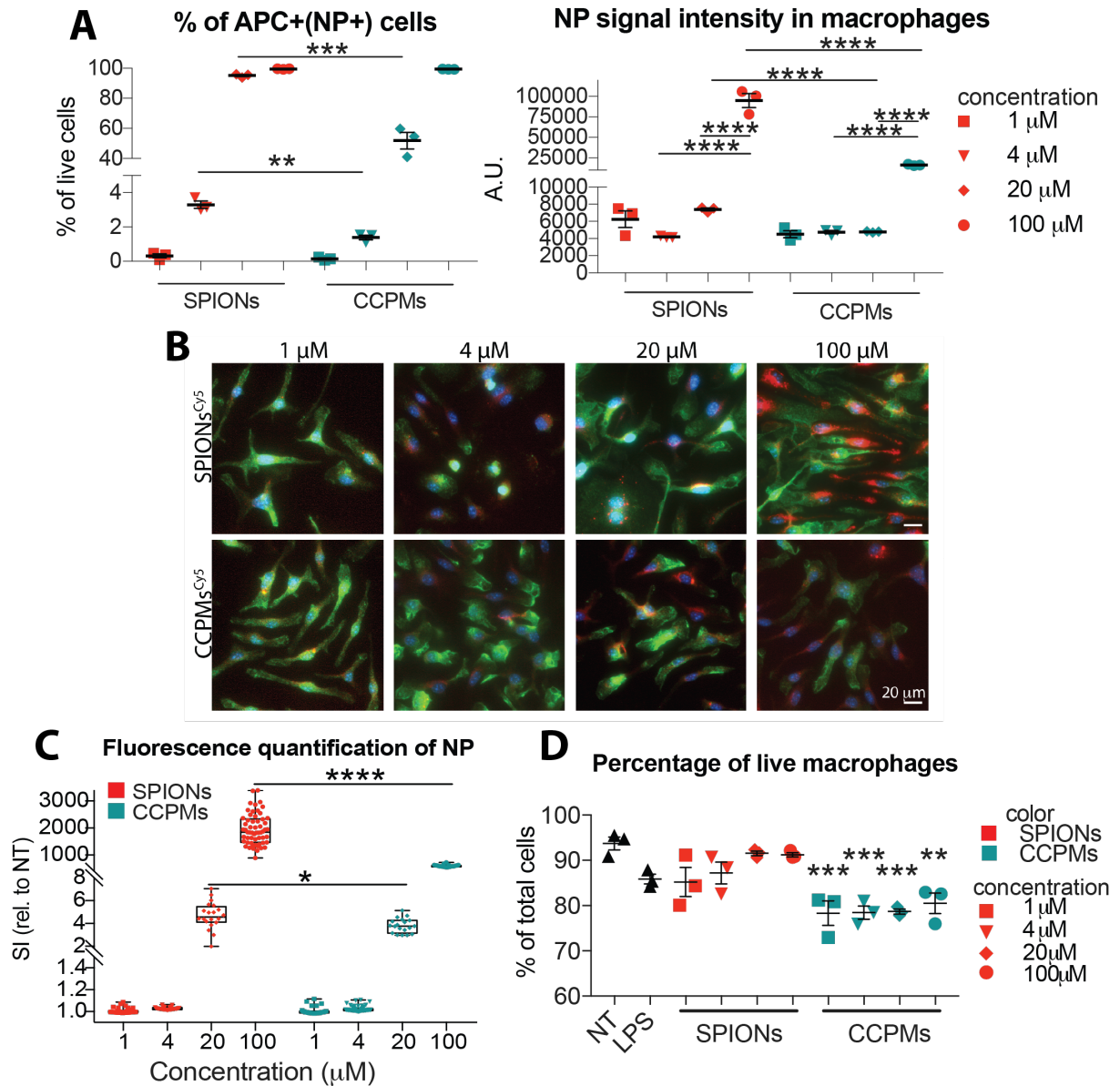
Figure 3.2. Evaluation of SPIONs and CCPMs treatment on macrophages. **A-D**. BMDMs were treated with SPIONs, CCPMs in increasing concentrations, LPS or not for 24 h and evaluated for nanoparticle (NP) uptake, and viability by flow cytometry (**A** and **D**) or microscopy (**B** and **C**). **A**. Percentage of NP+ cells and NP signal intensity in BMDMs. **B**. Distribution of NP in BMDMs and quantification (**C**). **D**. Percentage of total live BMDMs after treatments. Data reported as n ± Standard Error of the Mean (SEM) and representative of 3 independent experiments. One-way ANOVA to not treated condition (NT) unless otherwise indicated: * p < 0.01, ** p < 0.001, *** p < 0.0001.

Since previous data indicate that iron treatments can induce an inflammatory activation of macrophages[73,74,189], the inflammatory response in macrophages after NP treatment was evaluated. As a control, lipopolysaccharide (LPS) was used as it is a component of bacterial cell walls that stimulates a strong and well-characterized inflammatory response in macrophages[234–236]. Macrophages engaged in this programming produce high levels of CD86, CD80 and MHCII cell surface proteins as well as inflammatory cytokines[19,237]. By contrast, anti-inflammatory macrophages can be categorized by the presence of the cell surface protein CD206 as well as the production of IL4 and IL10 cytokines. CD206 surface expression was neither induced by treatment with NP or in our LPS-treated control (Figure 3.3A). However, CD86 surface expression was increased in cells treated with 20 and 100 µM SPIONs at a magnitude comparable to LPS treated cells (Figure 3.3B). When comparing the prevalence of CD86 expression to the intensity of SPION treated BMDMs, CD86 expression increased in a dose-responsive manner with respect to SPION concentration up to 100 µM (Figure 3.3C). Importantly, CCPMs did not stimulate either CD206 or CD86, indicating an inert control (Figure 3.2A and B). Overall, both NP are internalized in BMDMs, and that SPIONs trigger an inflammatory response, whereas CCPMs do not, suggesting that the iron core is a determinant factor in macrophage simulation.
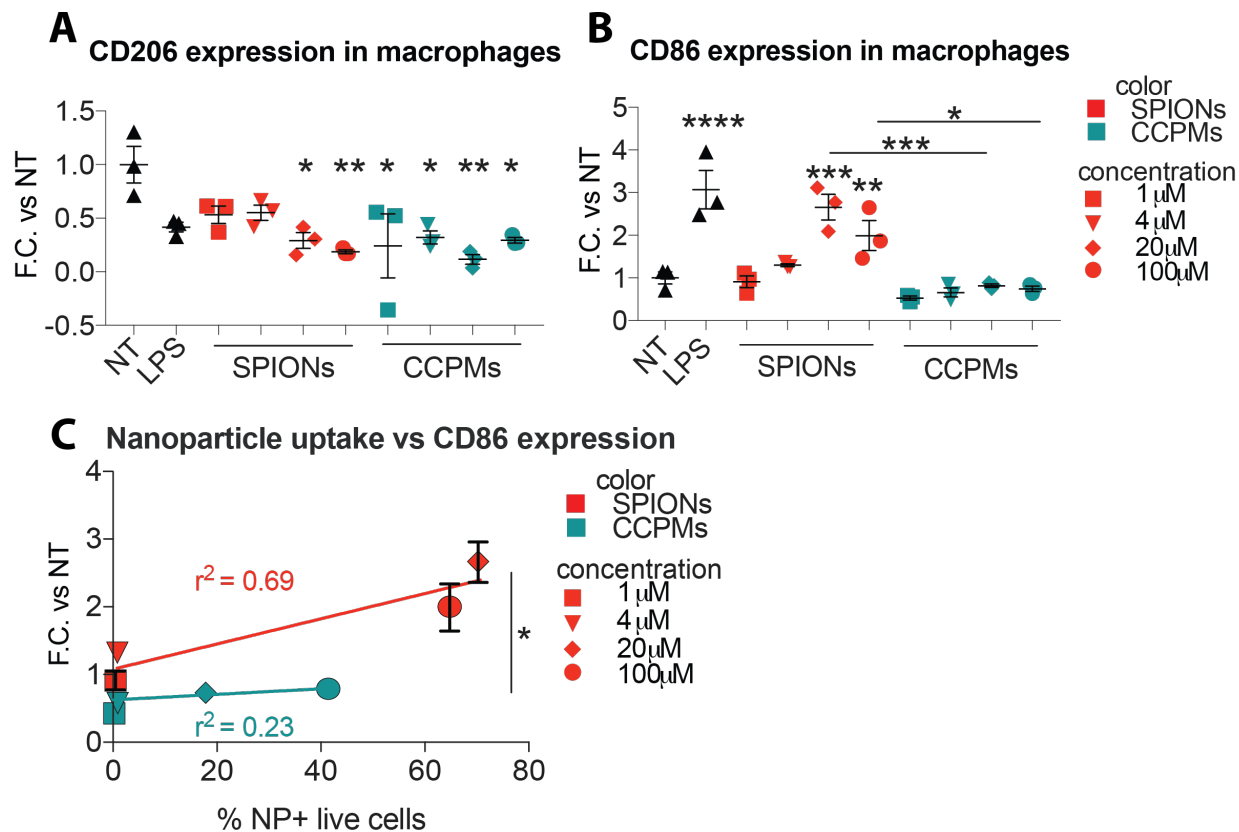
Figure 3.3. Stimulation of macrophages by SPIONs and CCPMs. CD206 levels (**A**), CD86 levels (**B**) and CD86 levels in comparison to NP uptake (**C**) measured by flow cytometry in BMDMs after 24 h of treatment. Data reported as n ± Standard Error of the Mean (SEM) and representative of 3 independent experiments. One-way ANOVA to not treated condition (NT) unless otherwise indicated: * $p < 0.01$, ** $p < 0.001$, *** $p < 0.0001$.

Since the aim was to specifically target macrophages with iron sources, the ability of non-macrophage cells to internalize the NP was addressed by comparing SPION and CCPM uptake in different cell types to BMDMs. Primary mouse hepatocytes were chosen due to their specialized role in iron and drug metabolism in the body[66,238,239]. As a cancer cell model, we used Lewis Lung carcinoma cells (LLC), an epithelial cancer cell line previously used to test iron NP[189]. Since 20 µM SPIONs was as effective as 100 µM in stimulating pro-inflammatory programming in macrophages (Figure 3.3B), for subsequent experiments, 20 µM was used as the standard working concentration to decrease the chances of off-target effects that may result from higher concentrations. Each cell type was treated with NP, and fluorescence microscopy was used to initially evaluate the cellular uptake and distribution of NP. In primary murine hepatocytes, there was little fluorescent signal, indicating little to no uptake of SPIONs or CCPMs (Figure 3.4A). Consistent with results in Figure 3.2, uptake of NP in BMDM cells showed more SPIONs internalized than CCPMs. In LLC cells, we observed intense CCPM fluorescence signal and dim SPION fluorescence signal in treated cells (Figure 3.4A). In all cells positive for NP fluorescence signal, signal was within the cytoplasm and not at the cell periphery.

To determine the level of NP uptake in the different cell lines, flow cytometry was used to quantitatively evaluate cell-associated NP fluorescence signal. Consistent with microscopy results, LLC cells internalized CCPMs 26.8X more than SPIONs. Since LLC cells are a *Kras* mutation-driven murine lung adenocarcinoma cell line isolated from C57Bl/6 mice[240,241], another murine *Kras* mutation-driven cell line, B16 cells, were evaluated, a melanoma immortalized cell line derived from C57Bl/6 mice that have comparable growth and metastatic qualities as LLC cells[242]. The uptake of NP in this cell line was similar to NP uptake in LLC cells in that CCPMs were internalized more than SPIONs (Figure 3.4B). To address whether this phenotype was conserved in human cells, NP uptake was quantitatively tested in different human cells (Figure 3.4B). Since kidney cells are a site of drug metabolism in the body, immortalized human embryonic kidney (HEK) 293 cells were chosen as a representative model[239]. H838 cells, a human non-small cell lung cancer (NSCLC) cell line, were chosen as a model to parallel LLC cells. To compare to BMDMs, human macrophages differentiated from patient buffy coat (peripheral blood mononuclear cells) samples were used. In HEK293 cells, a similar pattern of NP uptake was observed as in LLC and B16 cells. In contrast, H838 cells showed very little fluorescence uptake for either NP. Interestingly, in buffy coat-derived macrophages, CCPMs were taken up more than SPIONs. This may be due to infiltration of

other non-macrophage-like cells within culture, as the differentiation protocol of PBMCs does not filter out non-macrophage cell types prior to culturing. Importantly, SPIONs were taken up to a larger extent in buffy coat macrophages than in either HEK293 or H838 cells. Apart from the SPION treated buffy coat-derived macrophages, all other cells were unaffected by NP treatment when compared to their respective NT condition (Figure 3.4B, left). In buffy coat macrophages, despite a decrease in viability in control conditions, there was no significant change observed between the SPION, CCPM or untreated cultures. These results suggest that SPIONS do not elicit harmful effects on cells and are taken up more by macrophage cells compared to other human or mouse non-macrophage cells. This points to a promising path of macrophage-specific targeting.
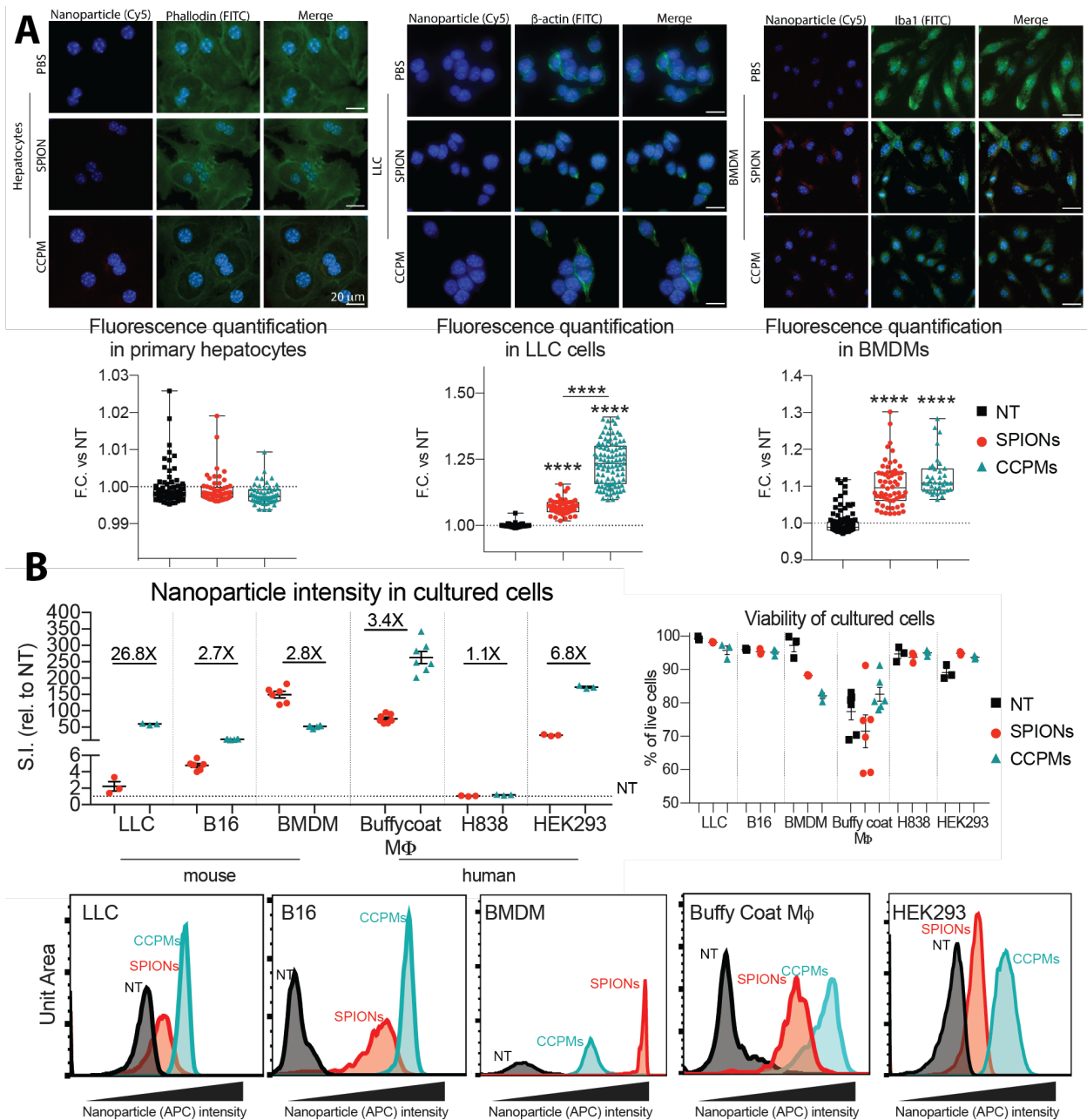
Figure 3.4. SPION and CCPM uptake in other cell types. A and **B**. Cells were treated with SPIONs, CCPMs or not for 24 h and evaluated by microscopy (**A**) or flow cytometry (**B**). **A**. Hepatocytes and LLC cells were stained with phallodin-FITC or β-actin-FITC, respectively. BMDMs were stained with Iba1-FITC. Quantification of NP signal intensity inside cells is shown below. **B**. Flow cytometry detection of NP signal intensity in LLC, B16, BMDM, buffy coat macrophages, H838 and HEK293 cultured cells. Representative flow cytometry fluorescent intensity plots are shown below. Viability of cultured cells was determined by quantification of % of 7-AAD negative cells. Data reported as n ± Standard Error of the Mean (SEM). One-way ANOVA in comparison to not treated (NT) condition unless otherwise indicated: * p < 0.01, ** p < 0.001, *** p < 0.0001.

Although significant changes were not observed in total macrophage cell numbers at 24 h post-NP treatment in Figure 3.2, macrophage viability could still be affected over a longer time course. To verify that cell viability is not affected in macrophages, four parallel methods were used, each elucidating a different aspect of cell death to gain a comprehensive view of cell viability following NP treatment. In general, cell death is either characterized by necrosis, an unregulated form of cell death due to an external insult, or apoptosis, a regulated signaling program of intracellular breakdown. In both scenarios, the cell membrane becomes permeable, cytoplasmic contents are released and metabolic enzymes like lactate dehydrogenase (LDH) accumulate in the surrounding media[243]. Cell membrane permeability can be measured in a variety of methods, one of which is by detecting the internalization of dye, such as 7AAD, while another is by the release of LDH from permeabilized cells, both of which are commonly used as convenient readouts for cell viability. Since evaluation by 7AAD internalization using flow cytometry had been done (Figure 3.2 and 3.4), the focus here will be on quantifying LDH release in treated BMDMs. Iron sources, such as ferric ammonium citrate (FAC) or iron dextran, were included as positive iron controls. To test cell viability in our system, BMDMs were incubated with iron controls, SPIONs or CCPMs, and LDH levels in the supernatant were quantified over a 72 h time course. Starting from 24 h, untreated BMDMs or BMDMs treated with CCPMs showed a decrease in viability compared to SPIONs and iron treated cells, and this trend continued up to 72 h post-treatment (Figure 3.5A). Next, these results were compared to 2 other common methods for studying cell viability; the measurement of cellular ATP levels to evaluate cellular energy levels, as well as cytosolic redox enzyme activity. Both methods require intact cells for measurement and are therefore an indication of intracellular cell death programming associated with apoptosis. Both methods found a similar trend as for LDH measurements (Figure 3.5B and C). BMDMs treated with SPIONs showed increased ATP levels in cell lysates and increased cytosolic redox activity in intact cells starting from 24 h. This trend with macrophages was not observed treated with CCPMs or iron in either assay.

Given that cytosolic redox activity increased in SPION treated BMDMs over time, a change in redox enzyme activity could be correlated to an increase in ROS levels upon SPION treatment in BMDMs. The generation of reactive oxygen species (ROS) was measured in untreated BMDMs, or BMDMs treated with SPIONs, CCPMs or iron dextran over time. Iron dextran was chosen as the iron control because of the similar increase of redox enzyme activity to SPION treated BMDMs over time observed in Figure 3.5C. CellROX green and CellROX orange are probes that locate to either the nuclear/mitochondrial or cytosolic areas in the cell,

respectively. Once applied to treated BMDMs, the probes release fluorescence signal upon oxidization by ROS species, which can then be quantified by subsequent flow cytometry measurement. After 18 h of SPION or CCPM treatment but not iron dextran treatment, increased ROS activity was observed in the cytoplasmic compartment of BMDMs (Figure 3.4D). At the 36 h time point, nuclear and mitochondrial ROS was increased in SPION and iron dextran treated BMDMs. Importantly, CCPMs did not increase nuclear or mitochondrial ROS levels in BMDMs, suggesting that iron triggers a specific response to ROS (Figure 3.4D). Previous studies have shown that the release of detectable iron into the intracellular compartment of BMDMs stimulates an increase in ROS production[244,245]. Given that an increase in ROS was observed, iron accumulation was addressed in BMDMs with the use of the histological stain Perls' Prussian Blue on BMDMs. FAC was used as our iron control because visualization of iron by Perls' Prussian blue occurs rapidly in BMDMs upon treatment with FAC. Iron accumulation in BMDMs treated with SPIONs occurred starting at the 24 h time point (Figure 3.5E), similar to levels of FAC treated BMDMs, indicating that iron released from SPIONs is stored within the cell. The shift in ROS detected first at cytosolic then at nuclear/mitochondrial areas illustrates the timing of SPIONs internalization and iron release into the intracellular areas (high cytosolic ROS) where it is stored (Perls' Prussian blue stain) as well as utilized for cellular processes (nuclear/mitochondrial ROS).

Since iron accumulation in BMDMs occurred when treated with SPIONs, the degradation of SPIONs in BMDMs could then correlate with a decrease in NP intensity in BMDMs. This was evaluated by flow cytometry where NP were taken up by almost all macrophages in culture treated with either SPIONs or CCPMs after 24 h of incubation and continued until 72 h (Figure 3.5F). The intensity of NP-treated BMDMs showed a sudden increase in SPION intensity at 24 h and then decreased at 48 h and 72 h. The spike in SPION intensity at 24 h correlates with the observations of iron accumulation (Figure 3.5E) and ROS increase (Figure 3.5D) that starts at 24 h. The evaluation of the total number of living to dead cells over time was done by flow cytometry using 7AAD. Heme was used as an iron control due to its potent cytotoxicity on BMDMs[20]. At 24 h, live-cell counts for BMDMs treated with SPIONs and CCPMs were comparable to non-treated cells (Figure 3.5F). At 48 h and 72 h, while SPION treated macrophages remained at ~80% viability, CCPM treated cells decrease in cell viability at the same rate as the non-treated (~30% reduction compared to SPION treated BMDMs). In contrast, heme reduces the macrophage live cell count in culture by 40% at the 24 h timepoint.

The increase in fluorescence intensity over time in CCPM treated BMDMs by flow cytometry (Figure 3.5F) suggests that CCPMs, the shell of SPIONs, are stable in solution. After 24 h of incubation, there was an increased SPION signal in SPION treated BMDMs at the same time as increases in cell viability by flow cytometry count, as well as LDH levels, redox enzyme activity, ROS, and iron accumulation. Sustained viability of SPION treated BMDMs at 48 h, and 72 h was observed in all four methods of live cell measurement, indicating that a sustained iron release profile of SPIONs which correlates to prolonging the lifespan of macrophages in culture. Overall, the accumulation and the slow degradation of SPIONs in BMDMs could be because of a slow release of iron profile from SPIONs that would then sustain BMDM viability in culture and suggests a stable composition of SPIONs in biological solutions.

A BMDM LDH release

B BMDM ATP levels

C BMDM redox enzyme activity

E Perls' Prussian Blue and Nucelar Fast Red

6 h

15 h

24 h

NT   FAC   SPIONs   CCPMs

20 μM

D Nuclear/mitochondrial ROS

Cytosolic ROS

F NP+ BMDMs

NP intensity in live BMDMs

Live BMDMs overtime

68
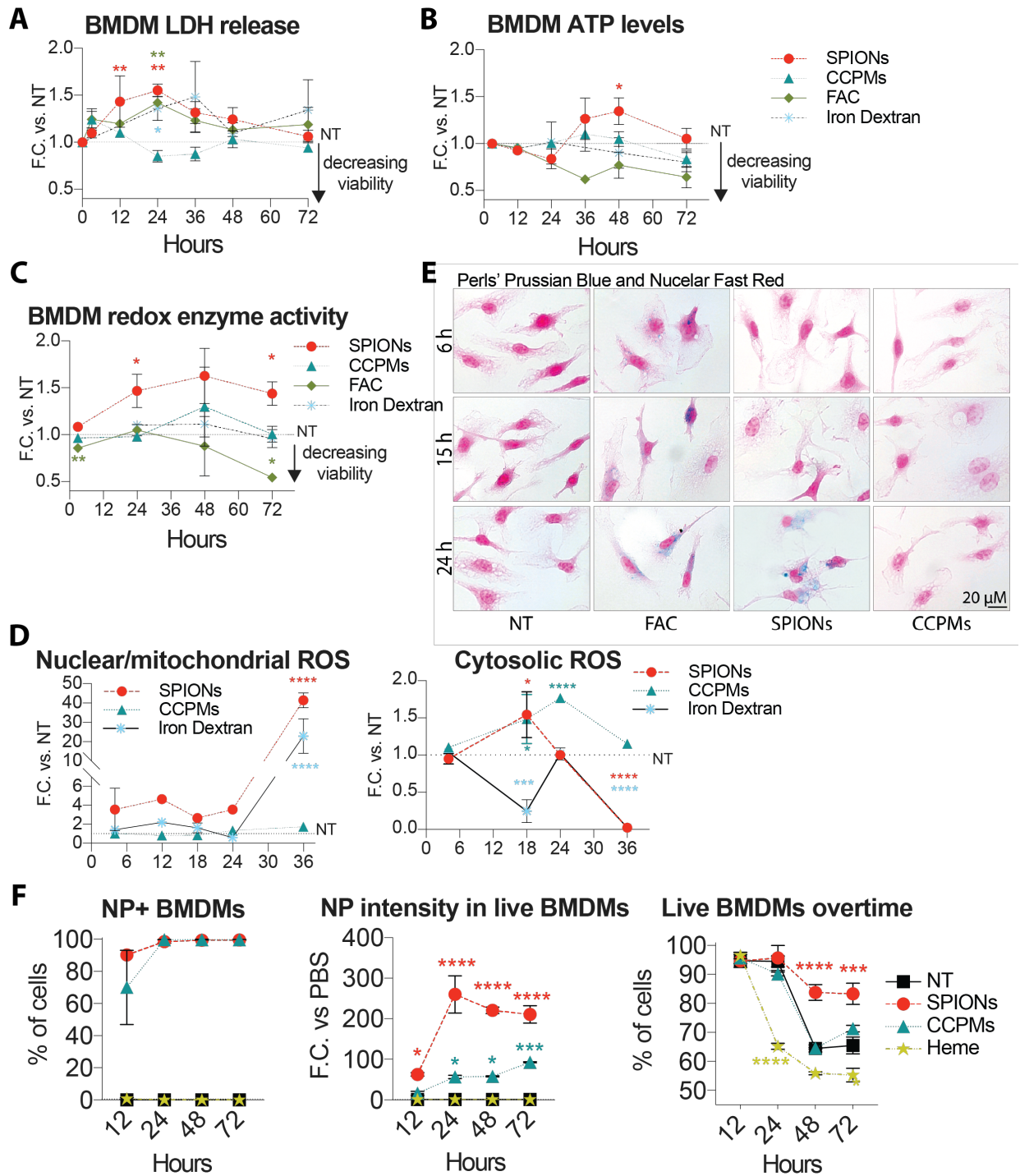
Figure 3.5. SPIONs are degraded slowly, releasing iron and activating macrophages. A-F. BMDMs were treated with SPIONS, CCPMs, iron dextran, FAC or heme for up to 72 h. LDH release (**A**), ATP levels in cell lysates (**B**) or redox enzyme activity (**C**) in BMDMs over time. **D**. Measurement of ROS production in BMDMs by flow cytometry. **E**. BMDMs were fixed and stained with Perls' Prussian Blue and Nuclear Fast Red. **F**. NP uptake and BMDM viability was measured by flow cytometry over time. Data reported as n ± Standard Error of the Mean (SEM) and representative of 3 independent experiments. One-way ANOVA in comparison to the non-treated (NT) condition: * $p < 0.01$, ** $p < 0.001$, *** $p < 0.0001$.

To understand whether iron is released from SPIONs, and is metabolically active in macrophages, the expression of inflammatory response proteins, enzymes, and transcription factors as well as, iron regulatory genes, were analyzed (Figure 3.6). BMDMs were treated with classical macrophage polarizing stimuli, inducing either the pro-inflammatory (100 ng/ml LPS) or anti-inflammatory (100 ng/ml interleukin-4 (IL4)) phenotype. In addition, BMDMs were treated with SPIONs, CCPMs and 20 µM of an iron source control (FAC or iron dextran or heme) for 6 h (Figure 3.6A) or 24 h (Figure 3.6B and C).

Inflammatory stimulation in BMDMs induces the expression of specific cytokines, including interleukin (il)-1α/β (Il1*B*), Il6, and tumor necrosis factor (TNF), enzymes such as inducible nitric oxide synthase (iNOS), as well as an iron retention phenotype[1]. On the other hand, anti-inflammatory macrophages do not accumulate iron and express *Ym1* mRNA, CD206, MerTK and CD163 cell surface proteins and enzymes such as arginase1 (ARG1). In SPION and LPS treated BMDMs at 6 h, an increase in *Nos2*, *Il1b*, *Il6*, *Cxcl10*, and *Tnf* mRNA transcripts (Figure 3.6A, blue, green, yellow panel) and decreased *Ym1* mRNA expression was observed (Figure 3.6A, red panel). At 24 h, BMDMs treated with SPIONs paralleled the inflammatory phenotype of LPS stimulated BMDMs by showing the expression of increased pro-inflammatory cell surface proteins, such as CD64, MHCII, CD172a, CD80, CD38, CD301, CD86, and decreased CD206 levels (Figure 3.6B). Conversely, CCPMs treated BMDMs expressed only *Slc7a11, Fth,* and *Cxcl10* mRNA transcripts and MHCII surface protein (Figure 3.6A, green panel and B), suggesting that iron released from SPIONs, and not the shell, stimulates the robust induction of inflammatory cytokine and surface marker expression in BMDMs. However, iron treatment on BMDMs resulted in the expression of inflammatory cytokines and surface markers that only partially paralleled SPION treatment on BMDMs (Figure 3.6A, blue, green, and yellow panel; Figure 3.6B, CD86 and MHCII). The differences observed between SPION treatment and iron treatment could be attributed to differences in uptake pathways of iron. Taken together, the expression profile of mRNA transcripts and surface proteins upon SPION treatment in BMDMs suggests that SPIONs induce an LPS-like pro-inflammatory phenotype in BMDMs.

LPS induced inflammatory activation in macrophages is accomplished through a well-characterized signaling pathway[234,246]. The expression of known LPS triggered transcription factors in SPION treated BMDMs was then analyzed. Increased expression of the transcription factors suppressor of cytokine signaling 3 (*Socs3*), hypoxia-inducible factor-1 alpha (*Hif1α*) and *Spi-C* was observed in both SPION treated and LPS treated cells (Figure 3.6A, green,

yellow, and red panel). Only LPS treated BMDMs expressed transcription factors signal transducer and activator of transcription 1 (*Stat1*), interferon regulatory factor 5 (*Irf5*), and the enzyme Arginase-1 (*Arg1*) (Figure 3.6A, red and yellow panel). Therefore, inflammatory stimulation in BMDMs by SPIONs followed partial LPS inflammatory signaling patterns.

Cells respond to an influx of iron by initiating protective mechanisms to reduce oxidative damage from freely available iron, leading to oxidative response signaling, iron export and iron sequestration[57]. Iron export from the cell is mainly mediated by the iron exporter protein ferroportin-1 (Fpn1)[247]. Oxidative stress targets the activation of the nuclear factor erythroid 2-like related factor-2 (Nrf2) and the CNC homolog 1 basic leucine zipper (bZIP) transcription factor 1 (Bach1) signaling pathway[248–250]. These responses are very well characterized in BMDMs treated with heme[251] (Figure 3.6A, yellow and red panel). Cells increased Fpn1 levels (*Ireg1* mRNA) upon SPION treatment (Figure 3.6A, red panel) and increased in the expression of Nrf2 target genes *Gstm1, Gclc, Nqo1, Gpx4, Slc7a11* and *Ho1* (Figure 3.6, red and green panel). Like with heme treatment, an iron sequestration phenotype was observed upon SPION treatment in BMDMs as expression of iron acquisition genes decreased, and iron storage genes increased (decreased *Tfrc* and *Cd163* mRNA expression (Figure 3.6, red panel); increased *FtH, FtL and Lcn2* (Figure 3.6A, green, yellow, and red panel) at 6 h; decreased TFR1 protein (Figure 3.6B) at 24 h). This iron sequestration phenotype was also observed in BMDMs treated with LPS providing further evidence supporting the LPS-like inflammatory phenotype that is induced in BMDMs upon SPIONs treatment.

Importantly, the inflammatory response to SPIONs was not restricted to mouse BMDMs as similar observations of mRNA transcripts, and protein levels were found in human buffy-coat macrophages (Figure 3.6C).

Taken together, SPIONs are observed to induce pro-inflammatory activation in BMDMs that follows a combination of iron and LPS-like inflammatory patterns, which are found both in the murine and human system.
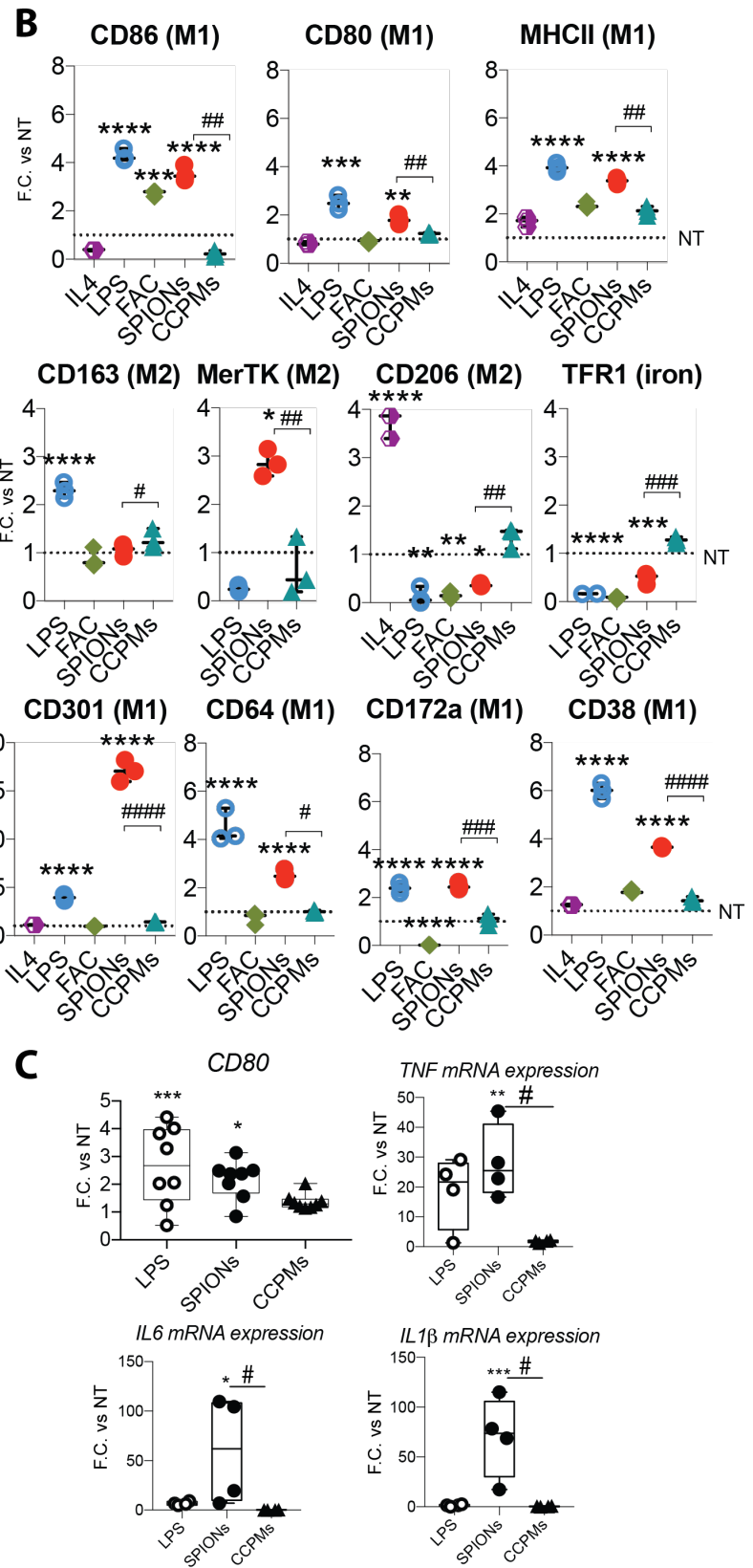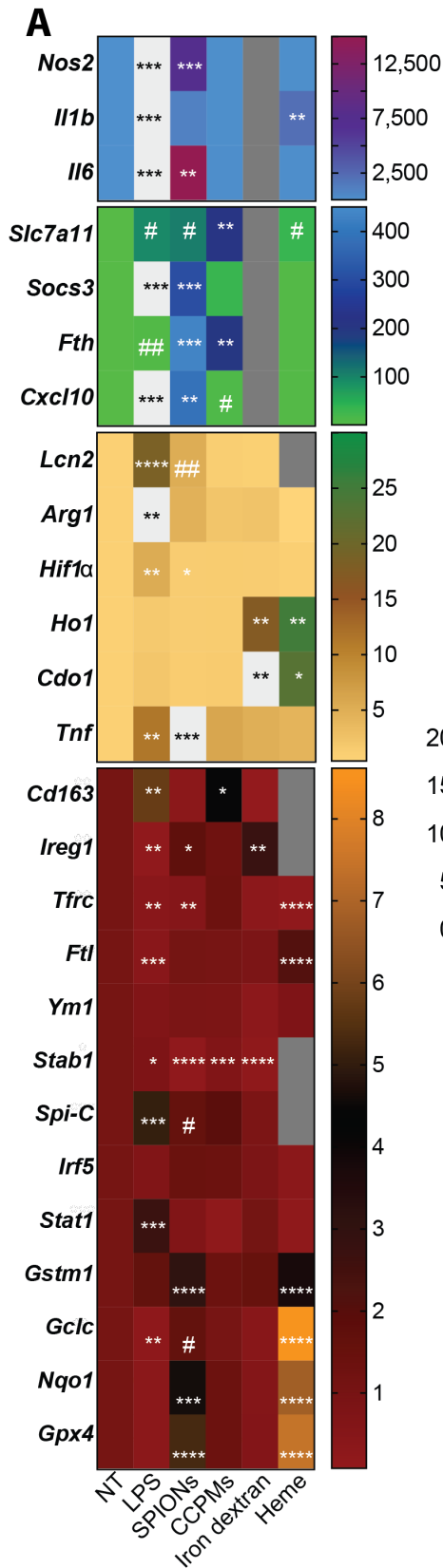
Figure 3.6. SPIONs activate inflammation in BMDMs. A, **B**. BMDMs were treated with SPIONs, CCPMs, LPS, IL4, iron dextran, FAC or heme for 6 h (**A**) or 24 h (**B**). All values are represented as fold change vs the non-treated condition (F.C. vs NT) **A**. Expression of mRNA transcripts in BMDMs; genes listed are in order of expression from highest relative expression to lowest: blue, green, yellow, red; grey indicates no value; white indicates off-scale value. Scale (right) indicates relative expression levels. **B**. Cell surface marker detection in BMDMs by flow cytometry. **C**. Measurement of the inflammatory protein CD80 and inflammatory cytokine mRNA expression in human buffy coat macrophages after 24 h of SPIONs, CCPMs, or LPS treatment. Data reported as n ± Standard Error of the Mean (SEM) and representative of 3 independent experiments. One-way ANOVA (*) in comparison to the non-treated (NT), or students' t-test (#) as indicated: * $p < 0.01$, ** $p < 0.001$, *** $p < 0.0001$.

SECTION 3.6: INFLAMMATORY RESPONSE IN SPION-LOADED MACROPHAGES IS TRIGGERED BY TLR4 SIGNALING AND IRON

Since stimulation by SPION and not CCPMs triggered an inflammatory phenotype in BMDMs (Figure 3.6), next the testing of whether the sequestration of iron by an iron chelator would reverse SPION mediated inflammation in BMDMs was addressed. Deferiprone (DFI) is an intracellular iron chelator[252] and was used to treat BMDMs in combination with SPIONs, CCPMs or LPS for 24 h. Cells were then analyzed by flow cytometry for NP uptake, and cell surface protein levels indicative of different stages of inflammation were examined. CD86, a receptor protein that initiates an adaptive immune response, was used as an indicator of early inflammatory phase activation in macrophages. MerTK is a tyrosine receptor kinase involved in the movement of lamellipodia, a mechanism necessary for phagocytosis, and has been implicated in the resolution phase of inflammation[253]. CD172a was used as an indicator of immune surveillance activity as it is an inhibitory receptor that serves as the "self" recognition receptor in the body. Its co-receptor, CD47, is expressed by all cells, and the lack of CD47 on cells, and therefore the absence of binding to CD172a, signals for phagocytic removal by macrophages[254,255]. In cells co-treated with NP and DFI, the intensity of SPION fluorescent signal in BMDMs was reduced by ~2-fold, whereas there was little to no change in the uptake of CCPMs (Figure 3.7A), suggesting that the degradation of SPIONs and release of iron is partially dependent on NP uptake. The levels of CD86 and MerTK were reduced in SPION treated cells upon iron chelation, whereas there was no change observed in CCPM treated cells (Figure 3.7B), suggesting that the expression of early phase inflammatory proteins and resolution phase inflammatory proteins are partially stimulated by iron. Iron chelation on LPS stimulated BMDMs reduced only CD86 protein levels, suggesting that iron contributes to the early inflammatory phase response when initiated by LPS in BMDMs. Iron chelation in BMDMs treated with SPIONs, CCPMs or LPS did not affect CD172a protein levels, indicating that stimulation by iron is not involved in the upregulation of the CD172a receptor and likely does not contribute to the immune surveillance function in macrophages. These data suggest that iron released from SPIONs partially contributes to the activation of the pro-inflammatory phenotype in macrophages.

LPS stimulation of macrophages is dependent on the toll-like receptor (TLR)-4 protein, which then initiates specific downstream activation of inflammatory responses in macrophages[234]. Additionally, the heme-driven pro-inflammatory phenotype in macrophages was previously described as TLR4-dependent[256]. Since many similarities between the molecular expression profiles of BMDMs stimulated with SPIONs, heme, and LPS were

74

observed (Figure 3.6), blocking the TLR4 receptor pathway would therefore inhibit the SPION stimulated inflammatory macrophage response. CLI-095 (CLI), also known as TAK242, is a small molecule inhibitor that blocks the intracellular domain of TLR4 from binding to the adaptor molecules Toll/interleukin-1 receptor domain-containing adaptor protein (TIRAP) or Toll/interleukin-1 receptor domain-containing adaptor protein inducing interferon-β-related adaptor molecule (TRAM) necessary for downstream inflammatory activation[257,258]. Blocking this pathway reduced SPION uptake in BMDMs by ~2.2-fold but did not affect CCPMs uptake (Figure 3.7E), suggesting that the degradation and release of iron from SPIONs induce TLR4 signaling, which contributes to NP uptake. While BMDMs treated with LPS expressed high levels of CD86 and CD172a, CLI treatment blocked the upregulation of CD86 and CD172a in LPS treated BMDMs confirming the effectiveness of CLI inhibition. SPION treatment on BMDMs showed increased levels of CD86, CD172a and MerTK, whereas the addition of CLI reduced levels to a greater extent than iron chelation (Figure 3.7F, G, and H), suggesting that TLR4 signaling is a major signaling pathway involved in SPION induced macrophage inflammation. Like conditions of iron chelation with DFI, no change was observed in the expression of the cell surface proteins upon treatment of BMDMs with CCPMs and CLI. Given that chelating iron and blocking TLR4 signaling reduced SPION uptake in BMDMs, the combination treatment of CLI and DFI would result in a more pronounced inhibition of SPION uptake in BMDMs. Co-treating BMDMS with DFI and CLI and NP resulted in little to no change, suggesting that NP uptake is dependent on both or neither iron signaling and TLR4 signaling pathways. Furthermore, this suggests that an additional compensatory pathway contributes to the uptake of NP. These data suggest that NP uptake is partially dependent on both iron release from the core of SPIONs and TLR4 signaling and likely includes other mechanisms that contribute to NP uptake.
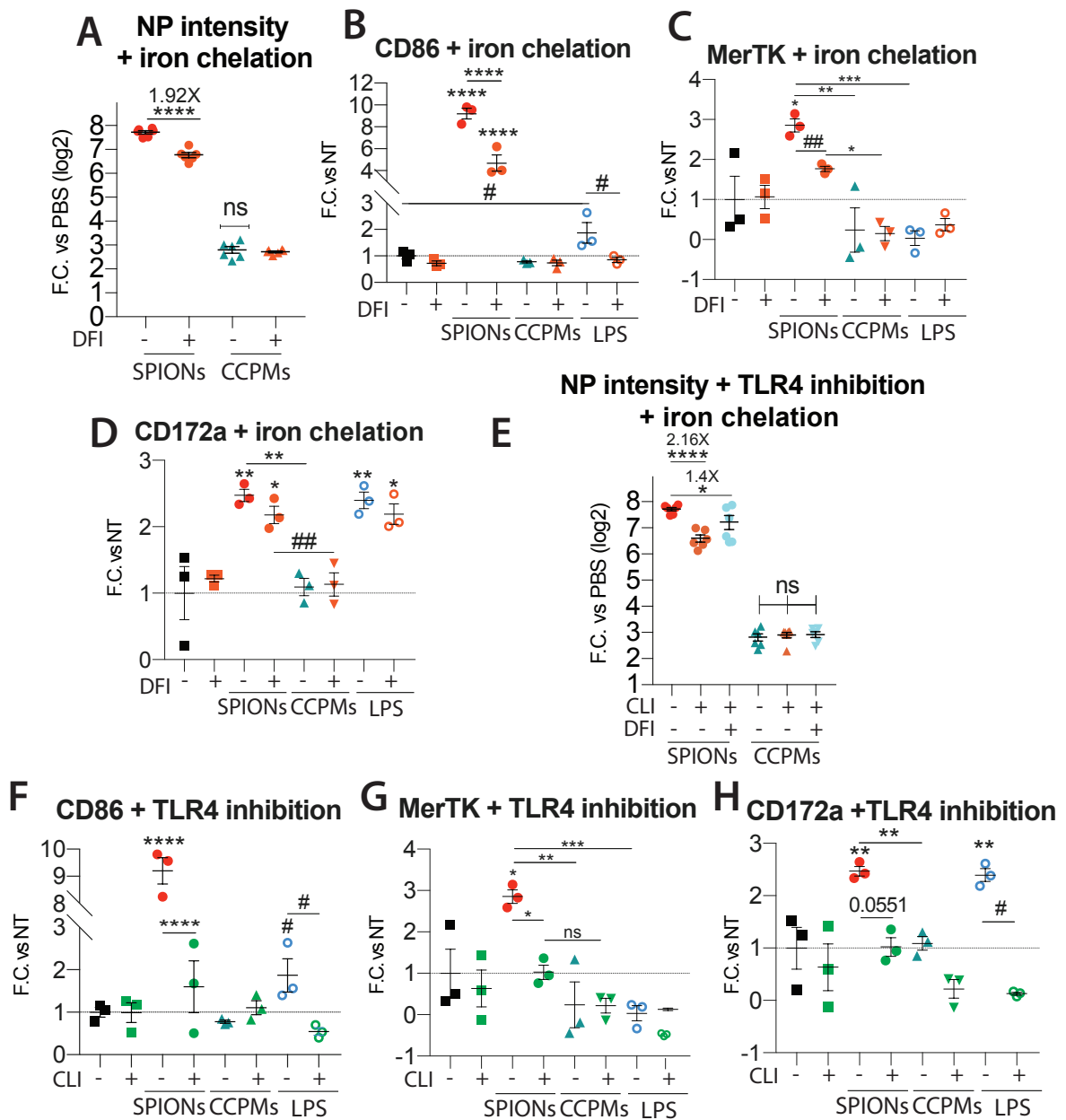
Figure 3.7. Iron released from SPIONs and TLR4 signaling mediates SPION stimulated macrophage inflammatory response. A-H. BMDMs were treated with SPIONs, CCPMs, LPS or left untreated for 24 h. NP uptake and cell surface proteins were evaluated by flow cytometry. **A-D**. BMDMs were treated with or without deferiprone. **E-G**. BMDMs were treated with or without CLI. Data reported as n ± Standard Error of the Mean (SEM) and representative of 3 independent experiments. One-way ANOVA (*) in comparison to the not treated (NT) condition unless otherwise indicated, students' t-test (#) comparison as indicated: * p < 0.01, ** p < 0.001, *** p < 0.0001.

SECTION 3.7: MACROPHAGE NP UPTAKE IS BY ACTIN-MEDIATED MECHANISMS

SPION uptake was affected upon both iron chelation and inhibition of TLR4-mediated signaling. Moreover, iron chelation, as well as TLR4 inhibition reduced the levels of MerTK and CD172a, cell surface proteins required for macrophage phagocytosis, in cells treated with SPIONs (Figure 3.7C and D). Therefore, inhibiting the assembly of cytoskeleton proteins required for phagocytosis would prevent SPION uptake in BMDMs. An actin polymerization inhibitor Cytochalasin D (CD) was used to block uptake in macrophages, which is a potent small molecule drug that disrupts cell motility, contraction and induces cell stiffness[259–262]. BMDMs were pre-treated for 1 h with CD, and then SPIONs or CCPMs were added for an additional 6 h or 18 h, where NP uptake was measured by flow cytometry. In the CCPM treated cells, NP uptake was reduced by half after 6 h and even further at 18 h, validating that CD inhibited phagocytosis (Figure 3.8A). Interestingly, after 6 h, SPION uptake increased by ~2-fold, suggesting that SPIONs may be internalized by a non-actin mediated mechanism. However, at 18 h, uptake of SPIONs by BMDMs treated with CD returned to normal levels, indicating that SPION treatment accelerates the degradation of CD. The extent of inflammatory activation was evaluated by the expression of *Tnf* mRNA as well as levels of CD86 protein by flow cytometry. There was no change in the expression of *Tnf* mRNA or the levels of CD86 upon CCPMs treatment in BMDMs with or without the treatment of CD (Figure 3.8B and C). CD treatment reduced *Tnf* mRNA expression, as well as levels of CD86 in SPION treated BMDMs, suggesting that SPION internalization was attenuated. CD treatment also reduced levels of the phagocytosis protein CD172a in BMDMs treated with SPIONs but not CCPMs at 6 h, further indicating that SPION internalization did not occur. The lack of inflammatory stimulation at 6 h in BMDMs treated with SPIONs and CD would suggest that SPIONs were not internalized. This could be explained by the preparation of macrophages for flow cytometry which did not include permeabilization and fixation steps. Therefore, the data suggest that the increase in SPION fluorescent signal in BMDMs upon CD treatment may be due to SPIONs immobilized at the cell membrane periphery. Taken together, macrophages are observed to phagocytose NP and that actin mediated mechanisms are involved in the SPION activation of BMDMs.
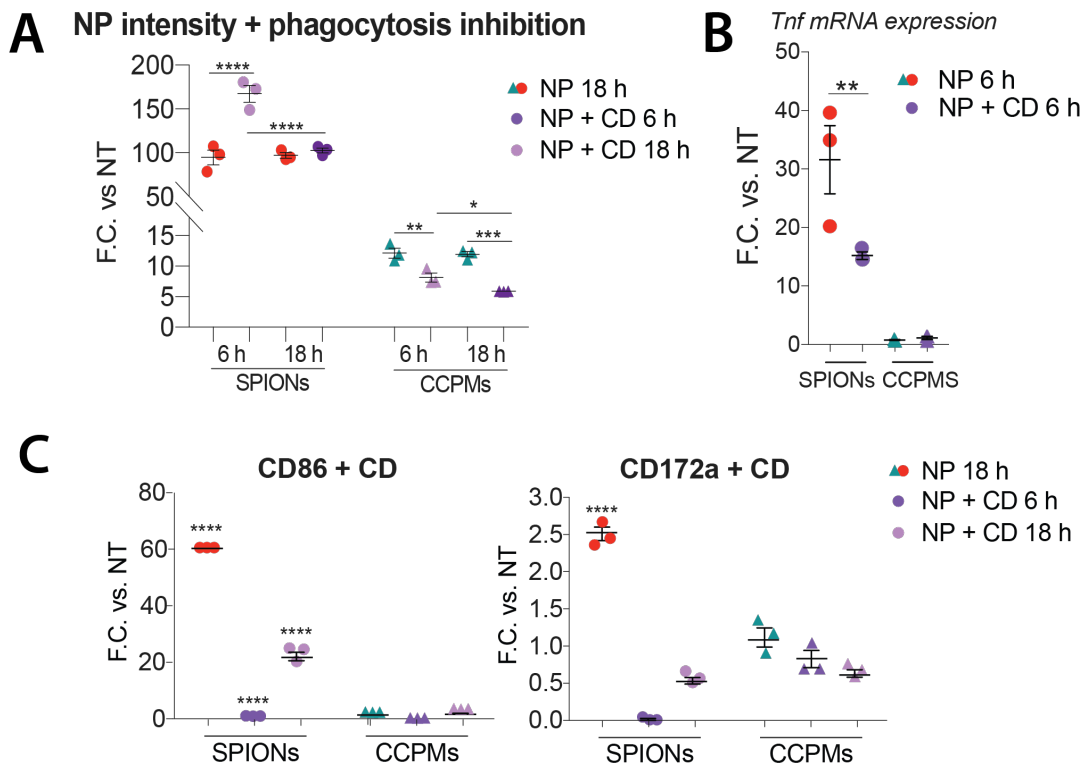
Figure 3.8. The SPION stimulated macrophage inflammatory response is phagocytosis dependent.
A-C. BMDMs were pretreated with Cytochalasin D (CD) for 1 h or not and then treated for 6 h or 18 h with SPIONs or CCPMs or left untreated. NP intensity and surface proteins were evaluated by flow cytometry. (**B**) *Tnf* mRNA transcript levels were measured after 6 h. Data reported as n ± Standard Error of the Mean (SEM) and representative of 3 independent experiments. One-way ANOVA (*) in comparison to the non-treated (NT) condition unless otherwise indicated: * $p < 0.01$, ** $p < 0.001$, *** $p < 0.0001$.

In cultured macrophages, maximal intensity of SPION uptake was observed at 24 h, which was sustained over the course of 72 h, leading to a strong inflammatory response in BMDMs. Building on cell culture analysis, whether a similar trend of iron release and inflammatory macrophage activation would occur *in vivo* was questioned. Intratracheally instillation of SPIONs into the lungs of C57Bl/6 mice was chosen as the route of administration as this organ provides the advantage of non-invasively administering SPIONs to a dense population of macrophages without adversely and directly affecting other organ systems. CCPMs were not included within this experiment as most phenotypic responses observed in macrophages treated with CCPMs were similar to non-treated macrophages, and the exclusion of this treatment group minimised the number of mice required. In 21 C57Bl/6N mice, administration of either SPIONs (10 mg/kg iron to body weight) or PBS was completed (Figure 3.9A). Mice were then sacrificed at 4, 24, 48 and 96 h post intratracheal instillation. At the first three-time points, the group distribution was n = 3 PBS vs. n = 2 SPION. At 96-h, the group distribution was n = 5 PBS vs. n = 4 SPION.

Uptake of SPIONs and inflammatory activation in pulmonary cell populations were evaluated by flow cytometry. At 4 h, immune cells had 5.8X more SPION signal intensity over background (Figure 3.9B). The greatest number of SPION+ immune (CD45+) cells was observed at 24 h and reduced only slightly over the next 48 h (Figure 3.9C). Within the population of CD45+ cells, SPIONs were predominantly found in innate immune cells. Within this population, innate immune cells other than macrophages were found to be positive for SPION signal and therefore were included in the analysis (Figure 3.9D). Interstitial macrophages (IM), as defined by the high levels of CD45+/CD11b+/Ly6C+/CD64+ cell surface markers, initially had the brightest SPION+ intensity at 4 h, whereas neutrophils, as defined by CD45+/CD11b+/Ly6G+, had the highest levels at 24 h. Other innate immune cells, such as eosinophils (CD45+/Siglecf+/CD11b+), were also positive for SPIONs at 24 h, albeit to a lesser extent. Dendritic cells had the brightest SPION intensity over background at 48 h. Expression of the inflammatory cytokines *Tnf*, *Il6*, and *Il1b* in lung tissue was increased at 24 h (Figure 3.9E), correlating with the detected increase in SPION uptake in cells (Figure 3.9C). Additionally, NRF2 target genes, such as *Ho-1*, *Nqo1* and *Slc7a11*, increased at 24 h followed by a second increase in expression at 96 h. These observations at 24 h parallel the characterization of the SPION induced inflammatory response in cultured macrophages (Figure 3.6).

Given that there was increased expression of inflammatory cytokines in the lungs next, the evaluation of whether this corresponded to inflammatory activation in cells within the lungs was addressed. To do so, inflammatory protein levels were evaluated on macrophages from the lungs of PBS, and SPION treated mice by flow cytometry. High levels of CD80 at 4 h and CD163 at 24 h, and reduced levels of MerTK at 4, 24 and 48 h were found on alveolar macrophages (AM) (defined by CD45+/SiglecF+/CD11c+) (Figure 3.9F), suggesting that SPION uptake induced pro-inflammatory activation in AM. At 24 h, IM expressed high levels of MHCII and MerTK, with a corresponding reduction in CD163 and TFR1, paralleling observations from cultured macrophages (Figure 3.9G and 3.6). Other innate immune cells were also responsive to SPION internalization. Eosinophils decreased expression of MHCII at 24 h (Figure 3.9H), and neutrophils increased in TFR1 expression at 48 h (Figure 3.9I). Cells from the adaptive immune system were also affected by SPION treatment as the percentage of CD71+ CD3+ T cells decreased at 24 h (Figure 3.9J).

Next, the systemic iron response to the introduction of SPIONs in the lungs of mice was evaluated by measuring iron levels in the serum and organs (Figure 3.10A and B). Unbound iron-binding capacity (UIBC) decreased at 96 h, and non-heme iron levels in the lungs reached a maximum at 96 h, indicating the time required for iron released from SPIONs to be absorbed into lung tissue and enter the systemic circulation. In line with this, at 96 h, iron levels in the spleen, liver and kidney increased, whereas the duodenum decreased, reflecting the redistribution of iron from the lungs iron into iron storage organs and the systemic response by decreasing iron uptake from the diet.

Overall, intratracheal administration of SPIONs in mice induced an inflammatory response that activated macrophages and as well as other innate and adaptive immune cells in an iron-responsive manner. In addition, iron intratracheally instilled entered the systemic circulation and added to bodily iron stores at 96 h, suggesting that iron introduced into the lungs can enter and contribute to the systemic iron stores of the body. Importantly, validation of SPIONs was done and found to possess the capability to polarize macrophages *in vivo* in a similar fashion as SPION stimulated cultured macrophages.
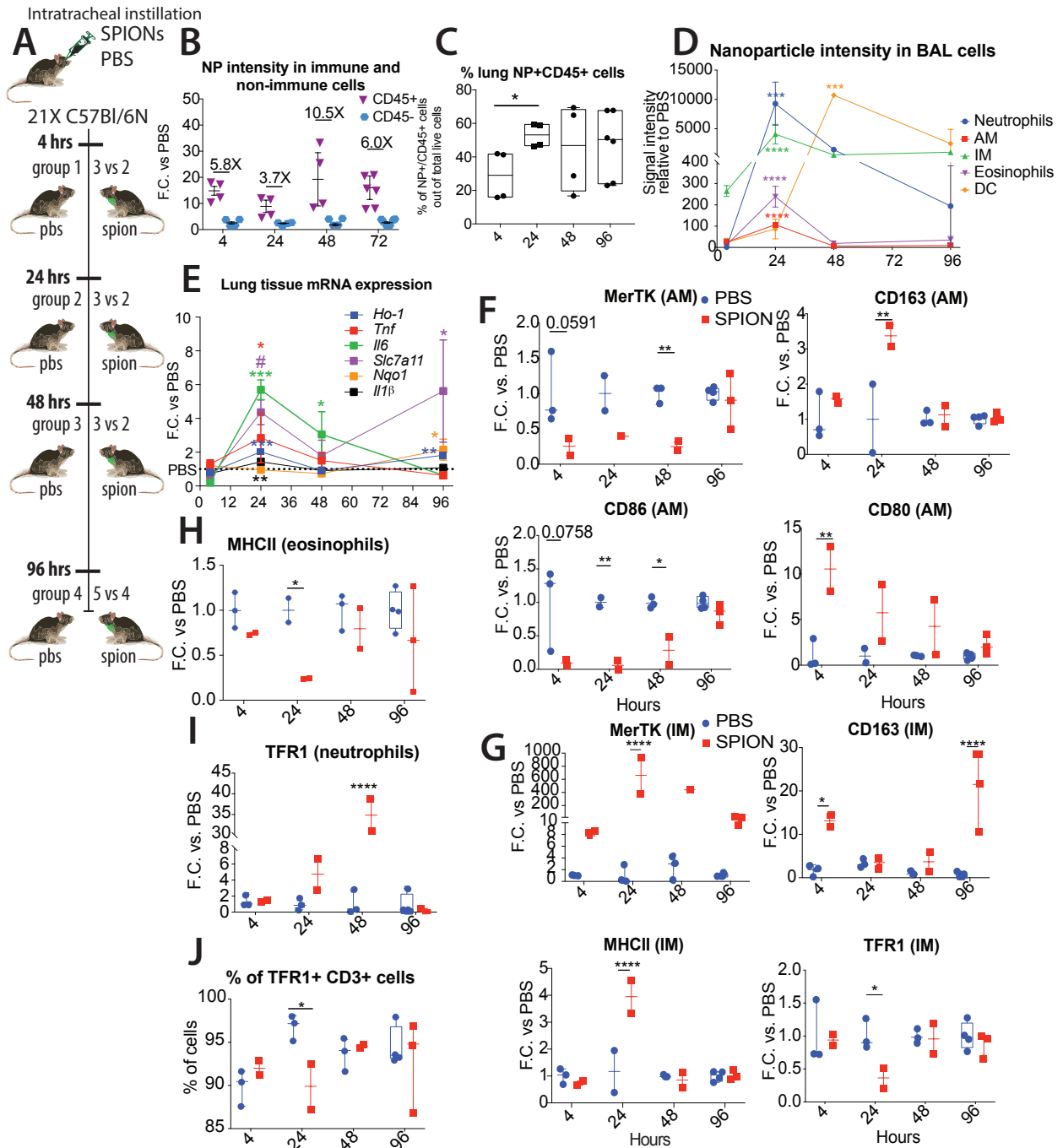
Figure 3.9. SPIONs induce acute inflammation in vivo. A. 21 mice were intratracheally instilled with SPIONs or PBS and sacrificed at 4 h, 24 h, 48 and 96 h. SPION uptake in immune cells (CD45+) compared to non-immune cells (CD45-) (**B**), the percentage of SPION+ immune cells (**C**) and SPION intensity in different populations of innate immune cells (**D**) was evaluated by flow cytometry. Inflammatory cytokines and Nrf2 target gene mRNA expression in lung tissue (**E**). Cell surface protein levels in alveolar macrophages (AM)(**F**), in interstitial macrophages (IM) (**G**), eosinophils (**H**), neutrophils (**I**) and CD3+ T-cells (**J**). Data reported as n ± Standard Error of the Mean (SEM). One-way ANOVA (*) or students' t-test (#), comparisons are as indicated: * p < 0.01, ** p < 0.001, *** p < 0.0001. *Experiment was in collaboration with AG Rocio Sotillo at the DKFZ, Heidelberg, Germany; experiment was constructed, implemented and analyzed by me.*

81
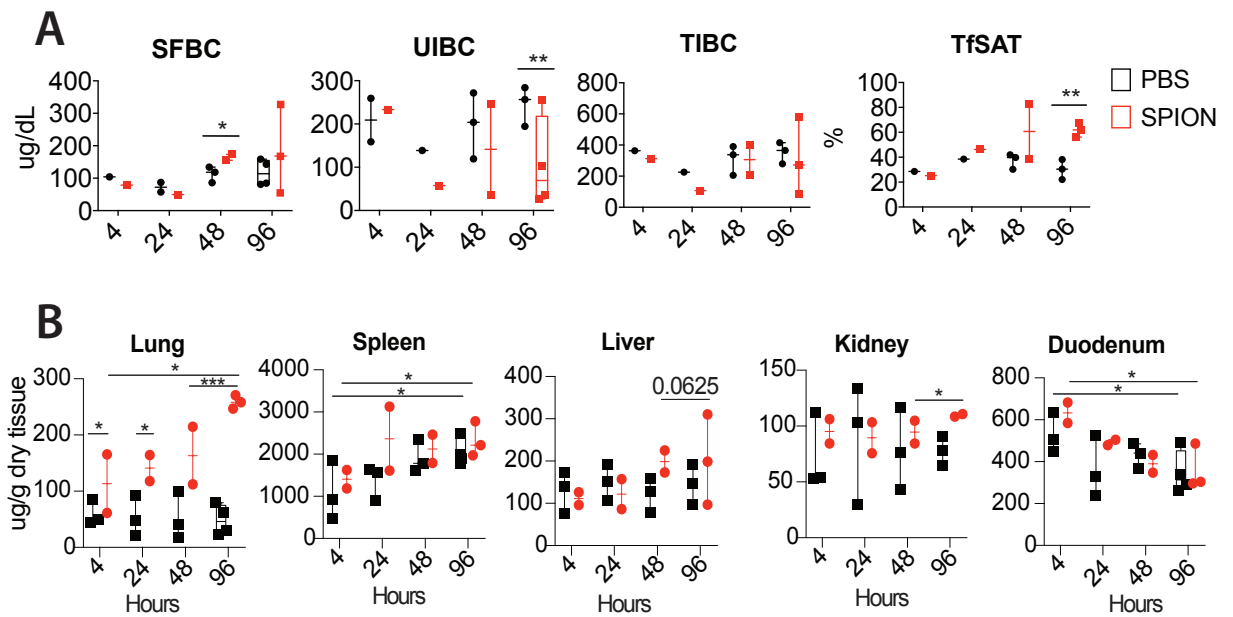
Figure 3.10. Intratracheally instilled SPIONs increase iron in blood and tissues of mice. Serum iron (**A**) and tissue iron levels (**B**) were quantified in mice intratracheally instilled with PBS or SPIONs. Data reported as n ± Standard Error of the Mean (SEM). One-way ANOVA (*) comparison as indicated: * $p < 0.01$, ** $p < 0.001$, *** $p < 0.0001$. *Experiment was in collaboration with AG Rocio Sotillo at the DKFZ, Heidelberg, Germany; experiment was constructed, implemented and analyzed by me.*

Section 3.9: Discussion

Previous studies have shown that iron induces a pro-inflammatory phenotype in macrophages[69]. When delivered to tumors, iron induces pro-inflammatory responses in tumor-associated macrophages (TAMs), which correlated with reduced tumor growth in mice[189]. The development of superparamagnetic iron oxide nanoparticles (SPIONs) as an iron delivery system was done to activate TAMs and induce anti-cancer mechanisms when applied to lung cancer tumors. Also included were control nanoparticles, CCPMs, which lack iron and allow for the specific examination of the role of iron in activating the pro-inflammatory phenotype in macrophages. The initial characterization in BMDMs found that SPIONs and not CCPMs induce pro-inflammatory activation in BMDMs, suggesting that iron is responsible for triggering the pro-inflammatory phenotype in macrophages. The activation of inflammation in SPION treated BMDMs was mediated by iron released from SPIONs and TLR4 signaling. In comparison to non-treated and CCPM treated BMDMs, SPION treated BMDMs had prolonged lifespan in culture and accumulated iron over time, suggesting that SPIONs are stable and slowly release iron within biological systems. Moreover, the uptake of both SPIONs and CCPMs by BMDMs involves phagocytotic mechanisms. The *in vivo* SPION treatment experiments in wildtype C57Bl/6 mice showed that the response in cultured macrophages could be recapitulated *in vivo* as lung macrophages, both alveolar and interstitial, were induced to a pro-inflammatory status. Other innate immune cells in the lung were found to also internalize to SPIONs. The inflammatory response triggered by SPIONs was resolved at 96 h, indicating an acute inflammatory response. Insight into how iron homeostasis in the lungs contributes to systemic iron regulation was elucidated as iron released from SPIONs in the lungs entered systemic iron distribution and accumulated in the liver and the kidneys after 96 h. These data demonstrate that SPIONs lead to pro-inflammatory macrophage activation in cultured cells and in mice, illustrating the potential of SPIONs as an immunostimulatory agent. Therefore, these analyses laid the foundation for the next phase of research, which will evaluate SPION treatment in lung cancer co-culture experiments and in mouse models. The summary figure outlining data shown in this chapter is found in Figure 3.11.
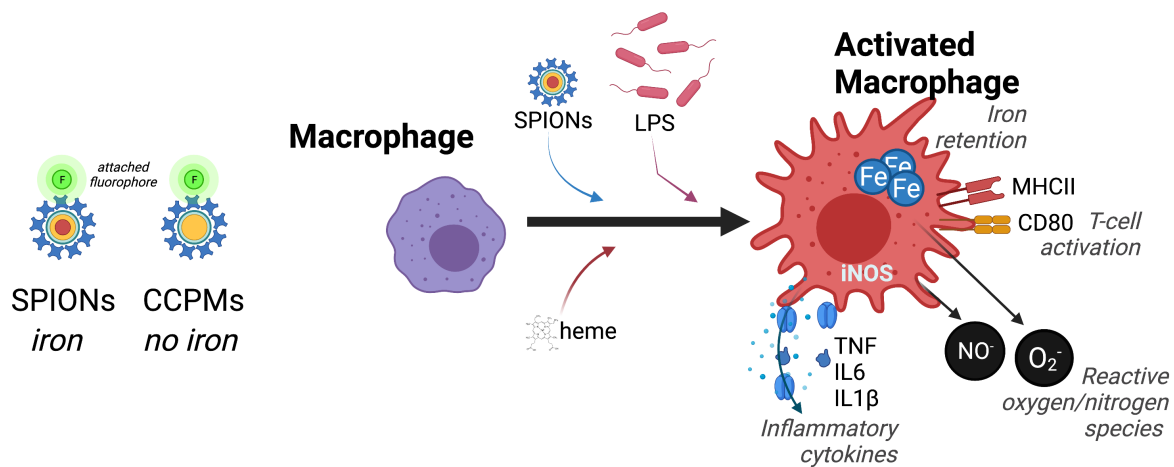
Figure 3.11. Summary schematic of Chapter 3: SPIONs induce a pro-inflammatory phenotype in macrophages. Macrophages when treated with known stimulators such as LPS or heme can stimulate pro-inflammatory activation. SPIONs can induce a similar pro-inflammatory phenotype, which retain and store intracellular iron; upregulate MHCII and CD80 protein levels; increase production of reactive oxygen/nitrogen species release; upregulate expression of inflammatory cytokines such as TNF, IL1, IL6 and IL1β. Figure adapted and updated from previously published studies[73,317,343,374,375].

Macrophages that were activated by SPIONs showed a pro-inflammatory profile that paralleled LPS and heme stimulation. However, SPION activated BMDMs showed subtle differences compared to LPS and heme activation as one key distinction was the levels of MerTK (Figure 3.6B). MerTK is a macrophage cell surface receptor that has been found to be involved in the resolution of atherosclerotic plaques, where macrophages that express MerTK engage in efferocytosis, a process of clearing apoptotic bodies[263]. The receptor protein is characterized as a "scavenger receptor" that is expressed at the leading edge of the plasma membrane, where it facilitates the uptake of dead cells and debris. While many studies associate this marker with M2/anti-inflammatory macrophages, a few studies have noted that the relative abundance of this marker varies on macrophage subtypes depending on the stage of development of the atherosclerotic plaque[264]. SPION treatment specifically increased the levels of this marker which was not seen in LPS or heme treatment. Both the removal of iron by iron chelation and TLR4 inhibition decreased the expression of MerTK in SPION stimulated BMDMs, suggesting that a combination of iron and TLR inflammation triggers the upregulation of this protein. Furthermore, this argues that SPION released iron induces a type of inflammatory subtype in macrophages that triggers both early phase inflammation responses, CD86+CD80+MHCII+, as well as mechanisms involved in resolving inflammation in macrophages, MerTK+.

This data supports a role of iron, released from SPIONs, for activating macrophage inflammatory responses. The inflammatory protein CD86 and the immunosurveillance protein CD172a were increased upon SPION treatment but not CCPMs treatment in BMDMs. Antigen presentation and immune surveillance are integral functions of macrophages that mediate inflammatory responses[1]. CD86 is a co-stimulatory antigen-presentation receptor on antigen presenting cells (APCs) important for stimulation of T-lymphocyte cells (T cells) and subsequent T cell activation[265–267]. Upon SPION treatment, the levels of CD86 were reduced (~2-fold) in BMDMs after iron chelation with the intracellular iron chelator deferiprone (DFI). Levels of CD86 were reduced to a greater extent upon Toll-like receptor 4 (TLR4) inhibition by the specific TLR4 inhibitor CLI (~4-fold), suggesting that stimulation by iron only partially contributes to the APC function of macrophages. CD172a on the other hand, is a negative response receptor necessary for immune surveillance that is constitutively expressed on macrophage cell surfaces[268]. A lack of interaction between CD172a and its ligand CD47 initiates pro-phagocytic mechanisms in a myosin II-dependent manner and initiates clearing of apoptotic cells. The expression of CD172a was heavily upregulated, indicating an increase in surveillance mechanisms initiated by SPION treatment in macrophages. This would suggest

that SPION activation stimulates intracellular pathways that are specific to immune surveillance and clearing of cells. Inhibiting TLR4 mediated signaling but not iron stimulation reduced the levels of CD172a on SPION stimulated macrophages, indicating that while both stimuli contribute to the function of apoptotic cell clearance by macrophages, TLR4 signaling contributes in a more pronounced manner. Activation of TLR4 signaling is classically defined by the binding of LPS to the TLR4 receptor[269]. Other stimuli, such as heme, have also been observed to activate TLR4 signaling in macrophages[270] yet the underlying mechanisms of TLR4 activation by heme or other stimuli are still elusive. Direct activation of TLR4 through a heme-binding site has not yet been determined[270]. Many reports show that heme can activate TLR4 signaling through several indirect methods, including the oxidation of phospholipids[271], the generation of ROS[272], interactions with or disruption of proteins associated with lipid rafts[273,274], the activation of the NOD-like receptor family pyrin domain containing 2 (NLRP3) inflammasome[275], or other unknown interactions. Considering that SPIONs activate macrophages in a similar manner as heme, it may be possible that SPION activation of TLR4 follows the same indirect interactions as heme with TLR4. Although the precise mode of activation is still unclear, from these observations, the degree to which signaling pathways contribute and determine the SPION-induced macrophage subtype can be elucidated.

Both iron-induced signaling and TLR4-mediated signaling contribute to the uptake of SPIONs in BMDMs. Treating macrophages with an actin polymerization inhibitor, Cytochalasin D (CD), reduced the activation of SPION inflammation in macrophages as production of *Tnf* mRNA and CD172a and CD86 protein levels were reduced (Figure 3.7). Despite this, an increase of SPION uptake in BMDMs treated with CD after 6 h. CD treatment inhibits cell ruffling, cell motility and initiates cell stiffness by inducing rounding of the cell shape[259,276]. Treatment with CD prevents microfilament function and polymerization, thus blocking phagocytosis and phagosome formation. One reason for the increased uptake of SPIONs when BMDMs were treated with CD could be that cell stiffness immobilized SPIONs to the outside periphery of the macrophage. Similar observations were found when BMDMs were cultured with *Legionella pneumophila* and treated with CD[277]. Interestingly, a difference in uptake of SPIONs and CCPMs in CD-treated BMDMs was observed. Both nanoparticles are of similar size and shape yet differ in mass. A recent study reported that the softness of nanoparticles affects the rate of phagocytosis in macrophages[278]. Actin filaments are responsible for wrapping the cell membrane around a foreign body and dragging it inwards for digestion. A harder (or denser) nanoparticle would be more easily dragged into the cell, whereas a softer particle would be harder to capture and can easily escape engulfment, akin to

engulfing a bowling ball to a feather in a fluid. In these experiments, SPIONs could be immobilized to the outside of BMDMs due to their density, whereas CCPMs may diffuse throughout the medium, evading phagocytosis. In these experiments with flow cytometry, cells were not fixed or permeabilized and therefore remained intact for evaluation. Under these experimental conditions, the immobilized SPIONs at the periphery of BMDMs would still appear as an "increase" in SPION internalization. Further evaluation by confocal fluorescence microscopy should be done to address this question.

In the initial assessment of SPION uptake, macrophages accumulated more SPIONs than CCPMs, suggesting that macrophages preferentially take up SPIONs (Figure 3.2). In human macrophages, although an increase in SPION uptake compared to non-myeloid derived cells was observed, CCPMs uptake was more than SPION uptake. One hypothesis for this difference could be that the isolation and differentiation protocol for human buffy coat macrophages from blood did not filter out all the non-myeloid cell types prior to culturing. In either case, the increase in SPION uptake was consistent between both BMDMs and buffy coat macrophages, indicating that SPIONs are targeting myeloid-derived cells.

SPIONs were found to be primarily taken up by innate immune cells when instilled intratracheally in mice (Figure 3.9 and 3.10). An increase in inflammatory cytokine expression in the lungs of SPION treated mice was also observed, indicating an inflammatory reaction. Specific evaluation of lung macrophages showed the increased expression of inflammatory proteins, which paralleled the characterization of BMDMs. Interestingly, differences were found in activation profiles of alveolar macrophages (AM) (CD11c+/SiglecF+) and interstitial macrophages (IM) (CD11b+/CD64+). While both types of macrophages are noted as tissue-resident[279], the location of residence within the lungs are different[279–283]. AMs mainly reside within the alveolar space deep within the lungs, while IMs are primarily found within the interstitium and bronchi space. Therefore, the differences in their activation could be due to timing, as the application of SPIONs by intratracheal instillation is applied to the bronchi of the lungs. Indeed, IMs had a higher intensity of SPION signal than AMs at 4 h. Additionally, IMs and AMs reside in vastly different tissue environments, and likely are primed for distinct responses due to environmental stimuli. For example, IMs express MHCII at 24 h and CD80/86 were not detectable. On the other hand, AMs had high levels of CD80, low levels of CD86 and no detectable levels of MHCII. These observations are in line with previous studies noting that AMs have the capacity to express more robust inflammatory signals than IMs[284] and that IMs can express higher levels of MHCII than AMs[285]. The differences in magnitude and timing of

protein levels indicate the varying physiological roles for these different macrophage populations within the lungs.

A single instillation of SPIONs to the lungs of mice caused an acute immune reaction at 24 h. Previous reports have shown that an acute immune response occurs upon intratracheal instillation of iron oxide nanoparticles[286–291]. However, most report either a single acute (24 h or 48 h) or chronic (90 d) time-points providing only a brief recording of the inflammatory response. Here immune cells, other than macrophages, were responsive to SPION instillation. At 24 h, neutrophils have significantly accumulated SPIONs in comparison to other innate immune cells. While many studies have shown that infiltration of neutrophils to the lungs occurs at 24 h upon nanoparticle instillation [292], the presence of TFR1 levels on neutrophils has not been reported. At 48 h, neutrophils expressed high levels of TFR1. Since neutrophils typically have lifespans that last for 24 h[293], the increase in TFR1 levels likely reflects the response to environmental stimuli by newer populations of neutrophils recruited to the lungs. At 24 h, eosinophils accumulated SPIONs while also decreased MHCII expression. Eosinophils have been shown to have APC-like functions by expressing MHC II and regulating T-cell immune responses in the lung[294]. Since eosinophils have decreased MHCII expression, this would suggest repression of immune responses at 24 h upon SPION internalization. Lastly, CD3+ T cells have been shown to require iron for clonal expansion and production of pro-inflammatory cytokines[295]. A decrease in the amount of TFR1+ CD3+ T cells at 24 h indicates that CD3+ T cells are responsive to the increase in iron in the lungs and infers that clonal expansion of T cells is underway. Whether TFR1+ CD3+ T cells were cytotoxic CD8+ T cells (Th1 response) or CD4+ T cells (Th2 response) was not recorded. The implications of these observations are not very well understood and present an opportunity for further investigation. Importantly, these observations begin to elucidate the immunostimulatory properties of SPIONs in the lungs.

Previous studies have shown that iron in the lungs is mainly taken up and regulated by macrophages[296]. On the other hand, epithelial cells also have the capacity to take up iron through TFR1 and the divalent metal transporter-1 (DMT1)[297]. Other iron-binding proteins, such as transferrin, ferritin and lactoferrin, have been found in the lungs and are thought to contribute to the regulation of iron homeostasis of lung tissue[80,82,298–302]. The intricacies of how iron distributes through the lungs over time is not yet clear[302]. In our system, serum iron measurements show an increase of iron entering the blood starting at 48 h post-SPION treatment, an indication that iron has entered the systemic circulation. Concurrent with that timing, the resolution of inflammation, inferred by the decreased expression of inflammatory

cytokines in the lung tissue and inflammatory marker levels on macrophages, was observed starting at 48 h, indicating that the redistribution of iron away from the lung tissue is an associated component of the resolution phase of inflammation in the lung. Complete resolution was observed at 96 h as the liver and kidney had high iron levels and inflammatory surface proteins on AMs, IMs and neutrophils returned to basal levels. This timeline highlights the kinetics of iron entry into the body from the lungs. Future studies looking at the precise localization of iron and the distribution of iron regulatory proteins within lung tissue by histological analysis over time would provide us with a clearer understanding of which specific cell types accumulate iron and how the distribution of iron affects molecular changes within the lung tissue.

These initial studies represent a proof of concept of SPIONs as an immunostimulatory agent. Iron was shown to induce a pro-inflammatory macrophage polarization in both cultured and *in vivo* settings, where macrophages polarize within 24 h and induce similar inflammatory responses. This data was used as a platform for the next section, which aims at developing and testing the anti-cancer activity of SPION-loaded macrophages in relevant cultured and *in vivo* models.

Chapter 4: SPION activated macrophages induce cancer cell death

Building on the characterization of SPION treatment in macrophages and other individual cell types, the next step was to characterize the impact of SPION activated macrophages on cancer cells when cultured together. BMDMs were co-cultured with LLC cells and treated with SPIONs or CCPMs for 24 h. The uptake and cellular distribution of nanoparticles was evaluated by fluorescence microscopy and flow cytometry (Figure 4.1A and B). A higher intracellular fluorescence signal was observed in BMDMs than LLC cells in co-cultures treated with SPIONs. In contrast, CCPMs had a more evenly distributed signal in both cell types. Quantitation by flow cytometry showed that BMDMs contained ~100-fold more SPIONs than LLC cells (Figure 4.1B). Consistent with mono-culture experiments, quantitative evaluation of CCPM uptake showed that LLC cells accumulated more CCPMs than SPIONs (Figure 4.1B). To determine if this effect was specific to LLC cells, our analysis expanded to look at another cancer cell type. B16 melanoma cancer cells are also a *Kras* mutation driven cell line[242] that share similar cell proliferation and expansion qualities as LLC cells[240,241]. When macrophages were cultured with B16 cells and treated with SPIONs, paralleling the observations of LLC cells, B16 cells internalized fewer SPIONs and more CCPMs than macrophages (Figure 4.1C). These results indicate that SPIONs are preferentially taken up by macrophages and not by cancer cells.
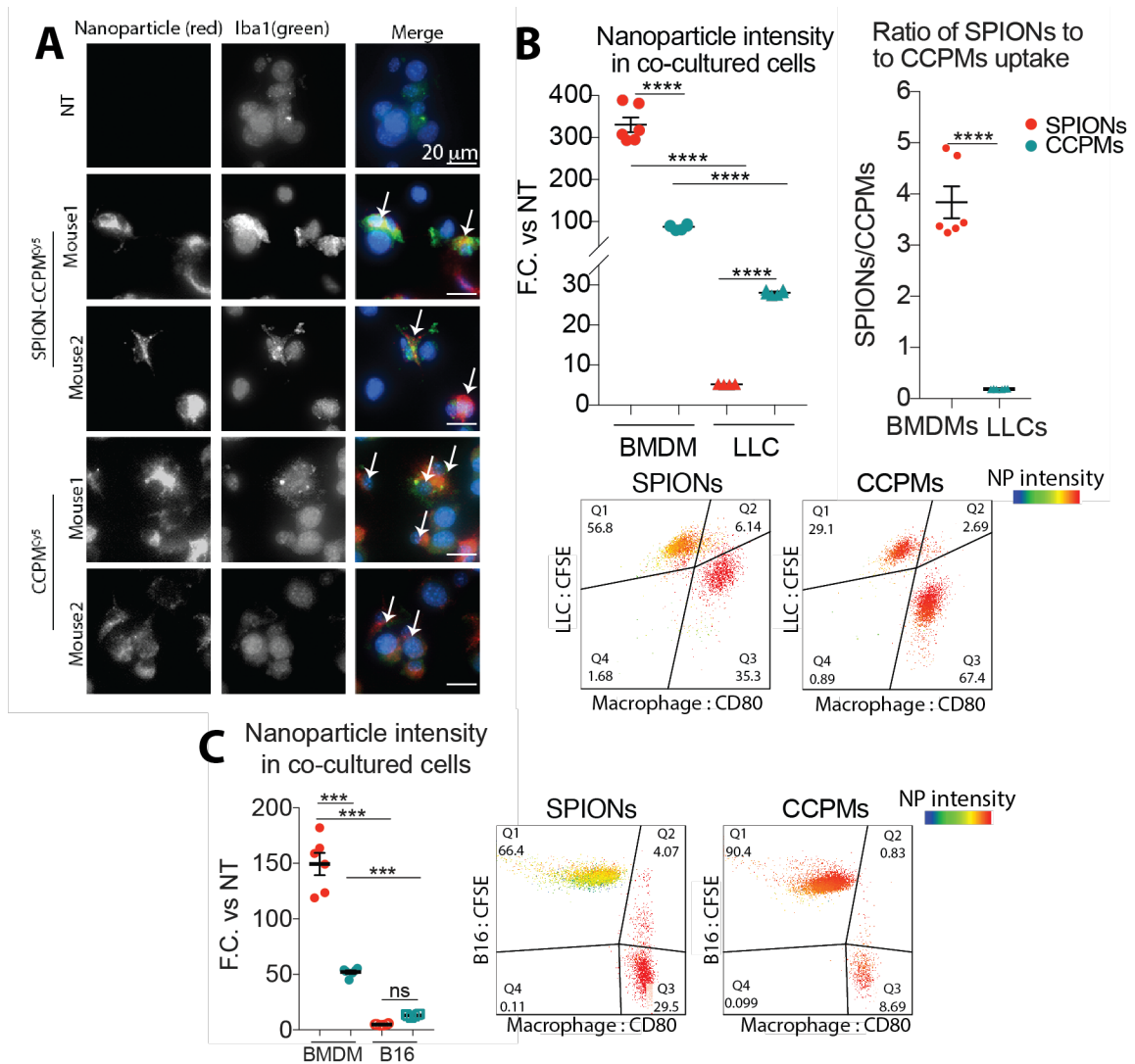
Figure 4.1. SPIONs are preferentially taken up by macrophages. A-C. Co-cultures of BMDMs and LLC cells (**B**) or BMDMs and B16 cells (**C**) evaluated by microscopy (**A**) or flow cytometry (**B** and **C**) after 24 h of treatment with SPIONs, CCPMs, or left untreated. **A**. Cells were fixed and stained for the macrophage marker Iba1. The white arrow indicates cells positive for NP. Representative images are from two biological replicates. Data representative of three independent experiments. Data reported as n ± Standard Error of the Mean (SEM). One-way ANOVA (*) with comparison indicated: * $p < 0.01$, ** $p < 0.001$, *** $p < 0.0001$.

SECTION 4.2: SPION-LOADED MACROPHAGES REDUCE THE GROWTH OF CANCER CELLS IN CULTURE

Previous reports have indicated a link between iron nanoparticle-activated macrophages and the occurrence of cancer cell death[189]. To determine if our SPION treated macrophages can cause cancer cell death, the survival and growth of cancer cells was evaluated when co-cultured with BMDMs over a 72 h time course. To evaluate co-cultured LLC cells and BMDMs separately, LLC cells were labeled with carboxyfluorescein succinimidyl ester (CFSE), a cell membrane permeable non-degradable nuclear stain[303]. This dye allows for an accurate evaluation of LLC cell numbers and the ability to track cell proliferation. Heme was used as the positive iron control because it is a naturally occurring source of iron and can be a potent stimulator of inflammation in macrophages[256]. The evaluation of cell viability for both BMDMs and LLC cells showed that in co-cultures treated with SPIONs, LLC cells had an overall stagnated growth curve (Figure 4.2A). On the other hand, LLC cells in co-cultures left untreated (NT) or treated with CCPMs increased in cell number starting from 24 h. It is well documented that cancer cells rapidly proliferate when given an abundance of freely accessible iron in culture[304]. With heme treatment, a significant increase in LLC cell number was observed (Figure 4.2A), indicating that iron in heme is accessible to cancer cells. Cell viability of BMDMs did not change in SPION treated co-cultures. On the other hand, a reduction in BMDMs was observed in cultures left untreated or treated with heme or CCPMs starting at 24 h (Figure 4.2B). The decrease in BMDMs over time parallels similar observations from our BMDM cultures in Chapter 3 (Figure 3.4).

Next, the proliferation of LLC cells was evaluated within the co-cultures. To do so, the signal intensity of CFSE reduces by half with each cell division allowing for a convenient evaluation of the rate of cell division by flow cytometry over time. In SPION treated co-cultures, an initial reduction in dividing LLC cells is noted starting at 24 h after treatment (Figure 4.2C). The profile of cell generations of each culture is shown by representative plots (Figure 4.2C, left). The reduction of dividing cells was more pronounced at 48 h and 72 h post-treatment (Figure 4.2C). Although LLC cells within SPION treated co-cultures are still dividing, the rate was less in comparison to the NT, heme or CCPM treated co-cultures after 24 h. Additionally, in SPION treated co-cultures, LLC-derived CFSE signal within BMDMs increased starting at 24 h post-treatment, indicating that BMDMs are actively internalizing LLC cell debris (Figure 4.2D). Internalization of LLC cell debris in BMDMs upon heme or CCPMs was less than SPION treated BMDMs. Consistent with observations in Figure 4.1, evaluation of nanoparticle uptake in BMDMs and LLC cells (Figure 4.2E) showed that a

greater uptake of SPIONs occurs in BMDMs, whereas CCPMs were taken up by both cell types. These results suggest that the specific activation of macrophages by SPIONs and not CCPMs adversely affects cancer cells by reducing the number of dividing cells in culture.
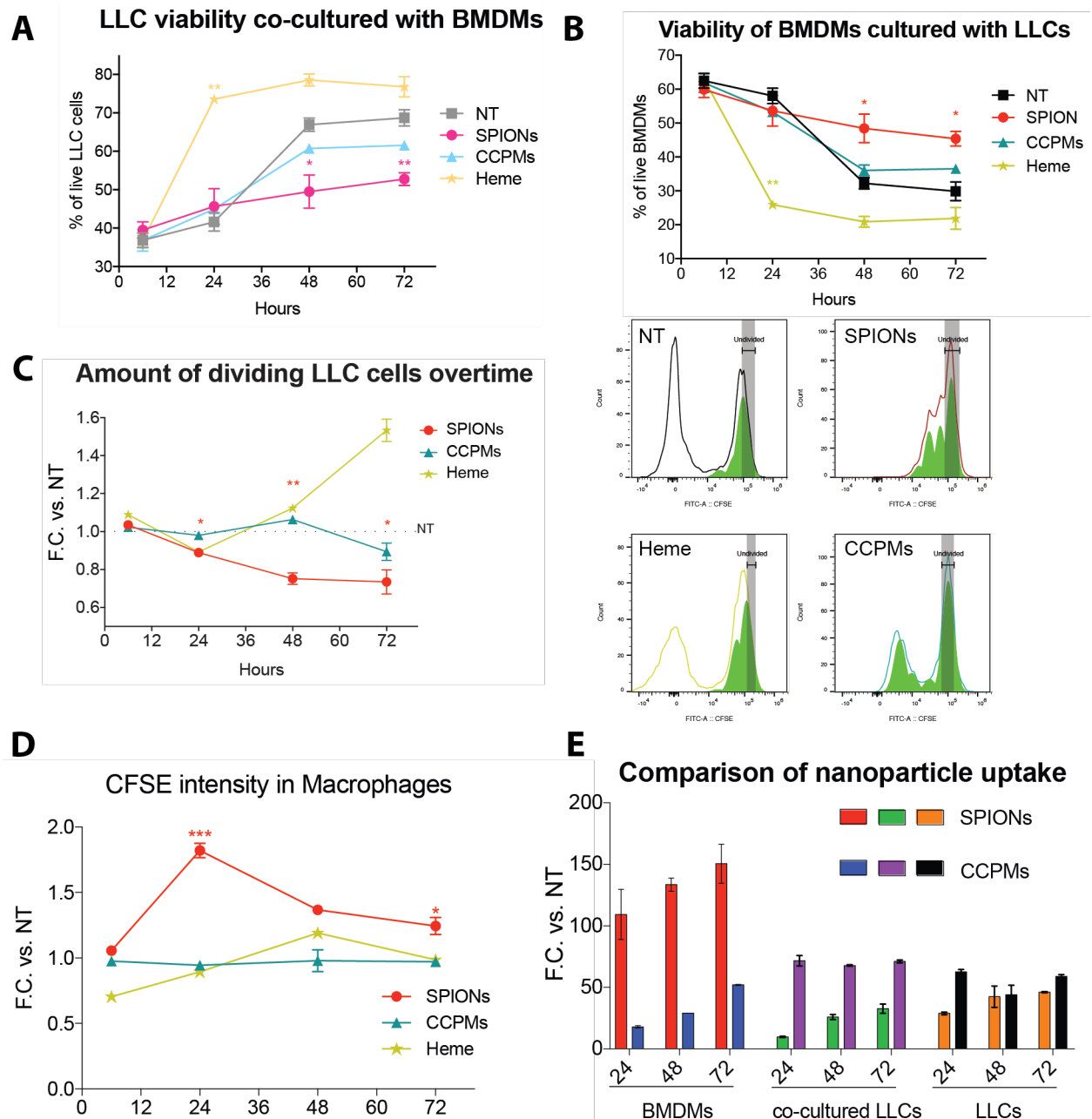
Figure 4.2. SPIONs loaded macrophages reduce LLC growth. A-E. Co-cultures of BMDMs and LLC cells were treated with SPIONs, CCPMs, heme or left untreated and analyzed by flow cytometry. LLC cells were stained with CFSE before co-culturing. Quantification of live LLCs (**A**) and BMDMs (**B**) in co-cultures over time. **C**. Division rate of LLC cells in co-cultures over time with representative division plots (left). **D**. LLC-derived CFSE signal intensity in BMDMs. **E**. Quantification of nanoparticle uptake in BMDMs and LLC cells co-cultured or mono-cultured over time. Data reported as n ± Standard Error of the Mean (SEM) and representative of three independent experiments. One-way ANOVA (*) in comparison to the non-treated (NT) condition: * $p < 0.01$, ** $p < 0.001$, *** $p < 0.0001$.

SECTION 4.3: SPION-INDUCED RESPONSES FROM MACROPHAGES CAUSE STRESS IN CANCER CELLS

The reduction in LLC cell number at 48 h seen in Figure 4.2 could be due to one of two possibilities: a buildup of harmful molecules secreted from activated macrophages that then limit cancer cell expansion or direct cancer cell clearance at early timepoints by macrophage phagocytosis. To address the former, the magnitude of differential mRNA expression in LLC cells and BMDMs were evaluated when treated with either SPIONs, CCPMs, or heme. Cultures of BMDMs, LLC cells or co-cultures of BMDMs with LLC cells were incubated with either SPIONs, CCPMs, heme or NT for 24 h or 48 h. At each time point, cells were separated into CD45+ (BMDMs) and CD45- (LLC cells) fractions by CD45+ microbeads, followed by lysis and analysis for differential gene expression by RT-qPCR. In mono- and co-cultures treated with SPIONs at 24 h, BMDMs expressed high levels of the inflammatory cytokine *Tnf*, the inflammatory enzyme iNOS (*Nos2*) and had reduced expression of the iron export protein Fpn1 (*Ireg1*) (Figure 4.3A), confirming that BMDMs were activated to an inflammatory and iron retaining phenotype within both cultured conditions. Conversely, under co-culture conditions, CCPM treated BMDMs showed lower levels of expression of *Tnf* and *Nos2* and high levels of *Fpn1* at 24 and 48 h in BMDMs. Heme treatment in BMDMs from either mono- or co-cultures did not induce inflammation (low levels of *Tnf, Nos2,* and increased *Fpn1*). These data suggest that iron released from SPIONs stimulates macrophages to pro-inflammatory and iron sequestration phenotype with or without cancer cells.

To understand the impact on LLC cells, genes were examined that have a negative role in the progression of the cell cycle or are initiated upon stress (Figure 4.3B). Aconitase2 (*Aco2*) is an iron-sulfur cluster containing enzyme that converts citrate to isocitrate, and increased expression redirects metabolic programming to favor slower cell division rates[305]. LLC cells from co-cultures treated with SPIONs expressed high levels of *Aco2* at 48 h post-treatment. This increase was not observed when co-cultures were treated with CCPMs or heme (Figure 4.3B). In response to oxidative stress, the transcription factor nuclear factor (erythroid-derived 2)-like 2 (Nrf2) induces the transcription of target genes such as NAD(P)H:quinone oxidoreductase (*Nqo1*), which then detoxifies and mitigates oxidative reactions[248,249,306,307]. Expression levels of *Nqo1* were increased from 24 h to 48 h in LLC cells from iron-treated co-cultures (both SPION and heme) but not in CCPM treated co-cultures. In contrast to CCPM treated LLC cells, SPION treatment on LLC cells cultured individually did not induce *Nqo1* or *Aco2* expression at any time point, suggesting that iron released from SPIONs in macrophages initiates the macrophages response may lead to reduced LLC cell division. Cancer cells exhibit

a higher requirement for iron than non-malignant cells and express iron regulatory genes that favor iron acquisition and retention, i.e., low levels of Fpn1 (*Ireg1*) and high levels of TFR1 (*Tfrc*)[166]. The status of iron handling in LLC cells from SPION treated co-cultures showed indications of reduced iron acquisition from 24 h to 48 h (*Ireg1* mRNA increased and *Tfrc* mRNA decreased) (Figure 4.3C), further supporting observations of reduced cancer cell growth in these co-cultures. Interestingly, CCPM treatment increased *Ireg1* mRNA and decreased *Tfrc* mRNA expression at 48 h in co-cultured LLC cells, suggesting that the components of the shell in SPIONs also contribute to the reduction of the growth rate of LLC cells. In support of this, CCPM treatment reduced LLC cell numbers at 48 h (Figure 4.2A). The expression of iron regulatory genes together with the increased expression *Aco2* and *Nqo1* mRNA at 48 h suggests that in LLC cells co-cultured with SPION treated BMDMs, an induction of oxidative stress responses and alterations in metabolism favor a slower rate of division.
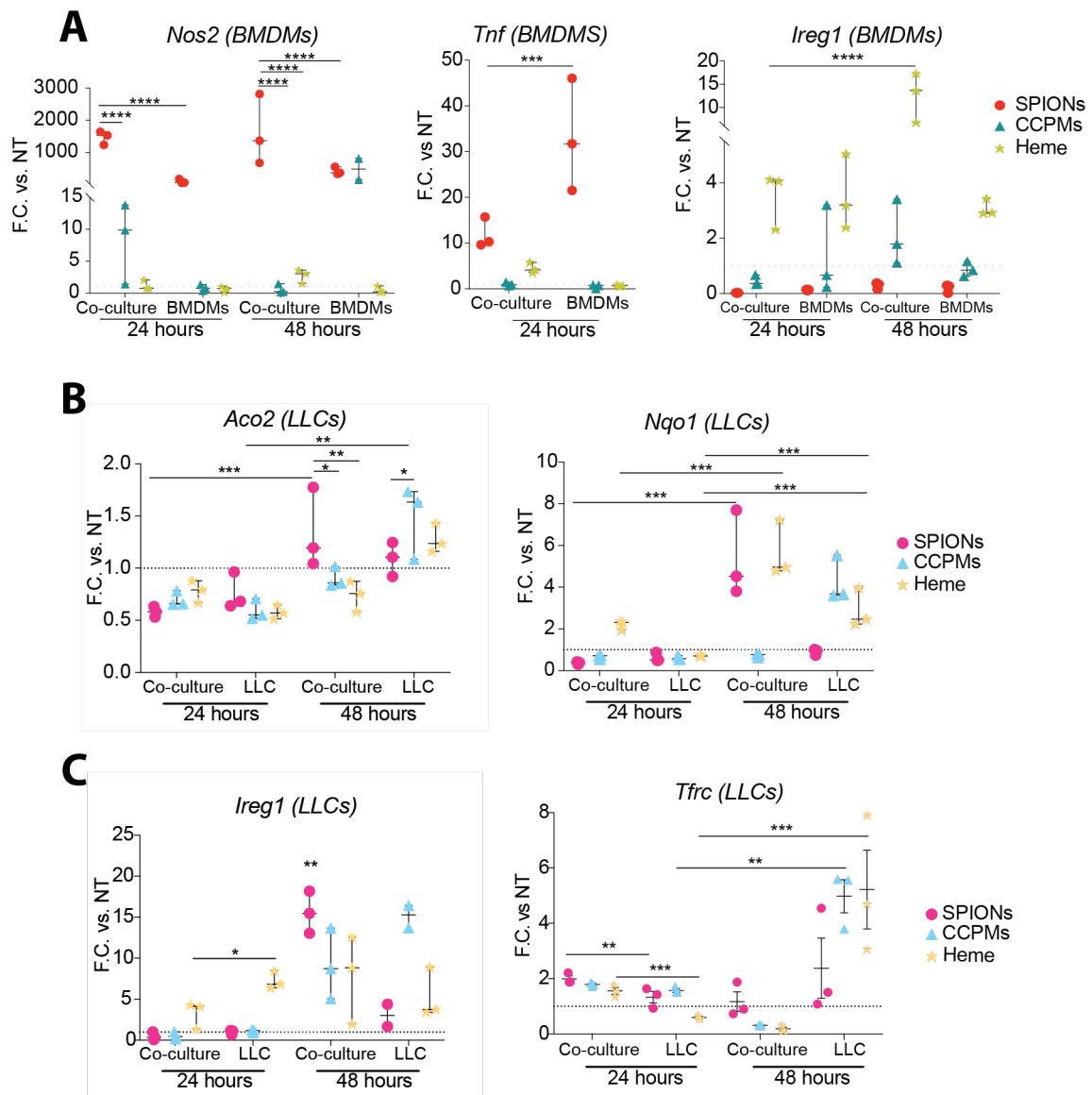
Figure 4.3. SPIONs loaded macrophages induce oxidative stress in co-cultured LLC cells.
A-C. BMDMs and LLC or BMDMs or LLC cells were treated with SPIONs, CCPMs, Heme or not for 24 h and 48 h, and separated using CD45+ microbeads for mRNA expression analysis. **A**. mRNA expression of *Nos2*, *Tnf* and *Ireg1* in BMDMs. **B** and **C**. mRNA expression of *Aco2*, *Nqo1*, *Ireg1* and *Tfrc* in LLC cells. Data reported as n ± Standard Error of the Mean (SEM). One-way ANOVA (*) in comparison to the non-treated condition unless otherwise indicated: * p < 0.01, ** p < 0.001, *** p < 0.0001.

The *Nos2* gene encodes for the inducible nitric oxide synthase (iNOS) enzyme, which produces nitric oxide (NO) that can react with intermediates to produce toxic reactive nitrogen species (RNS)[308]. Macrophages secrete RNS, which can induce oxidative stress and cytotoxic mechanisms correlating with death in cancer cells[309]. BMDMs were observed to produce high levels of iNOS in SPION treated co-cultures in addition to accumulating LLC-derived CFSE debris (Figure 4.2D and 4.3A), suggesting that SPION-loaded BMDMs secrete RNS. To address this, we tested whether toxic species secreted by macrophages would account for the reduced live LLC number at 48 h. Live LLC cell numbers were compared in co-cultures with BMDMs to live LLC cell numbers from a trans-well culture system after 48 h (Figure. 4.4A). An insert with 0.22 μm pore size was used for the trans-well culture system to allow solutes and nanoparticles to freely diffuse but also prevent cell movement between compartments. For the trans-well culturing, treatments of SPION, CCPM, or heme were applied to areas both in and out of the insert and accompanied with thorough mixing to ensure even distribution. As previously observed, fewer live LLC cells (~30%) were observed in SPION treated co-cultures than in untreated, CCPM or heme treated co-cultures (Figure 4.4B). For trans-well cultures, live LLC cell count also decreased by ~30% in SPION treated cultures when compared to LLC cells in non-treated and CCPM treated trans-well cultures (Figure 4.4B). Next, the proliferation profile of LLC cells was evaluated and showed that SPION treated LLC cells divided less in both systems when compared to non-treated, CCPM or heme treated cultures (Figure 4.4D). Interestingly, BMDMs in trans-well SPION treated cultures accumulated CFSE signal (Figure 4.4C). When comparing BMDMs between both culturing techniques, upon SPION treatments, brightness of CFSE signal in macrophages did not differ (Figure 4.4C) despite brighter nanoparticle intensity in BMDMs in the co-culture system (Figure 4.4E). Since the levels of LLC-derived CFSE signal in macrophages were similar between culturing systems (Figure 4.4C), the number of macrophages positive for LLC-derived CFSE signal differing between the two culturing systems was examined. There was no change in the amount of BMDMs positive for LLC cell CFSE signal in either SPION treated cultures (Figure 4.4F), suggesting that contact to cancer cells is unnecessary for SPION induced macrophage cancer cell death. The equivalent levels of LLC cell death (Figure 4.4A) and CFSE uptake in BMDMs (Figure 4.4C) in both co-culture and trans-well cultures indicate that macrophage-mediated cancer cell death occurs by the secretion of toxic species than direct cell contact.

BMDMs treated with SPIONs expressed higher levels of *Nos2* and *Tnf* mRNA transcripts when co-cultured with LLC cells compared to SPION treated BMDMs cultured separately (Figure 4.3B), suggesting that contact with LLC cells increase the degree of inflammatory activation in BMDMs. Next, evaluation was done on whether the extent of activation in BMDMs treated with SPIONs would differ if in contact with cancer cells. This was addressed by measuring the degree of expression of inflammatory cell surface proteins, such as CD86, CD80 and CD38, as well as the iron acquisition protein TFR1 by flow cytometry. The levels of inflammatory proteins, CD80 and CD86, show little difference in BMDMs treated with SPIONs between the two culturing systems, suggesting that the greater response in inflammatory activation in co-cultured BMDMs is due to secreted factors from cancer cells rather than from macrophage contact to cancer cells (Figure 4.4G). CD38 is a receptor involved in the process of macrophage chemotaxis[310]. BMDMs in the trans-well system showed a robust expression of CD38 upon SPION treatment compared to those from the co-culture system, suggesting BMDMs in the trans-well are migrating more than their co-cultured counterparts. Quantification of TFR1 levels showed that SPION treated BMDMs expressed higher levels of TFR1 when cultured in the trans-well system than in the co-culture system (Figure 4.4G). Differences could be attributed to SPION uptake in BMDMs when comparing co-cultured BMDMs to the trans-well cultured BMDMs (Figure 4.4E). Examination of all proteins on heme and CCPM treated BMDMs showed little to no difference between the two culturing systems. These results suggest SPION-loaded macrophages reduce LLC cell viability and proliferation by secreting toxic molecular species and that contact with cancer cells is not necessary for the reduction in cancer cells in culture.
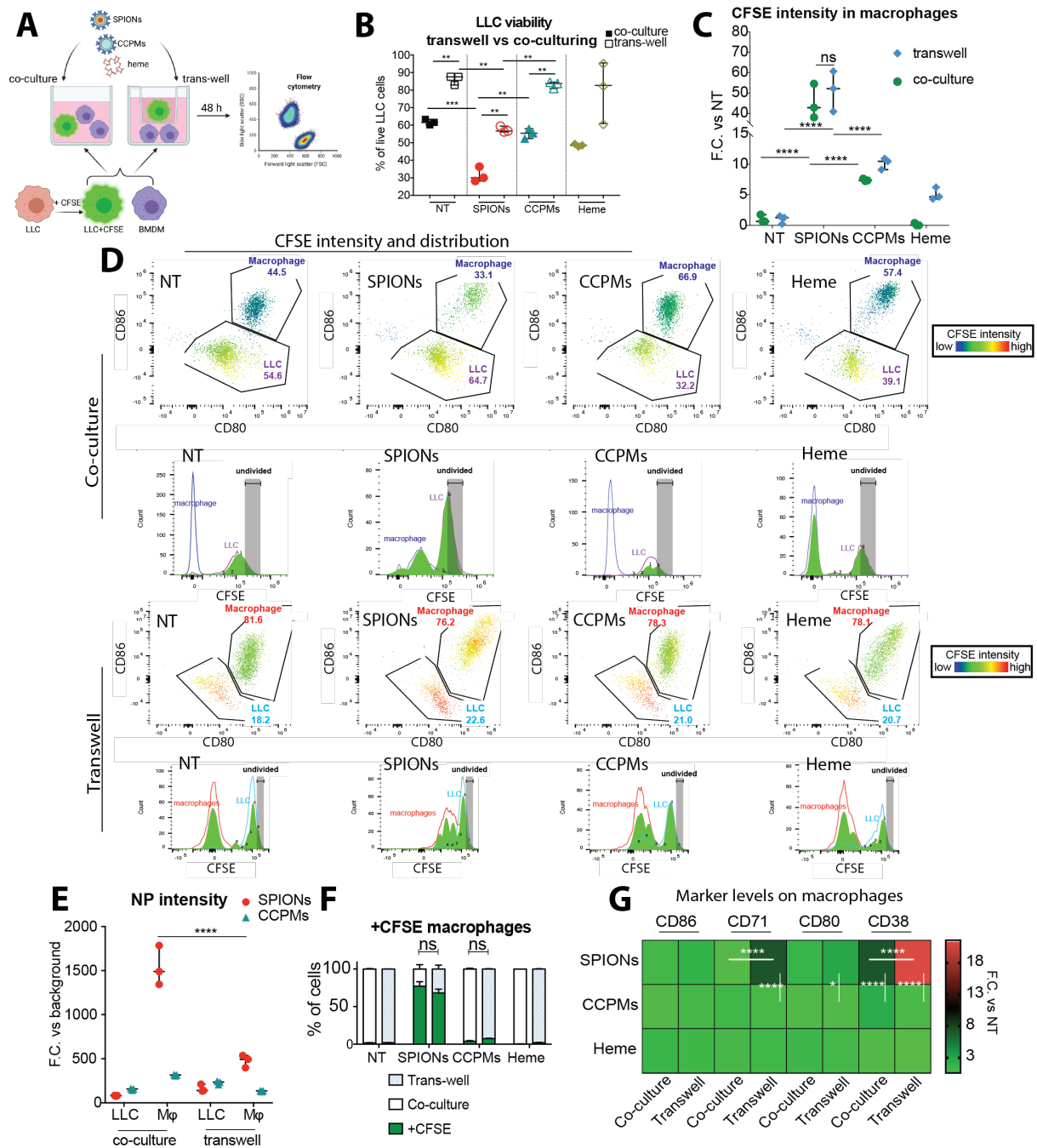
Figure 4.4. Cell-to-cell contact is not necessary for cancer cell killing by SPION activated macrophages. A. Schematic of co-culture and trans-well experiments. LLC cell viability (**B**), CFSE signal intensity in BMDMs (**C**), representative plots of LLC cell and BMDM growth dynamics (**D**), NP uptake (**E**), percentage of CFSE+ BMDMs (**E**), and cell surface markers on BMDMs (**F**) were evaluated using flow cytometry. Data reported as n ± Standard Error of the Mean (SEM) and representative of three independent experiments. NS – not significant. One-way ANOVA (*) in comparison to the non-treated (NT) condition unless otherwise indicated: * p < 0.01, ** p < 0.001, *** p < 0.0001.

Given that pro-inflammatory activation in macrophages by SPIONs is key to LLC cell death, inhibiting the inflammatory response was hypothesized to reverse cytotoxic effects on LLC cells. To address this, the impact on LLC cells was evaluated upon inhibition of specific triggered inflammation in SPION treated macrophages. Given that SPION activation in macrophages induced TLR4 signaling in Chapter 3 (Figure 3.6), an inflammatory response well-characterized by the stimulus lipopolysaccharide (LPS), the inhibition of this signaling pathway was evaluated in the co-culture system and LPS was included as a positive inflammatory control. To inhibit the TLR4 mediated inflammatory response, cells were treated with CLI-094 (CLI), a TLR4 specific inhibitor[257]. Co-cultures of LLC cells and BMDMs were incubated with or without CLI in addition to SPION or LPS treatment or left untreated for 48 h. The LPS treatments alone did not affect LLC live cell counts in mono-cultures or co-cultures with BMDMs (Figure 4.5A), suggesting that classical pro-inflammatory activation in macrophages does not induce significant cancer cell death. In co-cultures treated with CLI and SPIONs, SPION uptake was reduced by ~2-fold (Figure 4.5C) in BMDMs and live LLC cells increased by ~ 20%, indicating that TLR4 triggered inflammation is an essential mechanism of SPION-induced macrophage anti-cancer activity. Interestingly, in CLI and SPION treated co-cultures, the number of BMDMs as well as the magnitude of LLC-derived CFSE signal in BMDMs was reduced, indicating that likely a combination of both iron and TLR4 induced inflammation from SPION activated BMDMs is needed to cause LLC cell death and internalize LLC debris.

Since inflammatory activation mediated by iron in macrophages was key to induce cancer cell death, sequestration of iron with an iron chelator in macrophages would prevent SPION-loaded macrophage cancer cell death. With or without SPIONs or LPS the intracellular iron chelator deferiprone (DFI) was added to co-cultures of LLC cells and BMDMs for 48 h. Mono- and co-cultures treated with DFI had reduced LLC cell counts, apart from SPION treated cultures. Co- and mono-cultures treated with SPIONs showed no change in LLC cell count (Figure 4.5B), yet SPION uptake was reduced by ~2-fold (Figure 4.5C), suggesting that anti-cancer activity by SPION-loaded BMDMs is dependent on a minimum threshold of iron stimulation. The amount of live CFSE+ macrophages (Figure 4.5B, right) did not change between SPION treated co-cultures with and without DFI, indicating that the amount of dead LLC cells and the internalization of LLC debris by macrophages is not affected by the sequestration of iron by DFI.

To verify inflammatory activation occurred in macrophages from co-cultures, protein markers for the anti-inflammatory phenotype CD206 and the inflammatory phenotype CD64 were examined. From Figure 4.4A and 4.4B, a dynamic population of BMDMs within the co-cultures was noted, where a proportion of BMDMs were positive for LLC-derived CFSE signal and others were not. Therefore, the BMDM populations were separated into either CFSE+ or CFSE- macrophages to analyze the surface protein levels. In LPS treated BMDMs, CD206 levels were increased when TLR4 signaling was inhibited, confirming the efficacy of CLI (Figure 4.5D). SPION treated co-cultures showed an increase in CD206 levels in CFSE+ macrophages compared to CFSE- macrophages (Figure 4.5D). Recent studies have identified CD206 as a bona fide marker of phagocytic macrophages[311–313] and is a scavenging receptor important for the phagocytosis of apoptotic cells in the healing tissue[314]. The increase in CD206 indicates that SPION treatment contributes to phagocytosis activity in BMDMs. Upon TLR4 inhibition in SPION treated BMDMs, CD206 levels were reduced, correlating with reduced CFSE internalization in BMDMs and increased LLC cell number (Figure 4.5A). The levels of CD206 in SPION treated BMDMs were slightly reduced by iron chelation, suggesting that iron contributes to the production of this protein.

SPION and LPS treatment promoted a pro-inflammatory state as indicated by the increased levels of CD64 (Figure 4.5E). CD64 is upregulated under pro-inflammatory conditions where it functions as a receptor involved antibody-dependent cytotoxicity and immune complex clearance[315,316]. The treatment with CLI lead to a significant reduction in the levels of CD64 in SPION and LPS treated co-cultured macrophages (Figure 4.5E), verifying that pro-inflammatory activation was occurring. Iron chelation slightly reduced CD64 levels in SPION treated macrophages highlighting the minor role of iron in this type of inflammation.

Taken together, iron stimulation and TLR4 triggered inflammation are both necessary for the cytotoxic activity of SPION-loaded macrophages leading to LLC cell death.

A Co-cultured LLC cells + TLR4 inhibition
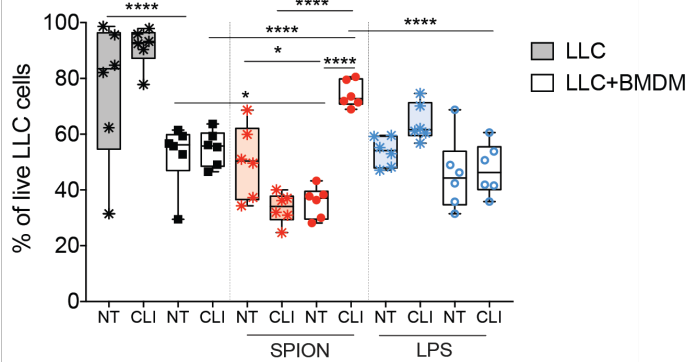
CFSE+ BMDMs
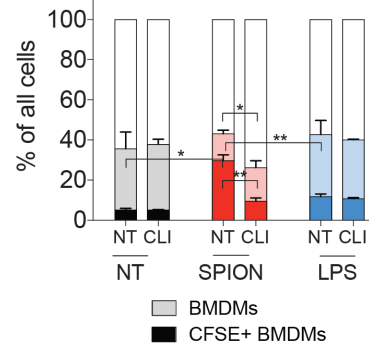
B Co-cultured LLCs + iron chelation
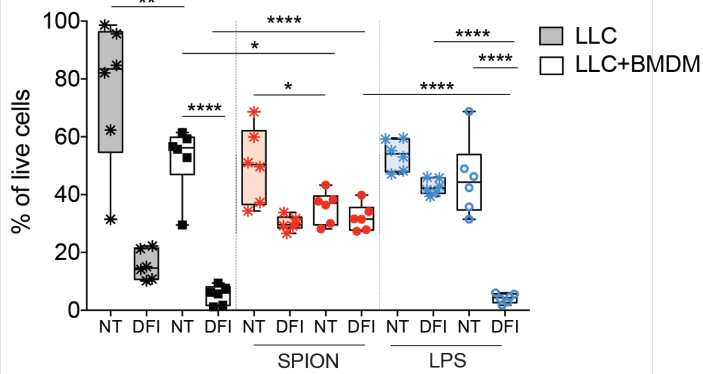
CFSE+ BMDMs

C SPION uptake

D CD206
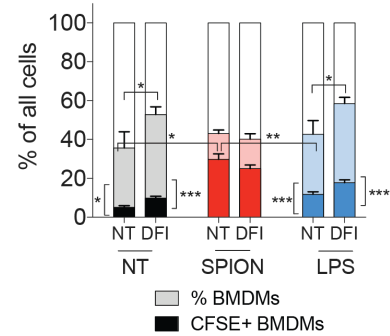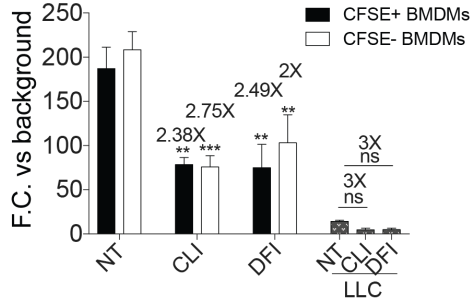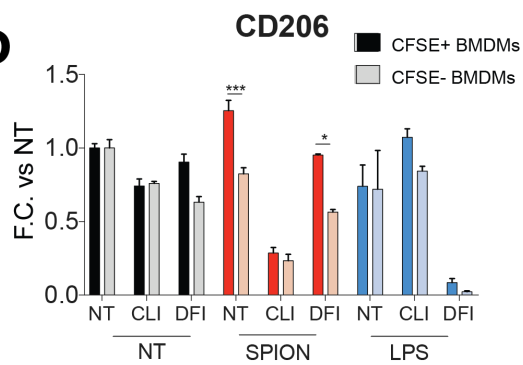
E CD64
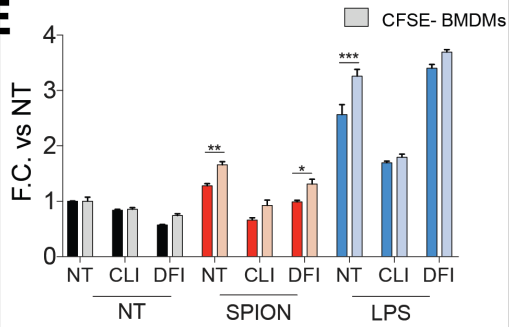
Figure 4.5. TLR4 signaling and iron stimulation are important for SPION mediated cancer cell death. A-F. Co-cultures of BMDMs and LLC cells were treated with either SPIONs, LPS or NT for 48 h and evaluated by flow cytometry. Percentage of live LLC cells in cultures treated with and without CLI (**A**, left) or DFI (**B**, left) and total live cells (**A** or **B**, right). **C**. SPION uptake in BMDMs and LLC cells is represented as fold change vs background. Macrophage markers, CD206 (**D**) and CD64 (**E**) were quantified in BMDMs from co-cultures. Data reported as n ± Standard Error of the Mean (SEM) and representative of three independent experiments. One-way ANOVA (*) in comparison to the non-treated (NT) condition unless otherwise indicated: * $p < 0.01$, ** $p < 0.001$, *** $p < 0.0001$.

Inflammatory activation of macrophages leads to the secretion of inflammatory cytokines and toxic molecules including reactive oxygen and nitrogen species (ROS/RNS) that induce cytostatic and cytotoxic effects in cancer cells[47]. Nitric oxide (NO) is a producrt of iNOS, which is a critical signal in initiating the pro-inflammatory phenotype in macrophages[317–319]. Additionally, previous studies have reported that intracellular oxidative species like NO and RNS are essential drivers for macrophage phagocytosis of dying or apoptotic cells[320,321]. Since blocking inflammatory activation by CLI in BMDMs increased LLC cell numbers, cancer cell death upon SPION treatment in BMDMs would be due to the secretion of NO/RNS and not by other secreted factors such as inflammatory cytokines. To test this, 1400W an irreversible and selective inhibitor for the iNOS enzyme was used to block the production of NO and RNS[322]. Our positive control was LPS as it is a potent activator of iNOS in macrophages. Treatments of 1400W in our co-culture system led to an increase in the number of live LLC cells (Figure 4.6A), suggesting that NOS/RNS produced by iNOS is an important mediator in LLC cell death by BMDMs. SPION uptake and the amount of CFSE+ macrophages significantly decreased in SPION treated co-cultured BMDMs (Figure 4.6B and C), which is consistent with previous reports of the role that NO/RNS drives phagocytosis activity in macrophages[323]. Treatment with 1400W and SPION also increased CD206 levels but CD64 levels were unchanged in co-cultured BMDMs (Figure 4.6D and E), indicating specific pathways of inflammatory signaling activated by SPIONs in BMDMs.

Antigen presentation is one of the main functions of macrophages[1]. MHCII, in conjunction with either CD80 or CD86, are receptors expressed for the induction of Th1 activation and proliferation. The expression of MHCII on BMDMs in all co-cultures under all treatments was examined and showed that MHCII was detected in CFSE- BMDMs that remained untreated or were treated with LPS (Figure 4.6F). CLI treatment in co-cultured BMDMs decreased MHCII expression by ~3-fold. MHCII expression was also reduced, by ~4-fold, when BMDMs were treated with DFI. Previous reports have suggested that MHCII presentation is regulated by NOS, where the induction of iNOS and production of NO causes an increase in antigen presentation[324]. Blocking NO production by 1400W treatment in co-cultured BMDMs reduced the expression of MHCII in LPS co-cultured BMDMs to near NT levels. Interestingly, MHCII expression increased in BMDMs treated with 1400W and SPIONs, suggesting that the release of free iron from SPIONs, which can induce the production

of reactive oxidative species, could compensate for the oxidative reactions necessary for MHCII expression in macrophages.

Since oxidative responses in macrophages are necessary not only for macrophage polarization but was also observed in LLC cells upon co-culturing with SPION-loaded BMDMs (Figure 4.3), the antioxidant response was evaluated by measuring total glutathione (GSH) or free GSH levels in cell lysates of BMDMs, LLC cells or co-cultures of LLC cells and BMDMs (Figure 4.6G). As a positive control, suberoylanilide hydoxamic acid (SAHA) was used, a pan-HDAC inhibitor, which prevents the induction of anti-oxidative mechanisms[325]. In BMDMs, LLC cells, and in co-cultures of BMDMs and LLC cells, SAHA reduced the oxidative capacity (total GSH levels) as well as the free GSH levels in cells. Conversely, for BMDMs or LLC cell lysates from mono-cultures, cells treated with SPIONs or CCPMs did not affect the oxidative capacity or the levels of free GSH. On the other hand, in cell lysates of BMDMs and LLCs, the oxidative capacity in cells was reduced upon treatment with either SPIONs or CCPMs. Evaluation of the free GSH levels showed SPION treatment in co-culture lysates with reduced GSH levels, whereas CCPMs treatment did not (Figure 4.6H), suggesting that SPION but not CCPM treatment induces an oxidative reaction that consumes free GSH in co-cultures.

Overall, SPION treatment showed induction of macrophage activation through the iNOS pathway, leading to an increase in secreted oxidative species and a paracrine cell death response in LLC cells. This mechanism elicits stress response mechanisms in cancer cells by consuming free GSH, resulting in reduced proliferation and cancer cell death.

A Co-cultured LLCs + iNOS inhibition
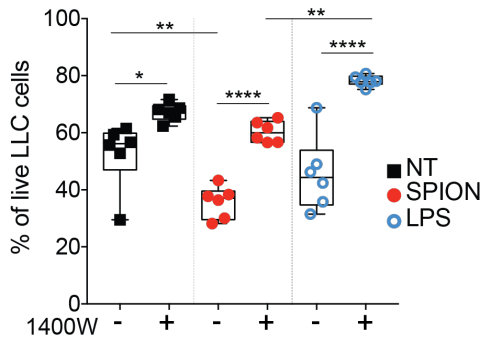
B CFSE+ macrophages
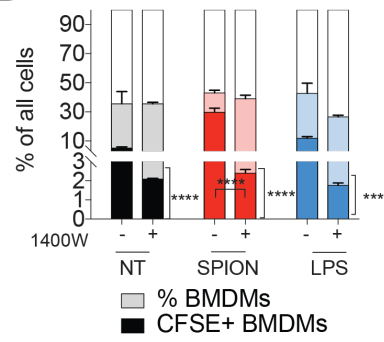
C SPION uptake
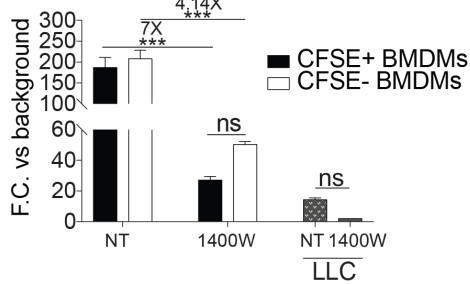
D CD206
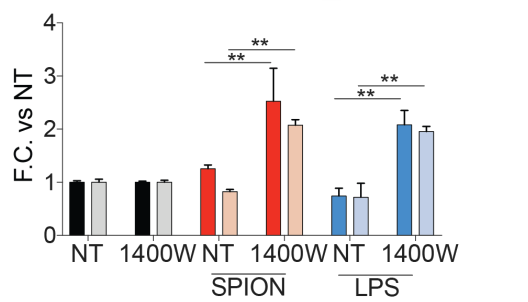
E CD64
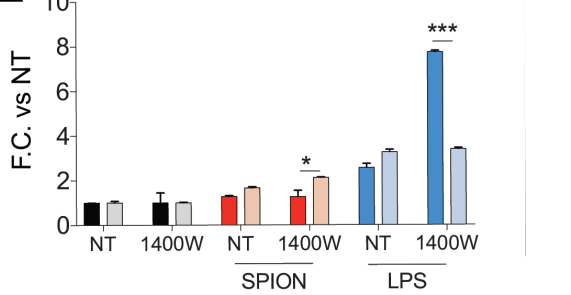
F MHCII (CFSE- BMDMs)
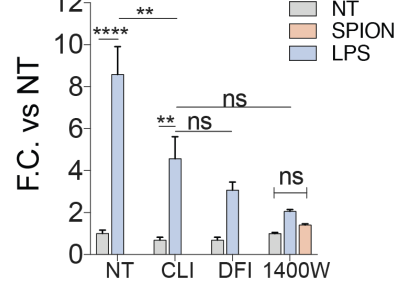
G BMDMs / Cancer / Co-culture
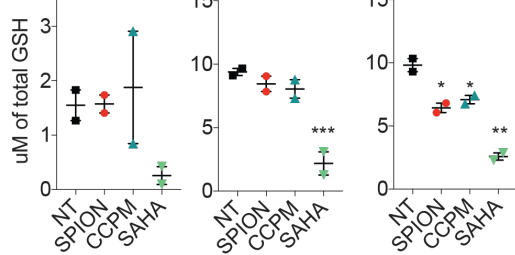
H Co-culture free GSH levels
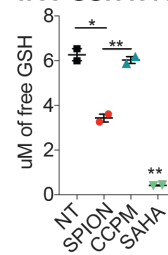
Figure 4.6. Secreted nitric oxide species by SPION activated macrophages are necessary for cancer cell death. A-D. Co-cultures of BMDMs and LLC cells were treated with SPIONs, LPS or NT, with and without 1400W for 48 h. Percentage of live LLC cells (**A**), % of BMDMs in co-cultures (**B**) and amount of SPION uptake (**C**) was evaluated by flow cytometry. **D** and **E**. Quantification of surface proteins levels of CD206 and CD64. **F**. Quantification of MHCII levels on CFSE- BMDMs. **G**. Total glutathione (**G**) or free glutathione levels (**H**) were measured in cell lysates of BMDMs, cancer cells, or co-culture of BMDMs and cancer cells after treatment with SPIONs, CCPMs, SAHA or NT for 48 h. Data reported as n ± Standard Error of the Mean (SEM), NT – non-treated. One-way ANOVA (*): * $p < 0.01$, ** $p < 0.001$, *** $p < 0.0001$.

Since SPIONs were preferentially taken up by cultured macrophages and pulmonary macrophages and SPION activated macrophages induced death in cultured cancer cells, we postulated that when administered in a lung cancer mouse model, SPIONs would target macrophages localized at lung tumors, thereby limiting cancer cell growth. Therefore, the efficacy of SPIONs was tested in a lung cancer orthotopic mouse model to determine if SPIONs could be developed as an adjuvant anti-cancer therapy. The administration of SPIONs or CCPMs was done intravenously as the administrative route to parallel conventional clinical administrative methods. Using C57Bl/6N mice, 1 million LLC cells were intratracheally instilled and mice were allowed to rest for one week before starting SPIONs or CCPMs treatment (Figure 4.7A). Three administrations at an interval of five days apart were done over the course of two weeks for a total experimental time of three weeks (or 21 days) (Figure 4.7A). Within 2 h of the first injection of either SPIONs or CCPMs, fluorescent signal was detected in the urine and reached a maximum intensity at 8 h (Figure 4.7B). Using an IVIS *in vivo* imaging system, CCPMs signal was detected throughout the bodies of mice (Figure 4.7C). SPION administered mice showed weaker signal than the CCPM group (Figure 4.7C, right), paralleling observations from co-cultures of LLC cells and BMDMs (Figure 4.1).

On day 21, mice were sacrificed and tumor size as well as nanoparticle distribution were evaluated. No visible tumors were observed in most lungs of mice and there was no difference in body to lung weight among the three groups (Figure 4.7D). Lung cell populations were evaluated and found that mice treated with SPIONs recruited more immune cells to the lungs than mice treated with CCPMs or PBS. Specifically, an increase of neutrophils and eosinophils in SPION treated mice was noted and not in mice administered CCPMs (Figure 4.7G) despite little to no LLC cells in the lungs of all mice.

Since there were no visible tumors in the lungs, the initial analysis focused on the distribution of SPIONs and CCPMs throughout the body. Evaluation of cells positive for nanoparticle signal by flow cytometry found that immune cells (CD45+) and not CD45- cells were positive for SPIONs and CCPMs signal in the lungs and spleen of mice, organs that contain high populations of macrophages (Figure 4.7E). There were more immune cells positive for SPION signal in the spleen than in the lungs (Figure 4.7F), suggesting that SPIONs do not specifically target pulmonary macrophages. Immune cells accumulated more SPIONs than CCPMs (12X in the spleen and 9.25X in the lungs). There was no significant difference in nanoparticle signal intensity in lung immune cells of mice administered either SPIONs or CCPMs (Figure 4.7E). The number of immune cells positive for CCPM signal was similar in

both the lungs and spleen. Overall, SPION and CCPM uptake *in vivo* follows a similar trend to observations in cultured cells, where SPIONs were taken up by immune cells and to a lesser extent by other cells.

Next, whether the distribution of SPIONs and CCPMs caused any side effects in the organs of mice was evaluated. Lung iron levels were increased in mice administered SPIONs (Figure 4.8A) with an associated increase in levels of the oxidative stress response protein glutathione peroxidase 4 (GPX4) when compared to mice administered PBS, suggesting that iron released from SPIONS in the lungs may induce an oxidative stress response (Figure 4.8B). In mice administered CCPMs, high iron levels were detected in the lungs as well as heterogeneous levels of GPX4 protein and TFR1 protein, suggesting CCPMs induce dysregulation of iron in the lungs. Increased levels of iron were found in both the spleen and liver of mice administered SPIONs (Figure 4.8A and C) which correlated to increased levels of GPX4 and the iron storage protein ferritin (FTL) (Figure 4.8D). In the liver, heme oxygenase 1 (HO1) protein levels were increased in mice administered both SPIONs and CCPMs (Figure 4.8D), suggesting that the polymer shell of the nanoparticles induces Nrf2 oxidative stress response mechanisms. A reduction in iron levels in the duodenum and spleen but not the liver of mice administered CCPMs was observed (Figure 4.8A), indicating that CCPMs disrupt systemic iron distribution within the body. This observation was supported by decreased Fpn1 (*Ireg1*) mRNA in the liver of mice administered CCPMs (Figure 4.8F). An up-regulation of cytochrome P450 gene *CYP2C67* was found*,* an oxidoreductase enzyme that catabolically processes exogenous drugs and lipids[326], suggesting that in addition to dysregulation of systemic iron, CCPMs but not SPIONs induce toxicity in the liver (Figure 4.8F).

From these experiments, insight was garnered into the biological distribution and effect of SPIONs *in vivo*. Importantly, CCPMs but not SPIONs induce systemic adverse effects. SPION treatment caused an infiltration of immune cells into the lungs of mice, indicating potential lung adjuvant efficacy. However, SPIONs were also taken up by immune cells in organs densely populated with macrophages other than the lungs. Since our experimental mouse models were without lung tumors, a conclusion on the efficacy of SPIONs as a cancer adjuvant cannot be confirmed.
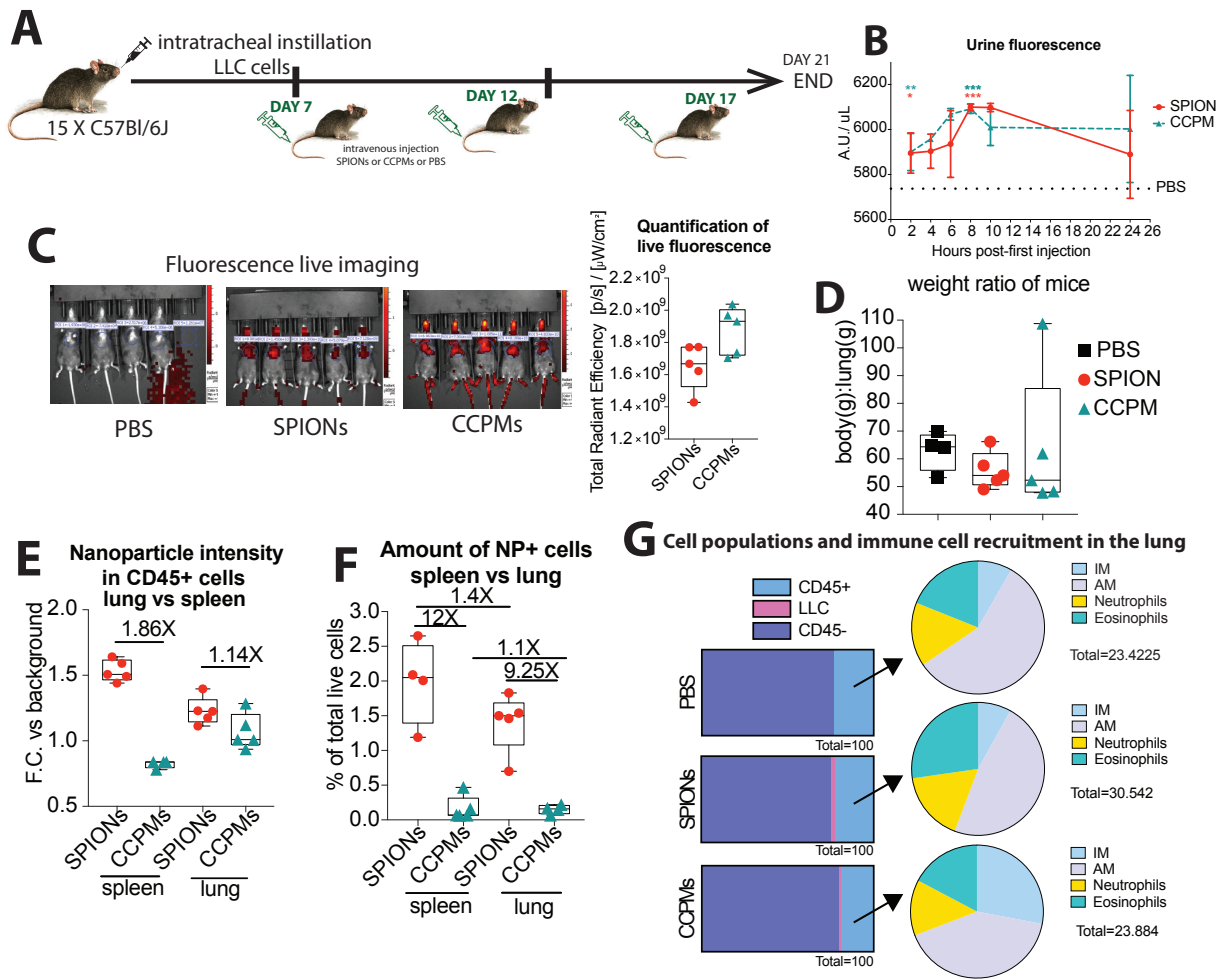
Figure 4.7. SPIONs, but not CCPMs, induce immune cell recruitment to the lung but are also taken up by cells of the spleen and liver. A. C57Bl/6 mice were intratracheally instilled with LLC cells. SPIONs, CCPMs, or PBS were intravenously injected one week later for a total of three administrations. **B**. Detection of nanoparticle fluorescence in urine of mice administered SPIONs or CCPMs. **C**. Live nanoparticle fluorescence detection and quantification in mice. **D**. Ratio of body to lung weight of mice. Nanoparticle intensity (**E**) and cell uptake (**F**) was evaluated in the lungs and spleen of mice by flow cytometry. **G**. Changes in cell populations of the lung. Data reported as n ± Standard Error of the Mean (SEM). One-way ANOVA (*): * p < 0.01, ** p < 0.001, *** p < 0.0001. *Experiment was in collaboration with AG Rocio Sotillo at the DKFZ, Heidelberg, Germany; experiment was constructed, implemented and analyzed by me.*
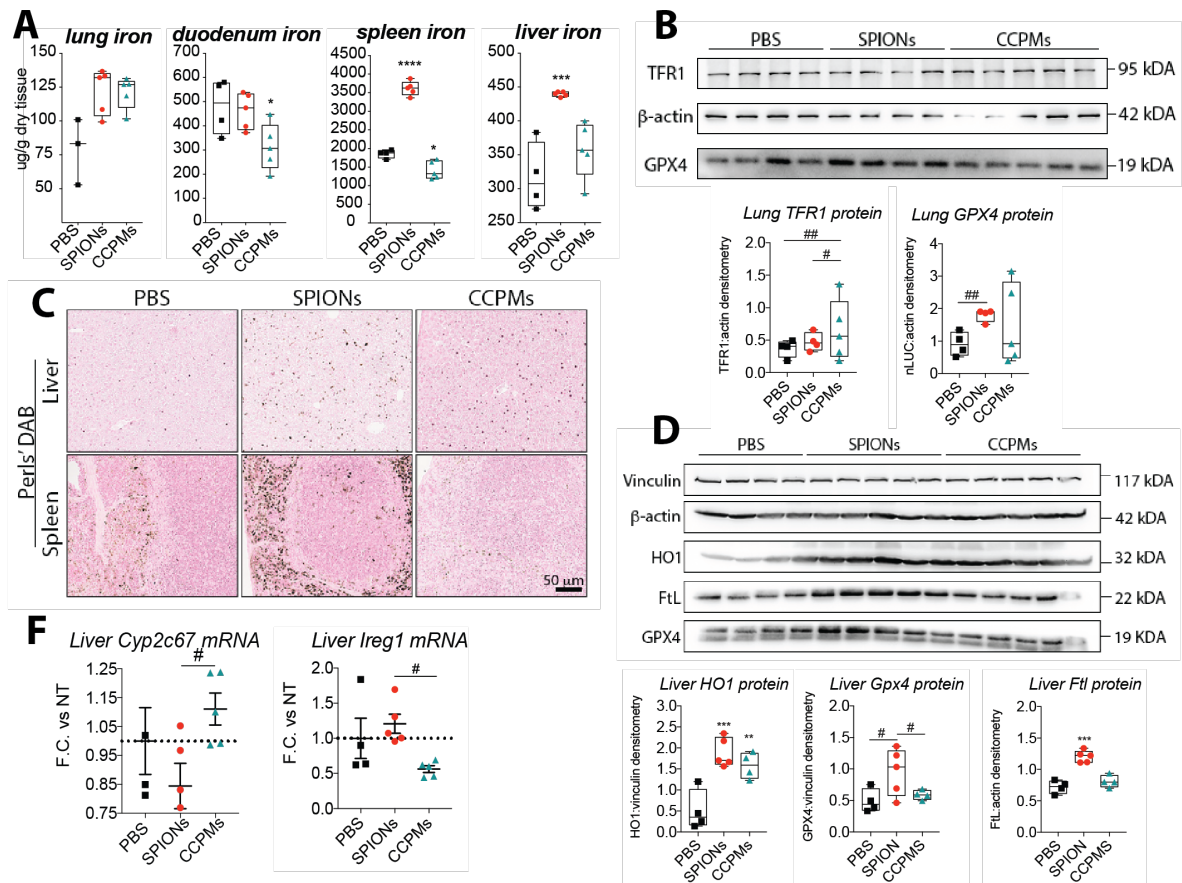
Figure 4.8. Iron and protein levels in response to SPION, CCPM or PBS administration in mice. A. Non-heme iron tissue in the lung, duodenum, spleen, and liver of SPION, CCPM and PBS administered mice. **B**. TFR1 and GPX4 protein levels in lungs of mice. **C**. Perls' blue Prussian DAB staining in the spleen and liver. **D**. HO1, FtL and GPX4 protein levels in the liver. **F**. Liver mRNA expression of *CYP2C67* and *Ireg1*. Data reported as n ± Standard Error of the Mean (SEM). One-way ANOVA (*) or students' t-test (#): * p < 0.01, ** p < 0.001, *** p < 0.0001. *Experiment was in collaboration with AG Rocio Sotillo at the DKFZ, Heidelberg, Germany; experiment was constructed, implemented and analyzed by me.*

Section 4.9: Discussion

Cell specific targeting is an important part of adjuvant therapies[327]. Since the efficacy of anti-cancer therapies is dependent on the amount of anti-inflammatory tumor-associated macrophages (TAMs) within the tumor micro-environment (TME)[328,329], the ability to target macrophages and reduce their interference in lung cancer is a promising therapeutic strategy. This data shows that SPIONs are preferentially taken up by macrophages and that SPION treated macrophages activate to a pro-inflammatory phenotype. When co-cultured with cancer cells, SPION-activated macrophages reduced cancer cell proliferation and induced cancer cell death (Figure 4.2). Oxidative stress occurred in LLC cells when treated with SPIONs, and not CCPMs, in co-cultures with BMDMs (Figure 4.3) demonstrates the triggered response in macrophages by iron that then induces cancer cell effects. The mechanism by which SPION-activated macrophages induce cell death in LLC cells was through the secretion of toxic oxidative species, including nitric oxide and reactive nitrogen species (ROS/RNS) (Figure 4.4, 4.5 and 4.6). LLC cell death was also dependent on the activity of TLR4 mediated and iron stimulated pathways in macrophages (Figure 4.5). The addition of other pro-inflammatory stimulants, such as heme or LPS, to co-cultures did not produce the same response in LLC cells, indicating the unique effect of SPIONs to activate macrophages and the associated cancer cell death. A schematic figure showing a summary of this data is shown in Figure 4.9.
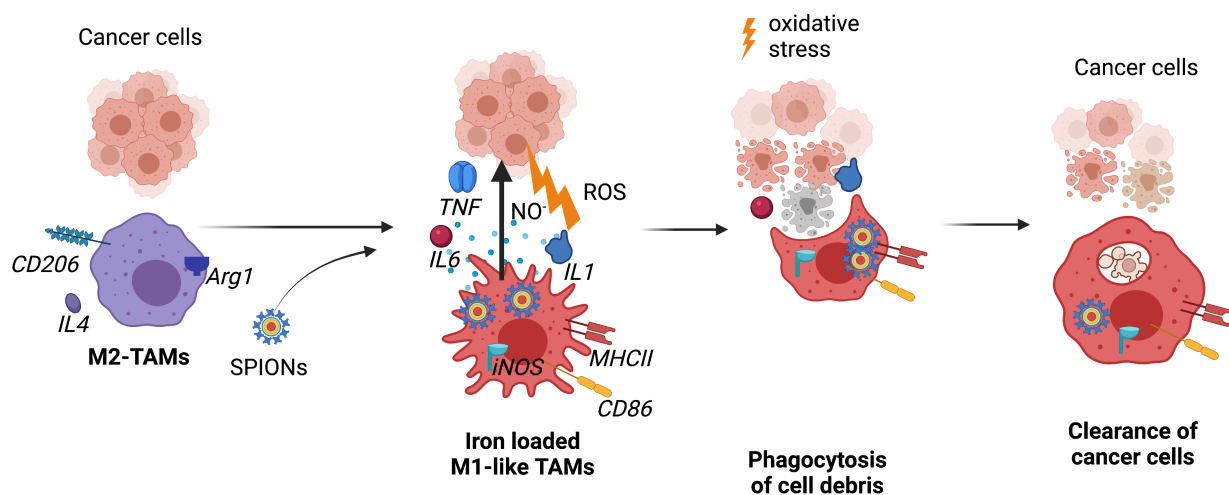
Figure 4.9. Summary schematic of Chapter 4: SPION-loaded macrophages reduce cancer cell proliferation and induce cancer cell death. Bone marrow-derived macrophages when co-cultured with LLC cancer cells are in an anti-inflammatory/suppressive phenotype. Upon treatment of SPIONs, macrophages are induced to a pro-inflammatory phenotype, where an increase in pro-inflammatory cytokines, such as TNF and IL6, as well as oxidative reactive species (ROS), such as nitric oxide (NO), occurs. Macrophages increase the levels of the enzyme iNOS and the surface proteins CD86 and MHCII. The secretions from macrophages induce oxidative stress in cancer cells and result in a decrease in cancer cell proliferation or cancer cell death. Macrophages then engage in efferocytosis and clear dead cell debris.

Inflammatory macrophages secrete toxic oxidative species and inflammatory cytokines as well as clear away dying cells by phagocytosis. From the initial characterization of the SPION induced macrophage phenotype the activation of inflammatory macrophages by SPIONs was observed to occur as early as 6 h (Figure 3.6). In SPION treated co-cultures at 24 h, LLC-derived CFSE signal increased in macrophages (Figure 4.2D). However, a decrease in cancer cell numbers was only detected at 48 h which suggests that an inflammatory burst from macrophages could have caused cell death in a small portion of LLC cells at an earlier time point. The inability to detect the difference in cell numbers may be due to exponential growth dynamics of LLC cells, where the reduction of cell numbers is not detected until a prolonged exposure to toxic oxidative species secreted from macrophages over time significantly decelerates the rate of LLC cell division. LLC cells were observed to experience an Nrf2 response at 48 h, suggesting that the latter may be a primary factor mitigating LLC cell death and would then parallel models of chronic inflammation[103].

From these experiments, one question that arises is the duration of the inflammatory activation of macrophages. Biphasic responses have been observed for many innate immune cells, including macrophages and are necessary to prevent chronic inflammation and inflammatory exhaustion[330]. Studies have shown that prolonged exposure of macrophages to inflammatory stimuli results in functionally exhausted resident macrophages in the lungs, which exhibit reduced efferocytosis, impaired phagocytosis and chronic expression of inflammatory cytokines[167,168]. Under chronic inflammatory conditions, such as within the tumor microenvironment (TME), prolonged exposure of macrophages to anti-cancer therapies could result in exhausted macrophage inflammatory responses manifesting in problematic responses such as immune tolerance to therapy or immune evasion of cancer cells. Under these conditions, the magnitude and duration of the inflammatory response by pro-inflammatory macrophages is still unclear[103]. Gaining deeper insights into this would provide an understanding of how to strategically design an efficacious regimen for SPION therapy to activate macrophages within the TME in lung cancer. A heterogeneous population of CFSE+ and CFSE- macrophages were observed in the co-cultures, suggesting a dynamic population of phagocytotic and non-phagocytic macrophages. The switching between macrophage polarized states (from anti-inflammatory to pro-inflammatory, and vice versa) could constantly be occurring, depending on the immediate stimuli of their environment as well as cell-intrinsic negative feedback signals. This could also indicate that the inflammatory activation of a macrophage is brief or cyclical, where macrophages move between activated and "de-activated" states. A high interval time course experiment evaluated by flow cytometry

examining the amount of phagocytosis (determined by internalized LLC-derived CFSE) in conjunction with the expression of pro-inflammatory markers in macrophages from SPION treated co-cultures could help elucidate whether macrophages that cycle through activated states over time correlate with phagocytic activity, as well as provide information about the magnitude of inflammatory macrophage response under chronic inflammatory conditions.

The stimulation of the adaptive immune system through the activation of CD4+ T cells by antigen-presenting cells (APCs) requires the presentation of MHCII as well as one of the CD80/CD86 co-stimulatory signals[331]. Studies have shown that, upon maturation, APCs increase expression of both MHCII and CD80/CD86 while concurrently decreasing phagocytic activity[332]. On the other hand, an increase in phagocytosis in conjunction with increased MHCII expression has been observed only in macrophages upon phagocytosis of endotoxin-containing particulates[333]. In this study, macrophages positive for LLC cell debris expressed low amounts of CD86/CD80 and MHCII, whereas macrophages that had not internalized cell debris had higher levels of CD86/CD80 and MHCII. Additionally, the expression of CD80/CD86 was greater on macrophages in the trans-well culturing system compared to the co-culturing system. This would indicate that the internalization of cell debris reduces APC function in macrophages and thus reduces the population of pro-inflammatory macrophages. Indeed, our co-culture time course showed that the percentage of CFSE+ macrophages increased over time, which suggests that a decrease in the population of pro-inflammatory macrophages is occurring and could likely contribute to a reduction of cancer cell death. Therefore, for continued cancer death to occur, a replenishment of either new unstimulated macrophages or a reactivation of macrophages is required. It is likely that, for sustained cytotoxicity, pulsing treatments of SPIONs will be necessary to maintain a pro-inflammatory activation in macrophages.

SPION induced macrophages have a specific phenotype that relies on both iron release from SPIONs and TLR4 activated inflammatory pathways. In co-cultures treated with LPS, TLR4 inhibition did not affect cancer cell viability, suggesting that inflammatory cytokines and oxidative species secreted from classical LPS activated macrophages do not adversely impact cancer cells. In SPION treated cultures, inhibiting TLR4 in macrophages substantially increased LLC cell viability. Both results demonstrate that while TLR4 stimulation of macrophages triggers inflammation, iron stimulation is needed for a specific type of inflammation in macrophages to mediate cancer cell death. However, it is important to note that LLC cells are known to express TLR4[334] and therefore the treatment of CLI, the TLR4 inhibitor, could be a contributing factor in these experiments. TLR4 stimulation of

macrophages has been shown to increase inflammatory cytokine production as well as nitric oxide[335]. Iron stimulated macrophages produce high amounts of reactive oxygen and nitric oxide species in addition to inflammatory cytokines[336]. Secretion of metabolites and oxidative species from SPION stimulated macrophages that differ from LPS treated macrophages explain the difference in live LLC cell numbers. Evaluation of secreted proteins and metabolites in the supernatant of co-cultures could provide insight into the secretions that are responsible for the cancer death mediated by SPION stimulated macrophage.

The type of cell death that is stimulated by SPION induced macrophages in LLC cells is still not well understood. The evaluation of cell viability by flow cytometry used the viability stain 7AAD, which is internalized by dead cells. Considering that cells internalize 7AAD when cell membrane leakiness occurs, an indication of late-stage apoptosis or necrosis[337], the oxidative stress responses in LLC cells may be an indication that apoptotic cell programmed cell death is induced rather than other forms of cell death, such as necroptosis or ferroptosis. In our system at the early time points (6 h and 24 h), LLC cells were not detected to undergo cell death and only effects at 48 h were observed. The expression of phosphatidylserine (PS) on the outside layer of the plasma membrane on cells is characterized as an early step in triggered apoptotic programming and is recognized by scavenger receptors on macrophages[318]. To identify at what timepoint cells are initiating apoptosis, quantification of PS+ apoptosing LLC cells over time could be done by flow cytometry using the PS specific stain annexin V. Once a timeframe has been established, proteome profiling of the co-cultured LLC cells as well as BMDMs could be done to assess the intricacies of cell death induced by the SPION-loaded macrophage.

To test SPIONs in a mouse model, intratracheal instillation of LLC cells, a lung adenocarcinoma cell line, was followed by intravenous injection (i.v.) of SPIONs. Surprisingly, very few LLC cells in the lungs of mice were found upon necropsy. One possibility for this is that LLC cells could have quickly metastasized to other regions of the body. This question was addressed by evaluating tissue sections from the liver, spleen, heart, kidney, and brain. Evidence of cancer cell metastases was found within the liver and brain sections of mice in all three experimental groups. Similar phenotypes are observed in human patients with lung adenocarcinoma, where the progression of disease is usually characterized by smaller tumors that metastasize quickly and are difficult to detect[88,150,338]. Despite the low levels of tumors, the preliminary testing still allowed for the evaluation of the distribution and uptake of SPIONs. It was found that SPIONs, and to a lesser degree CCPMs, localize primarily to organs that contain dense populations of macrophages. SPIONs induced inflammatory and oxidative stress

responses within the lungs, indicating the potential of SPIONs as an adjuvant therapy against lung cancer. Future testing will include other lung cancer mouse models that reliably generate lung tumors, such as the genetically engineered mouse model that harbors the *EML4-ALK* transposon mutation. Additionally, a specific targeted approach will be the focus of future SPION testing, where SPIONs are administered to the lungs of mice and to pulmonary macrophages. The test of intratracheal instillation of SPIONs in wildtype mice from Chapter 3 provides data to strategically design a dosing regimen.

Chemotherapies for lung cancer are traditionally given via i.v. which in effect significantly exposes the entire body to chemotherapeutics[339]. For some types of lung cancers that primarily remain in the lungs, the i.v. method of administration is not an efficient method for patients simply due to dose-limiting off-target and adverse effects that are associated with systemic administration[340]. For lung adenocarcinoma patients, systemic exposure of chemotherapeutics throughout the body could inadvertently be beneficial as i.v. injection could prime organs, such as the liver, for an inhospitable environment thus preventing metastasis[150,338]. Therefore, the injection of SPIONs intravenously could also be beneficial for specific types of lung adenocarcinoma patients.

Chapter 5: Conclusions and future directions

5.1 SPION-MEDIATED MACROPHAGE POLARIZATION

Several studies have found that macrophages with an anti-inflammatory phenotype are disease potentiators in cancer and therefore represent promising therapeutic targets[10,341]. Accumulation of iron in macrophages has been shown to activate macrophages to a pro-inflammatory phenotype[73,74,77,342,343], thus providing an avenue for iron-based anti-cancer therapies. This observation has initiated numerous investigations into the iron-mediated mechanisms that can facilitate macrophage polarization from anti-inflammatory to pro-inflammatory phenotypes. Since treatment with free iron is highly toxic, researchers have begun to explore a variety of alternative iron delivery mechanisms.

Nanoparticle delivery systems are of particular interest for drug development due to the high versatility in composition and biocompatibility. Nanoparticles that carry iron, such as super-paramagnetic iron oxide nanoparticles (SPIONs), have been available for use in medical procedures for several years, but their potential in initiating a pro-inflammatory phenotype in macrophages has only recently been discovered[189,228]. This discovery has sparked many questions about iron biology in macrophages and how iron can be used to manipulate macrophages as a tool against diseases[195,275,327,344]. In this study, the biological impact of a novel class of SPIONs was examined. The analysis compared an iron-loaded SPION to a control particle lacking an iron core, which provided important insights into the specific mechanisms of iron-induced pro-inflammatory macrophage activation. Specifically, SPIONs triggered a robust inflammation response in bone marrow-derived macrophages (BMDMs) compared to conventional iron sources, such as heme or iron dextran. This inflammatory response involved SPION uptake by phagocytosis and led to a pattern of inflammatory marker expression that paralleled heme and LPS induced activation in macrophages.

Intratracheal instillation of SPIONs into C57Bl/6 wildtype mice initiated an acute inflammatory reaction in the lung. This response led to an innate immune response that included inflammatory activation of macrophages, neutrophils, and eosinophils, as well as decreased the numbers of specific adaptive immune cells in the lung. The response was acute as resolution of the inflammatory response started at 48 h post-SPION administration, highlighting a short but robust mode of action. This pulse-like stimulation of the immune system is an indication that SPIONs could serve as adjuvants with other immunizing agents to boost anti-cancer immune responses.

One major flaw of many macrophage polarization studies has been the inability to translate work from mono-culture cell studies to *in vivo* systems[16]. A reason for this is the failure to recapitulate complex tissue settings in cell culture, which are necessary to provide the diversity and variability of environmental stimuli responsible for the macrophage subtype. Early studies that initially defined M2/anti-inflammatory subtypes were based on macrophage responses in reaction to a single cytokine stimulus, IL4[17,345]. While this served to set the foundations of the macrophage polarization field, studies published later were unable to identify these macrophage phenotypes *in vivo*[1]. At the same time, macrophage subtypes were being classified based on the differential expression of a discrete and limited panel of proteins and mRNA transcript levels in non-physiological culture systems, which was later found to be inconsistent with macrophages found in complex *in vivo* settings[345]. With current advances in flow cytometry methods, immunohistochemistry, and the ongoing revolution of technologies capable of single-cell resolution, macrophages are being described with an unbiased level of precision, allowing for the revision of the knowledge surrounding macrophages and macrophage phenotypes. These technologies allow not only for the spatial resolution in complex tissues but also for analyses under virtually any biological condition[5]. This has resulted in refining the macrophage polarization paradigm to a multidimensional model of activation, redefining classical macrophage phenotypes in the context of their associated functionality and microenvironmental tissue factors[26,109].

Defined macrophage subtypes have significant implications in potentiating diseases, and as a result, new subtypes are continuously being defined. The transient role of iron within the acute inflammatory responses is suspected to be mainly mediated by innate immune responses[346]. Since iron is the most prevalent metal within the body that regulates several necessary cellular processes, the control of iron levels both locally and systemically is extremely important. Therefore, a better characterization of the iron-loaded macrophage would provide us both with an understanding of how iron is regulated locally at the interface between host and pathogen, as well as how iron-loaded macrophages contribute to systemic iron regulation. A description of the iron-loaded macrophage is currently underway[73,249,256,306,347–349] though there are still inconsistencies in defining the specific iron-related metabolic and catabolic processes that regulate and define the model of the iron-induced pro-inflammatory phenotype[26,350]. Our results show that SPIONs induce a specific inflammatory macrophage phenotype that occurs both in cultured settings and within the body. An initial characterization of the SPION-loaded macrophage based on whole population (flow cytometry) and bulk techniques (mRNA expression) has been described, which provides a framework for iron-

loaded macrophages. To further verify this framework, future experiments will focus on isolating and single-cell sequencing macrophages from lung tissue and comparing differential mRNA expression of lung macrophages to our framework. Not only would this approach confirm our SPION focused data but also provide an in-depth insight into the heterogeneity of the iron-loaded macrophage phenotype. Future approaches would also include an in-depth multi-omics approach, where macrophages isolated from lung tissue would be evaluated by single-cell sequencing combined with mass cytometry and metabolomics to provide a clear model of the iron-loaded macrophage. This in-depth characterization would contribute to establishing the iron-loaded macrophage as a bona fide macrophage subtype.

Another major open question in the macrophage polarization field is the fate or lifetime of inflammatory macrophages. Tissue-resident macrophages have been shown to possess proliferative properties and remain in tissues for long periods of time, whereas monocytic-derived macrophages are generally short-lived[351]. Studies have postulated that macrophages that polarize to an M1/inflammatory phenotype either "de-activate" or undergo apoptosis upon the resolution of inflammation[19]. While it would seem logical for the process of de-activation to occur in tissue-resident macrophages, there is still a lack of data supporting this process for recruited monocytic-derived macrophages. Similarly, the process of de-activation in the iron-loaded macrophage (M1/inflammatory phenotype) is unclear in both the tissue-resident, such as the alveolar, as well as monocytic-derived macrophages. Studies that are investigating the multidimensional model of macrophage activation lack in-depth resolution to decipher cell-to-cell variability in macrophage responses, and as such, current investigations are working on elucidating the heterogeneous response in specific subtypes[4,26,45]. In the context of the iron-loaded macrophages, the cell fate likely has a significant impact on the local environment, as apoptosis of an iron-loaded macrophage could cause a flood of iron into the surrounding micro-niche, in effect reversing the initial protective macrophage role. The fate of iron-loaded macrophages could also have several implications in diseases such as cancer, where different macrophage subtypes have been found in varying micro-niche areas of the tumor microenvironment, influencing the surrounding tissue areas in different ways[175,352]. *In vivo* cell tracking of these macrophages would shed light on the lifespan as well as migration of iron-loaded macrophages under acute inflammatory conditions, such as infection, or chronic inflammatory conditions, such as cancer, and contribute to understanding iron homeostasis. Our fluorescently tagged SPIONs provide a useful tool for identifying and tracking SPION-loaded (and therefore iron-loaded) macrophages to answer these questions.

5.2 ANTI-CANCER POTENTIAL OF SPION ACTIVATED MACROPHAGES

Reported here is the fact that SPIONs induce a robust inflammatory response in macrophages, which negatively impacts cancer cell proliferation and induces cancer cell death. Our data indicated that the mechanism of cancer cell death is through the secretion of inflammatory and oxidative molecules from SPION activated macrophages. The inhibition of the TLR4 mediated inflammation as well as the inhibition of iNOS, responsible for producing reactive nitrogen species, resulted in a decrease in macrophage-mediated cancer cell death. The induced cancer death was further illustrated by an oxidative stress response in LLC cells co-cultures of SPION treatment. Together, our results suggest that SPIONs are a promising adjuvant anti-cancer therapy.

Analysis of SPION treated macrophages co-cultured with LLC cells indicated a strong potential as an anti-cancer therapeutic, leading us to test SPIONs in *in vivo* systems. Adjuvants are immune stimulants that are used in combination with immunotherapies to boost immune anti-cancer activity. Many vaccines currently employ adjuvants along with pathogen epitopes to induce a more robust immune response and increase antibody or T cell responses[353]. Some adjuvants for anti-cancer therapies being investigated are directed to specifically trigger TLR4 responses in the innate immune system[354]. SPION treatment triggered both iron and TLR4 signaling pathways in macrophages along with other innate immune cells, indicating opportunity as an adjuvant therapy when administered intratracheally (Section 4.4). However, despite obvious advantages of administering SPIONs via inhalation for lung cancer, intravenous (i.v.) injection is still the preferred administrative method[340]. Therefore, our initial testing of SPIONs in a lung cancer mouse model followed the conventional i.v. route. To implant lung cancer, LLC cells were intratracheally instilled into mice and administered three doses of nanoparticles intravenously, each one week apart. The mice showed no tumors, likely due to the highly metastatic nature of LLC adenocarcinoma cells. While an obvious solution to address this problem could have been to increase the number of cells instilled into each mouse, the observation of metastases in the liver and brain of mice prevented further experimentation with this model. Despite the specific lack of lung tumors, the immune cell and systemic iron distribution could still be evaluated in these mice. Changes in cell populations within the lungs upon treatment showed that SPIONs injection caused recruitment of innate immune cells to the lungs, pointing towards potential immune-boosting properties of this therapy. This experiment highlighted a few important details: i.v injection of SPIONs showed a less robust immune response in the lungs than intratracheal instillation of SPIONs, the

maximal rate of excretion of nanoparticles via urination occurred at 8 h after i.v. injection, indicating rapid clearance from the body, iron accumulated in organs that are heavily populated with macrophages other than the lungs, such as the spleen and the liver, and an oxidative stress response was recorded in the liver as evidenced by GPX4 protein levels. These all demonstrate sufficient reason to test SPIONs with a more directed approach in a lung cancer mouse model by intratracheal instillation for future studies.

Adjuvant therapies are currently being developed as non-specific innate immune system inducers in lungs[353]. Diseases such as influenza program the lung toward a more anti-inflammatory response, thus ensuring its penetrance and infection into the lung. Therefore, reprogramming pulmonary macrophages has the potential to protect against influenza and is currently being investigated with adjuvants. Intratracheal instillation of nanoparticles encasing *Streptococcus pneumoniae* bacterial lysates, in a pulse-like fashion, once a week for ten weeks, primed the innate immune system and reduced infection rates in mice[355]. In principle, the use of SPIONs as an immunostimulant for lung cancer patients would follow a similar principle and be highly applicable for those patients that have reached immune tolerance or exhausted traditional therapy routes. Considering that conventional chemotherapies are directed at killing cancer cells, administration of SPIONs to the TME after chemotherapy administration, as an adjuvant, could both potentiate anti-cancer cytotoxic effects as well as facilitate the clearing of apoptotic cells. Data from our intratracheal instillation experiment shows that an inflammatory pulse by SPION treatment could be as frequent as every five days. For clinical application, several obstacles may exist for this therapy. First, SPIONs must be able to aerosolize easily and therefore require stringent testing for physical gaseous properties, which may prolong the pre-clinical phase of testing. Secondly, the amount of SPIONs required for an acute response will likely need to be in a concentrated dose and dependent on the regimen, therefore requiring high volumes of supply. Without a permanent production from a manufacturer, SPION testing can be stalled at the pre-clinical phase of testing due to short supply. Third, the initiation of an acute immune reaction in patients is likely painful, which could affect patient compliance. The first three obstacles will require optimization of SPIONs administration as well as a stable supply of SPIONs from an industry-grade manufacturer.

Another caveat to discuss is that SPION administration will deposit iron within the body. For some lung cancer patients, an increased amount of iron in the body could induce adverse side effects. More specifically, this means that since increased iron stimulates cell growth and there is no dedicated route for iron excretion in the body, higher levels of circulating iron could be detrimental by providing an additional supply of iron that is accessible for cancer

126

cells. In our study, SPIONs were observed to be specifically internalized by phagocytic cells and less so by epithelial or endothelial cells. Upon internalization, we observed that inflammatory responses initiated by SPIONs lowered iron export by decreasing Fpn1 levels in macrophages co-cultured with LLC cells. Within the TME, iron released from SPIONs within macrophages would likely be retained and therefore not aid in tumor cell growth. Moreover, studies have indicated that in cancer patients, anemia (hemoglobin levels less than 10.0 g/dL) is an independent variable that affects overall survival and disease-free survival rates: ~39% of cancer patients upon diagnosis and 67% of patients receiving chemotherapy are anemic[356,357]. In fact, lung cancer patients diagnosed with preoperative anemia were found to experience a 19% increase in the risk of death[358]. An etiological factor for cancer-related anemia is high levels of chronic inflammation. Under these conditions, the presence of inflammatory cytokines, such as TNF and IL6, stimulate hepatocytes to increase levels of serum hepcidin which then, by binding to Fpn1, blocks the release of iron from macrophages, lowering circulating serum iron levels, giving rise to functional iron deficiency (FID)[359]. It is possible that our therapy could be beneficial to lung cancer patients beyond the direct effects of tumor reduction by providing a supplement of iron which would then help to alleviate FID. However, it remains to be determined how this source of iron impacts systemic iron stores over time warranting more comprehensive *in vivo* studies.

The application of adjuvants can result in a cytotoxic lymphocyte infiltration to the tumor and has been very promising to maximize the effectiveness of traditional chemotherapeutics in lung cancer[360]. However, the knowledge of whether neoadjuvant (administered before conventional chemotherapies) or adjuvant therapies (administered after conventional chemotherapies) offer a superior advantage in humans is also largely unknown. At the current stage in cancer research, the study of adjuvant therapy is still exploratory for NSCLC[361]. The two trials currently ongoing are with immune checkpoint therapies, anti-PD1 and anti-PDL1 agents, in combination with or without cisplatin-based chemotherapy[360–365]. While much of the ongoing progress of these trials are exhaustively detailed, the conclusive outcome from these trials will remain unknown until 2024-2027. Therefore, the detailed mechanisms, knowledge of efficacy and effectiveness as well applicability of adjuvant therapies in combination with conventional chemotherapies, remains unknown and highly reliant on pre-clinical mouse studies. Using our mouse system, a more in-depth understanding of the immune-stimulating effects of SPIONs within the lungs of mice has been elucidated. Chemotherapeutics kill cancer cells and so a SPIONs administration shortly after cisplatin-based chemotherapeutics would induce infiltration of immune cells, stimulate the clearing of

apoptotic and necrotic cells as well as induce further death of cancer cells. Therefore, it would be worthwhile to test SPIONs as an adjuvant with conventional cisplatin-based chemotherapeutics in lung cancer mouse models. Future testing will determine whether SPIONS are an effective avenue towards reducing tumor growth and improving lung cancer patient prognosis.

5.3 CONCLUSION

This work here has provided important insights into how iron, when released from SPIONs, activates macrophages, and is systemically regulated when administered to the lungs. More importantly, it has built the foundation for developing and testing an adjuvant anti-cancer therapy that can be used for lung cancer patients.

Chapter 6: Bibliography

1. Mills, C. D. & Ley, K. M1 and M2 macrophages: The chicken and the egg of immunity. **6**, (2014).

2. Dzik, J. M. The ancestry and cumulative evolution of immune reactions. *Acta Biochim Pol* **57**, 443–66 (2010).

3. Ginhoux, F. & Guilliams, M. Tissue-Resident Macrophage Ontogeny and Homeostasis. *Immunity* **44**, 439–449 (2016).

4. Lavin, Y. *et al.* Tissue-Resident Macrophage Enhancer Landscapes Are Shaped by the Local Microenvironment. *Cell* **159**, 1312–1326 (2014).

5. Bassler, K., Schulte-Schrepping, J., Warnat-Herresthal, S., Aschenbrenner, A. C. & Schultze, J. L. The Myeloid Cell Compartment—Cell by Cell. *Annu Rev Immunol* **37**, 1–25 (2019).

6. Jenkins, S. J. *et al.* Local macrophage proliferation, rather than recruitment from the blood, is a signature of TH2 inflammation. **332**, (2011).

7. Takata, K. *et al.* Induced-Pluripotent-Stem-Cell-Derived Primitive Macrophages Provide a Platform for Modeling Tissue-Resident Macrophage Differentiation and Function. *Immunity* **47**, 183-198.e6 (2017).

8. Varol, C., Yona, S. & Jung, S. Origins and tissue-context-dependent fates of blood monocytes. *Immunol Cell Biol* **87**, 30–38 (2009).

9. Mosser, D. M. & Edwards, J. P. Exploring the full spectrum of macrophage activation. *Nature Publishing Group* **8**, (n.d.).

10. Poltavets, A. S., Vishnyakova, P. A., Elchaninov, A. V., Sukhikh, G. T. & Fatkhudinov, T. K. Macrophage Modification Strategies for Efficient Cell Therapy. *Cells* **9**, 1535 (2020).

11. Cros, J. *et al.* Human CD14dim Monocytes Patrol and Sense Nucleic Acids and Viruses via TLR7 and TLR8 Receptors. *Immunity* **33**, 375–386 (2010).

12. Mantovani, A., Sozzani, S., Locati, M., Allavena, P. & Sica, A. Macrophage polarization: Tumor-associated macrophages as a paradigm for polarized M2 mononuclear phagocytes. **23**, (2002).

13. Murray, P. J. *et al.* Macrophage Activation and Polarization: Nomenclature and Experimental Guidelines. *Elsevier* **41**, (n.d.).

14. Italiani, P. & Boraschi, D. From monocytes to M1/M2 macrophages: Phenotypical vs. functional differentiation. **5**, (n.d.).

15. Orecchioni, M., Ghosheh, Y., Pramod, A. & Ley, K. Macrophage Polarization: Different Gene Signatures in M1(LPS+) vs. Classically and M2(LPS–) vs. Alternatively Activated Macrophages. *Frontiers in Immunology* **10**, 1084 (2019).

16. Martinez, F. O. & Gordon, S. The M1 and M2 paradigm of macrophage activation: time for reassessment. **6**, (n.d.).

17. Stein, M., Keshav, S., Harris, N. & Gordon, S. Interleukin 4 potently enhances murine macrophage mannose receptor activity: a marker of alternative immunologic macrophage activation. *J Exp Medicine* **176**, 287–292 (1992).

18. Nathan, C. F. Mechanisms of macrophage antimicrobial activity. *T Roy Soc Trop Med H* **77**, 620–630 (1983).

19. Murray, P. J. Macrophage Polarization. *Annu Rev Physiol* **79**, 541–566 (2016).

20. Mosser, D. M. The many faces of macrophage activation. *J Leukocyte Biol* **73**, 209–212 (2003).

21. Fleming, B. D. & Mosser, D. M. Regulatory macrophages: Setting the Threshold for Therapy. *Eur J Immunol* **41**, 2498–2502 (2011).

22. Mantovani, A. *et al.* The chemokine system in diverse forms of macrophage activation and polarization. **25**, (2004).

23. Gordon, S. & Martinez, F. O. Alternative activation of macrophages: Mechanism and functions. *Elsevier Inc.* **32**, (n.d.).

24. Martinez, F. O. Macrophage activation and polarization. *Front Biosci* **13**, 453 (2008).

25. Varga, T. *et al.* Highly Dynamic Transcriptional Signature of Distinct Macrophage Subsets during Sterile Inflammation, Resolution, and Tissue Repair. *J Immunol* **196**, 4771–4782 (2016).

26. Xue, J. *et al.* Transcriptome-Based Network Analysis Reveals a Spectrum Model of Human Macrophage Activation. *Elsevier Inc.* **40**, (2014).

27. Srikrishna, G. & Freeze, H. H. Endogenous Damage-Associated Molecular Pattern Molecules at the Crossroads of Inflammation and Cancer. *Neoplasia* **11**, 615–628 (2009).

28. Kawai, T. & Akira, S. Toll-like Receptors and Their Crosstalk with Other Innate Receptors in Infection and Immunity. *Immunity* **34**, 637–650 (2011).

29. Beutler, B. A. TLRs and innate immunity. *Blood* **113**, 1399–1407 (2009).

30. Sica, A. & Mantovani, A. Macrophage plasticity and polarization: in vivo veritas. **122**, (2012).

31. Lin, J.-D. *et al.* Single-cell analysis of fate-mapped macrophages reveals heterogeneity, including stem-like properties, during atherosclerosis progression and regression. *Jci Insight* **4**, e124574 (2019).

32. RANDOLPH, G. J. The fate of monocytes in atherosclerosis. *J Thromb Haemost* **7**, 28–30 (2009).

33. Sager, H. B. *et al.* Proliferation and Recruitment Contribute to Myocardial Macrophage Expansion in Chronic Heart Failure. *Circ Res* **119**, 853–864 (2016).

34. Cai, Y. *et al.* In Vivo Characterization of Alveolar and Interstitial Lung Macrophages in Rhesus Macaques: Implications for Understanding Lung Disease in Humans. *J Immunol* **192**, 2821–2829 (2014).

35. Shapouri-Moghaddam, A. *et al.* Macrophage plasticity, polarization, and function in health and disease. *Journal of Cellular Physiology* **233**, 6425–6440 (2018).

36. Grainger, J. R., Konkel, J. E., Zangerle-Murray, T. & Shaw, T. N. Macrophages in gastrointestinal homeostasis and inflammation. *Pflügers Archiv - European J Physiology* **469**, 527–539 (2017).

37. Murray, P. J. & Wynn, T. A. Protective and pathogenic functions of macrophage subsets. **11**, (n.d.).

38. immunology, M.-E. Delineating the origins, developmental programs and homeostatic functions of tissue-resident macrophages. (2018) doi:10.1093/intimm/dxy044.

39. Locati, M., Mantovani, A. & Sica, A. Macrophage Activation and Polarization as an Adaptive Component of Innate Immunity. *Elsevier Inc.* **120**, (2013).

40. Mantovani, A., Biswas, S. K., Galdiero, M., Sica, A. & Locati, M. Macrophage plasticity and polarization in tissue repair and remodelling. **229**, (2013).

41. Martinez, F. O., Helming, L. & Gordon, S. Alternative Activation of Macrophages: An Immunologic Functional Perspective. *Annu Rev Immunol* **27**, 451–483 (2009).

42. Jenkins, S. J. & Allen, J. E. Similarity and Diversity in Macrophage Activation by Nematodes, Trematodes, and Cestodes. *J Biomed Biotechnol* **2010**, 262609 (2010).

43. Mei, J. *et al.* Prognostic impact of tumor-associated macrophage infiltration in non-small cell lung cancer: A systemic review and meta-analysis. **7**, (2016).

44. Jackute, J. *et al.* Distribution of M1 and M2 macrophages in tumor islets and stroma in relation to prognosis of non-small cell lung cancer. *BMC Immunology* **19**, 3 (2018).

45. Lavin, Y. *et al.* Innate Immune Landscape in Early Lung Adenocarcinoma by Paired Single-Cell Analyses. *Cell* **169**, 750-765.e17 (2017).

46. Kieler, M., Hofmann, M. & Schabbauer, G. More than just protein building blocks: How amino acids and related metabolic pathways fuel macrophage polarization. *Febs J* (2021) doi:10.1111/febs.15715.

47. Modolell, M., Corraliza, I. M., Link, F., Soler, G. & Eichmann, K. Reciprocal regulation of the nitric oxide synthase/arginase balance in mouse bone marrow-derived macrophages by TH 1 and TH 2 cytokines. *Eur J Immunol* **25**, 1101–1104 (1995).

48. Molgora, M. *et al.* TREM2 Modulation Remodels the Tumor Myeloid Landscape Enhancing Anti-PD-1 Immunotherapy. *Cell* **182**, 886-900.e17 (2020).

49. Nairz, M. *et al.* "Ride on the ferrous wheel" - The cycle of iron in macrophages in health and disease. *Elsevier GmbH.* **220**, (2015).

50. Recalcati, S., Gammella, E. & Cairo, G. Ironing out Macrophage Immunometabolism. *Pharm* **12**, 94 (2019).

51. Soares, M. P. & Hamza, I. Macrophages and Iron Metabolism. *Elsevier Inc.* **44**, (n.d.).

52. Klei, T. R. L., Meinderts, S. M., Berg, T. K. van den & Bruggen, R. van. From the Cradle to the Grave: The Role of Macrophages in Erythropoiesis and Erythrophagocytosis. *Front Immunol* **8**, 73 (2017).

53. Gomes, A. C. *et al.* IFN-γ–Dependent Reduction of Erythrocyte Life Span Leads to Anemia during Mycobacterial Infection. *J Immunol* **203**, 2485–2496 (2019).

54. Hamza, I. & Dailey, H. A. One ring to rule them all: Trafficking of heme and heme synthesis intermediates in the metazoans. *Elsevier B.V.* **1823**, (2012).

55. White, C. *et al.* HRG1 is essential for heme transport from the phagolysosome of macrophages during erythrophagocytosis. *Elsevier Inc.* **17**, (2013).

56. Gozzelino, R. & Soares, M. P. Coupling Heme and Iron Metabolism via Ferritin H Chain. *Antioxid Redox Sign* **20**, 1754–1769 (2014).

57. Muckenthaler, M. U., Rivella, S., Hentze, M. W. & Galy, B. A Red Carpet for Iron Metabolism. *Elsevier Inc.* **3**, (2017).

58. Knutson, M. D., Oukka, M., Koss, L. M., Aydemir, F. & Wessling-Resnick, M. Iron release from macrophages after erythrophagocytosis is up-regulated by ferroportin 1 overexpression and down-regulated by hepcidin. **102**, (2005).

59. Arosio, P., Elia, L. & Poli, M. Ferritin, cellular iron storage and regulation. *IUBMB Life* **69**, 414–422 (2017).

60. Arosio, P., Ingrassia, R. & Cavadini, P. Ferritins: A family of molecules for iron storage, antioxidation and more. *Biochimica Et Biophysica Acta Bba - Gen Subj* **1790**, 589–599 (2009).

61. Donovan, A. *et al.* The iron exporter ferroportin/Slc40a1 is essential for iron homeostasis. **1**, (2005).

62. Nemeth, E. *et al.* Hepcidin Regulates Cellular Iron Efflux by Binding to Ferroportin and Inducing Its Internalization. *Science* **306**, (n.d.).

63. Sacco, A. *et al.* Iron Metabolism in the Tumor Microenvironment—Implications for Anti-Cancer Immune Response. *Cells* **10**, 303 (2021).

64. Simpson, I. a *et al.* A novel model for brain iron uptake: introducing the concept of regulation. *Nature Publishing Group* **35**, (2014).

65. Lal, A. Iron in Health and Disease: An Update. *Indian J Pediatrics* 1–8 (2019) doi:10.1007/s12098-019-03054-8.

66. Dev, S. & Babitt, J. L. Overview of iron metabolism in health and disease. (2017) doi:10.1111/hdi.12542.

67. Chen, C. *et al.* Snx3 Regulates Recycling of the Transferrin Receptor and Iron Assimilation. *Cell Metab* **17**, 343–352 (2013).

68. Kukulj, S. *et al.* Altered iron metabolism, inflammation, transferrin receptors, and ferritin expression in non-small-cell lung cancer. **27**, (2010).

69. Cairo, G., Recalcati, S., Mantovani, A. & Locati, M. Iron trafficking and metabolism in macrophages: Contribution to the polarized phenotype. **32**, (2011).

70. Recalcati, S. *et al.* Macrophage ferroportin is essential for stromal cell proliferation in wound healing. *Haematologica* **104**, haemat.2018.197517 (2018).

71. Sabelli, M. *et al.* Human macrophage ferroportin biology and the basis for the ferroportin disease. **65**, (2017).

72. "Pumping iron"—how macrophages handle iron at the systemic, microenvironmental, and cellular levels. (n.d.) doi:10.1007/s00424-017-1944-8.

73. Vinchi, F. *et al.* Hemopexin therapy reverts heme-induced proinflammatory phenotypic switching of macrophages in a mouse model of sickle cell disease. *Blood* **127**, 473–486 (2016).

74. Recalcati, S. *et al.* Differential regulation of iron homeostasis during human macrophage polarized activation. **40**, (n.d.).

75. Pereira, M. *et al.* Acute Iron Deprivation Reprograms Human Macrophage Metabolism and Reduces Inflammation In Vivo. *Cell Reports* **28**, 498-511.e5 (2019).

76. Recalcati, S., Locati, M., Gammella, E., Invernizzi, P. & Cairo, G. Iron levels in polarized macrophages: Regulation of immunity and autoimmunity. *Elsevier B.V.* **11**, (2012).

77. Zhou, Y. *et al.* Iron overloaded polarizes macrophage to proinflammation phenotype through ROS/acetyl-p53 pathway. *Cancer Medicine* **7**, 4012–4022 (2018).

78. Marques, O., Neves, J., Horvat, N. K., Altamura, S. & Muckenthaler, M. U. Mild Attenuation of the Pulmonary Inflammatory Response in a Mouse Model of Hereditary Hemochromatosis Type 4. *Front Physiol* **11**, 589351 (2021).

79. Neves, J. *et al.* Disruption of the Hepcidin/Ferroportin Regulatory System Causes Pulmonary Iron Overload and Restrictive Lung Disease. *The Authors* (2017) doi:10.1016/j.ebiom.2017.04.036.

80. Neves, J., Haider, T., Gassmann, M. & Muckenthaler, M. U. Iron Homeostasis in the Lungs—A Balance between Health and Disease. *Pharm* **12**, 5 (2019).

81. Siegel, R. L., Miller, K. D. & Jemal, A. Cancer statistics, 2020. *Ca Cancer J Clin* **70**, 7–30 (2020).

82. Marques, O. *et al.* Iron-Related Parameters are Altered Between C57BL/6N and C57BL/6J Mus Musculus Wild-Type Substrains. *Hemasphere* 1 (2019) doi:10.1097/hs9.0000000000000304.

83. Mahowald, N. M. *et al.* Atmospheric Iron Deposition: Global Distribution, Variability, and Human Perturbations*. *Annu Rev Mar Sci* **1**, 245–278 (2009).

84. Falcone, L. M. *et al.* Inhalation of iron-abundant gas metal arc welding-mild steel fume promotes lung tumors in mice. *Toxicology* **409**, 24–32 (2018).

85. Dixon, S. J. & Stockwell, B. R. The role of iron and reactive oxygen species in cell death. *Nature Chemical Biology* **10**, 9 (2014).

86. Ali, M. K. *et al.* Role of iron in the pathogenesis of respiratory disease. *Int J Biochem Cell Biology* **88**, 181–195 (2017).

87. Eeden, S. F. van & Akata, K. Macrophages—the immune effector guardians of the lung: impact of corticosteroids on their functional responses. *Clin Sci* **134**, 1631–1635 (2020).

88. Ferone, G., Lee, M. C., Sage, J. & Berns, A. Cells of origin of lung cancers: lessons from mouse studies. *Gene Dev* **34**, 1017–1032 (2020).

89. Lee, J.-H. & Rawlins, E. L. Developmental mechanisms and adult stem cells for therapeutic lung regeneration. *Dev Biol* **433**, 166–176 (2018).

90. Kim, C. F. Intersections of lung progenitor cells, lung disease and lung cancer. *European Respir Rev* **26**, 170054 (2017).

91. Leach, J. P. & Morrisey, E. E. Repairing the lungs one breath at a time: How dedicated or facultative are you? *Gene Dev* **32**, 1461–1471 (2018).

92. Byrne, A. J., Mathie, S. A., Gregory, L. G. & Lloyd, C. M. Pulmonary macrophages: key players in the innate defence of the airways. *Thorax* **70**, 1189 (2015).

93. Puttur, F., Gregory, L. G. & Lloyd, C. M. Airway macrophages as the guardians of tissue repair in the lung. *Immunol Cell Biol* **97**, 246–257 (2019).

94. Cordeiro, J. V. & Jacinto, A. The role of transcription-independent damage signals in the initiation of epithelial wound healing. *Nat Rev Mol Cell Bio* **14**, 249–262 (2013).

95. Dahl, M. *et al.* Protection against inhaled oxidants through scavenging of oxidized lipids by macrophage receptors MARCO and SR-AI/II. *J Clin Invest* **117**, 757–764 (2007).

96. Amit, I., Winter, D. R. & Jung, S. The role of the local environment and epigenetics in shaping macrophage identity and their effect on tissue homeostasis. *Nat Immunol* **17**, 18–25 (2015).

97. Ogger, P. P. & Byrne, A. J. Macrophage metabolic reprogramming during chronic lung disease. *Mucosal Immunol* 1–14 (2020) doi:10.1038/s41385-020-00356-5.

98. Arredouani, M. *et al.* The Scavenger Receptor MARCO Is Required for Lung Defense against Pneumococcal Pneumonia and Inhaled Particles. *J Exp Medicine* **200**, 267–272 (2004).

99. Arredouani, M. S. *et al.* The Macrophage Scavenger Receptor SR-AI/II and Lung Defense against Pneumococci and Particles. *Am J Resp Cell Mol* **35**, 474–478 (2006).

100. Arredouani, M. S. *et al.* MARCO Is the Major Binding Receptor for Unopsonized Particles and Bacteria on Human Alveolar Macrophages. *J Immunol* **175**, 6058–6064 (2005).

101. Zizzo, G., Hilliard, B. A., Monestier, M. & Cohen, P. L. Efficient Clearance of Early Apoptotic Cells by Human Macrophages Requires M2c Polarization and MerTK Induction. *J Immunol* **189**, 3508–3520 (2012).

102. Sipka, T. *et al.* Damage-Induced Calcium Signaling and Reactive Oxygen Species Mediate Macrophage Activation in Zebrafish. *Front Immunol* **12**, 636585 (2021).

103. Krzyszczyk, P., Schloss, R., Palmer, A. & Berthiaume, F. The Role of Macrophages in Acute and Chronic Wound Healing and Interventions to Promote Pro-wound Healing Phenotypes. *Front Physiol* **9**, 419 (2018).

104. Nguyen-Chi, M. *et al.* TNF signaling and macrophages govern fin regeneration in zebrafish larvae. *Cell Death Dis* **8**, e2979–e2979 (2017).

105. Simkin, J. *et al.* Macrophages are required to coordinate mouse digit tip regeneration. *Development* **144**, dev.150086 (2017).

106. Petrie, T. A. *et al.* Macrophages modulate adult zebrafish tail fin regeneration. *Development* **141**, 2581–2591 (2014).

107. Godwin, J. W., Pinto, A. R. & Rosenthal, N. A. Macrophages are required for adult salamander limb regeneration. *Proc National Acad Sci* **110**, 9415–9420 (2013).

108. Guilliams, M. *et al.* Dendritic cells, monocytes and macrophages: a unified nomenclature based on ontogeny. *Nat Rev Immunol* **14**, 571–8 (2014).

109. Ginhoux, F., Schultze, J. L., Murray, P. J., Ochando, J. & Biswas, S. K. New insights into the multidimensional concept of macrophage ontogeny, activation and function. *Nat Immunol* **17**, 34–40 (2016).

110. Schyns, J., Bureau, F. & Marichal, T. Lung Interstitial Macrophages: Past, Present, and Future. *J Immunol Res* **2018**, 1–10 (2018).

111. Guilliams, M. *et al.* Alveolar macrophages develop from fetal monocytes that differentiate into long-lived cells in the first week of life via GM-CSF. *J Exp Medicine* **210**, 1977–1992 (2013).

112. Chakarov, S. *et al.* Two distinct interstitial macrophage populations coexist across tissues in specific subtissular niches. *Science* **363**, eaau0964 (2019).

113. Evren, E. *et al.* Distinct developmental pathways from blood monocytes generate human lung macrophage diversity. *Immunity* **54**, 259-275.e7 (2021).

114. Gibbings, S. L. *et al.* Three Unique Interstitial Macrophages in the Murine Lung at Steady State. *Am J Resp Cell Mol* **57**, 66–76 (2017).

115. Jakubzick, C. *et al.* Minimal Differentiation of Classical Monocytes as They Survey Steady-State Tissues and Transport Antigen to Lymph Nodes. *Elsevier Inc.* **39**, (n.d.).

116. Sabatel, C. *et al.* Exposure to Bacterial CpG DNA Protects from Airway Allergic Inflammation by Expanding Regulatory Lung Interstitial Macrophages. *Immunity* **46**, 457–473 (2017).

117. Misharin, A. V., Morales-Nebreda, L., Mutlu, G. M., Budinger, G. R. S. & Perlman, H. Flow Cytometric Analysis of Macrophages and Dendritic Cell Subsets in the Mouse Lung. *Am J Resp Cell Mol* **49**, 130522202035005 (2013).

118. Yona, S. *et al.* Fate Mapping Reveals Origins and Dynamics of Monocytes and Tissue Macrophages under Homeostasis. *Elsevier* **38**, (2013).

119. Sorokin, S. P. & Brain, J. D. Pathways of clearance in mouse lungs exposed to iron oxide aerosols. *Anatomical Rec* **181**, 581–625 (1975).

120. Georgoudaki, A. *et al.* Reprogramming Tumor-Associated Macrophages by Antibody Targeting Inhibits Cancer Progression and Metastasis. **15**, (2016).

121. Deschemin, J.-C., Mathieu, J. R. R., Zumerle, S., Peyssonnaux, C. & Vaulont, S. Pulmonary Iron Homeostasis in Hepcidin Knockout Mice. *Front Physiol* **8**, 804 (2017).

122. Philippot, Q. *et al.* Increased Iron Sequestration in Alveolar Macrophages in Chronic Obtructive Pulmonary Disease. *Plos One* **9**, e96285 (2014).

123. Andrianaki, A. M. *et al.* Iron restriction inside macrophages regulates pulmonary host defense against Rhizopus species. *Nat Commun* **9**, 3333 (2018).

124. Lee, J. *et al.* Bronchoalveolar lavage (BAL) cells in idiopathic pulmonary fibrosis express a complex pro-inflammatory, pro-repair, angiogenic activation pattern, likely associated with macrophage iron accumulation. *Plos One* **13**, e0194803 (2018).

125. Niethammer, P., Grabher, C., Look, A. T. & Mitchison, T. J. A tissue-scale gradient of hydrogen peroxide mediates rapid wound detection in zebrafish. *Nature* **459**, 996–999 (2009).

126. Janssen, W. J., Stefanski, A. L., Bochner, B. S. & Evans, C. M. Control of lung defence by mucins and macrophages: ancient defence mechanisms with modern functions. *Eur Respir J* **48**, 1201–1214 (2016).

127. Anrather, J., Racchumi, G. & Iadecola, C. NF-κB Regulates Phagocytic NADPH Oxidase by Inducing the Expression of gp91 phox *. *J Biol Chem* **281**, 5657–5667 (2006).

128. Yoo, S. K., Starnes, T. W., Deng, Q. & Huttenlocher, A. Lyn is a redox sensor that mediates leukocyte wound attraction in vivo. *Nature* **480**, 109–112 (2011).

129. Bewley, M. A. *et al.* Impaired Mitochondrial Microbicidal Responses in Chronic Obstructive Pulmonary Disease Macrophages. *Am J Resp Crit Care* **196**, 845–855 (2017).

130. Taylor, A. E. *et al.* Defective macrophage phagocytosis of bacteria in COPD. *Eur Respir J* **35**, 1039–1047 (2009).

131. Frank, J. A., Wray, C. M., McAuley, D. F., Schwendener, R. & Matthay, M. A. Alveolar macrophages contribute to alveolar barrier dysfunction in ventilator-induced lung injury. *Am J Physiol-lung C* **291**, L1191–L1198 (2006).

132. Naidu, B. V. *et al.* Early activation of the alveolar macrophage is critical to the development of lung ischemia-reperfusion injury. *J Thorac Cardiovasc Surg* **126**, 200–207 (2003).

133. Albright, J. M. *et al.* Advanced Age Alters Monocyte and Macrophage Responses. *Antioxid Redox Sign* **25**, 805–815 (2016).

134. Knapp, S. *et al.* Alveolar Macrophages Have a Protective Antiinflammatory Role during Murine Pneumococcal Pneumonia. *Am J Resp Crit Care* **167**, 171–179 (2003).

135. Adjei, A. A. Lung Cancer Worldwide. *J Thorac Oncol* **14**, 956 (2019).

136. Chen, Z., Fillmore, C. M., Hammerman, P. S., Kim, C. F. & Wong, K.-K. Non-small-cell lung cancers: a heterogeneous set of diseases. *Nature Reviews Cancer* **14**, 535–546 (2014).

137. Sutherland, K. D. & Berns, A. Cell of origin of lung cancer. *Molecular Oncology* **4**, 397–403 (2010).

138. Frese, K. K. & Tuveson, D. A. Maximizing mouse cancer models. *Nature Reviews Cancer* **7**, 654–658 (2007).

139. Dutt, A. & Wong, K.-K. Mouse Models of Lung Cancer. *Clinical Cancer Research* **12**, 4396s–4402s (2006).

140. Tammela, T. & Sage, J. Investigating Tumor Heterogeneity in Mouse Models. *Annu Rev Cancer Biology* **4**, 1–21 (2019).

141. Day, C.-P., Merlino, G. & Van Dyke, T. Preclinical Mouse Cancer Models: A Maze of Opportunities and Challenges. *Cell* **163**, 39–53 (2015).

142. Hynds, R. E. *et al.* Progress towards non-small-cell lung cancer models that represent clinical evolutionary trajectories. *Open Biol* **11**, 200247 (2021).

143. Ambrogio, C. *et al.* Modeling Lung Cancer Evolution and Preclinical Response by Orthotopic Mouse Allografts. *Cancer Res* **74**, 5978–5988 (2014).

144. Jung, J., Seol, H. S. & Chang, S. The Generation and Application of Patient-Derived Xenograft Model for Cancer Research. *Cancer Res Treat* **50**, 1–10 (2018).

145. Sharpless, N. E. & DePinho, R. A. The mighty mouse: genetically engineered mouse models in cancer drug development. *Nat Rev Drug Discov* **5**, 741–754 (2006).

146. Weber, J. & Rad, R. Engineering CRISPR mouse models of cancer. *Curr Opin Genet Dev* **54**, 88–96 (2019).

147. Platt, R. J. *et al.* CRISPR-Cas9 Knockin Mice for Genome Editing and Cancer Modeling. *Cell* **159**, 440–455 (2014).

148. Maddalo, D. *et al.* In vivo engineering of oncogenic chromosomal rearrangements with the CRISPR/Cas9 system. *Nature* **516**, 423–427 (2014).

149. McFadden, D. G. *et al.* Mutational landscape of EGFR-, MYC-, and Kras-driven genetically engineered mouse models of lung adenocarcinoma. *Proceedings of the National Academy of Sciences* **113**, E6409–E6417 (2016).

150. Busch, S. E. *et al.* Lung Cancer Subtypes Generate Unique Immune Responses. *The Journal of Immunology* **197**, 4493–4503 (2016).

151. Heath, J. L., Weiss, J. M., Lavau, C. P. & Wechsler, D. S. Iron deprivation in cancer- potential therapeutic implications. **5**, (2013).

152. Jung, M., Mertens, C., Tomat, E. & Brüne, B. Iron as a Central Player and Promising Target in Cancer Progression. *International Journal of Molecular Sciences* **20**, 273 (2019).

153. Kuang, Y. & Wang, Q. Iron and Lung Cancer. *Cancer Lett* **464**, 56–61 (2019).

154. Zhang, C. & Zhang, F. Iron homeostasis and tumorigenesis: molecular mechanisms and therapeutic opportunities. **6**, (2015).

155. Torti, S. V. & Torti, F. M. Iron and Cancer: 2020 Vision. *Cancer Res* **80**, 5435–5448 (2020).

156. Richmond, H. G. Induction of Sarcoma in the Rat by Iron—Dextran Complex. *Brit Med J* **1**, 947 (1959).

157. Campbell, J. A. Effects of Precipitated Silica and of Iron Oxide on the Incidence of Primary Lung Tumours in Mice. *Brit Med J* **2**, 275 (1940).

158. Muka, T. *et al.* Dietary mineral intake and lung cancer risk: the Rotterdam Study. *Eur J Nutr* **56**, 1637–1646 (2017).

159. Boyd, J. T., Doll, R., Faulds, J. S. & Leiper, J. Cancer of the lung in iron ore (haematite) miners. *Brit J Ind Med* **27**, 97 (1970).

160. Edgren, G. *et al.* Donation Frequency, Iron Loss, and Risk of Cancer Among Blood Donors. *JNCI: Journal of the National Cancer Institute* **100**, 572–579 (2008).

161. Jian, J. *et al.* Effects of iron deficiency and iron overload on angiogenesis and oxidative stress-a potential dual role for iron in breast cancer. *Elsevier Inc.* **50**, (2011).

162. Ward, H. A. *et al.* Haem iron intake and risk of lung cancer in the European Prospective Investigation into Cancer and Nutrition (EPIC) cohort. *Eur J Clin Nutr* **73**, 1122–1132 (2019).

163. Iron Nutrition and Tumor Growth: Decreased Tumor Growth in Iron-deficient Mice1. (n.d.).

164. Lelièvre, P., Sancey, L., Coll, J.-L., Deniaud, A. & Busser, B. Iron Dysregulation in Human Cancer: Altered Metabolism, Biomarkers for Diagnosis, Prognosis, Monitoring and Rationale for Therapy. *Cancers* **12**, 3524 (2020).

165. Ren, J. *et al.* LF-MF inhibits iron metabolism and suppresses lung cancer through activation of P53-miR-34a-E2F1/E2F3 pathway. *Sci Rep-uk* **7**, 749 (2017).

166. Torti, S. V., Manz, D. H., Paul, B. T., Blanchette-Farra, N. & Torti, F. M. Iron and Cancer. *Annu Rev Nutr* **38**, 97–125 (2018).

167. Sharma, S. K. *et al.* Pulmonary Alveolar Macrophages Contribute to the Premetastatic Niche by Suppressing Antitumor T Cell Responses in the Lungs. *The Journal of Immunology* **194**, 5529–5538 (2015).

168. Loyher, P.-L. *et al.* Macrophages of distinct origins contribute to tumor development in the lungDual origin of macrophages in lung tumors. *J Exp Medicine* **215**, 2536–2553 (2018).

169. Lambrechts, D. *et al.* Phenotype molding of stromal cells in the lung tumor microenvironment. *Nat Med* **24**, 1277–1289 (2018).

170. Zilionis, R. *et al.* Single-Cell Transcriptomics of Human and Mouse Lung Cancers Reveals Conserved Myeloid Populations across Individuals and Species. *Immunity* **50**, 1317-1334.e10 (2019).

171. Franklin, R. A. & Li, M. O. Ontogeny of Tumor-Associated Macrophages and Its Implication in Cancer Regulation. *Elsevier Inc.* **2**, (2016).

172. Qian, B. Z. & Pollard, J. W. Macrophage Diversity Enhances Tumor Progression and Metastasis. **141**, (2010).

173. Guerriero, J. L. Macrophages: The Road Less Traveled, Changing Anticancer Therapy. *Trends in Molecular Medicine* (2018) doi:10.1016/j.molmed.2018.03.006.

174. Vitale, I., Manic, G., Coussens, L. M., Kroemer, G. & Galluzzi, L. Macrophages and Metabolism in the Tumor Microenvironment. *Cell Metab* **30**, 36–50 (2019).

175. Movahedi, K., Laoui, D., Gysemans, C. & Baeten, M. Different tumor microenvironments contain functionally distinct subsets of macrophages derived from Ly6C(high) monocytes. **70**, (2010).

176. Pollard, J. W. Tumour-educated macrophages promote tumour progression and metastasis. **4**, (n.d.).

177. Yang, M., McKay, D., Pollard, J. W. & Lewis, C. E. Diverse Functions of Macrophages in Different Tumor Microenvironments. *Cancer Res* **78**, 5492–5503 (2018).

178. Larionova, I. *et al.* Interaction of tumor-associated macrophages and cancer chemotherapy. *Oncoimmunology* **8**, 1–15 (2019).

179. Wu, P. *et al.* Inverse role of distinct subsets and distribution of macrophage in lung cancer prognosis: a meta-analysis. *Oncotarget* **7**, 40451–40460 (2015).

180. Sumitomo, R. *et al.* M2 tumor-associated macrophages promote tumor progression in non-small-cell lung cancer. *Exp Ther Med* **18**, 4490–4498 (2019).

181. Larionova, I. *et al.* Tumor-Associated Macrophages in Human Breast, Colorectal, Lung, Ovarian and Prostate Cancers. *Frontiers Oncol* **10**, 566511 (2020).

182. Mantovani, A., Bottazzi, B., Colotta, F., Sozzani, S. & Ruco, L. The origin and function of tumor-associated macrophages. **13**, (1992).

183. Zhu, Y. *et al.* Tissue-Resident Macrophages in Pancreatic Ductal Adenocarcinoma Originate from Embryonic Hematopoiesis and Promote Tumor Progression. *Immunity* **47**, 597 (2017).

184. Hirsch, F. R. *et al.* Lung cancer: current therapies and new targeted treatments. *Lancet* **389**, 299–311 (2017).

185. Huang, A. *et al.* Increased CD14+HLA-DR-/low myeloid-derived suppressor cells correlate with extrathoracic metastasis and poor response to chemotherapy in non-small cell lung cancer patients. *Cancer Immunol Immunother* **62**, 1439–1451 (2013).

186. Thielmann, C. M. *et al.* Iron accumulation in tumor-associated macrophages marks an improved overall survival in patients with lung adenocarcinoma. *Sci Rep-uk* **9**, 11326 (2019).

187. Thorsson, V. *et al.* The Immune Landscape of Cancer. *Immunity* **48**, 812-830.e14 (2018).

188. Oberndorfer, F. & Müllauer, L. Molecular pathology of lung cancer. *Curr Opin Oncol* **30**, 69–76 (2018).

189. Silva, M. C. da, Breckwoldt, M. O. & Vinchi, F. Iron Induces Anti-tumor Activity in Tumor-Associated Macrophages. **8**, (2017).

190. Valdiglesias, V. *et al.* Are iron oxide nanoparticles safe? Current knowledge and future perspectives. *Journal of Trace Elements in Medicine and Biology* **38**, 53–63 (2016).

191. Wilhelm, S. *et al.* Analysis of nanoparticle delivery to tumours. **1**, (2016).

192. Lammers, T. *et al.* Cancer nanomedicine: is targeting our target? *Nat Rev Mater* **1**, natrevmats201669 (2016).

193. Sengupta, S. Cancer Nanomedicine: Lessons for Immuno-Oncology. *Elsevier Inc.* **3**, (2017).

194. Shi, J., Kantoff, P. W., Wooster, R. & Farokhzad, O. C. Cancer nanomedicine: progress, challenges and opportunities. *Nature Reviews Cancer* **17**, nrc.2016.108 (2016).

195. Shi, Y. & Lammers, T. Combining Nanomedicine and Immunotherapy. *Accounts Chem Res* (2019) doi:10.1021/acs.accounts.9b00148.

196. Milling, L., Zhang, Y. & Irvine, D. J. Delivering safer immunotherapies for cancer. *The Authors* (2017) doi:10.1016/j.addr.2017.05.011.

197. Jiang, W. *et al.* Designing nanomedicine for immuno-oncology. *Macmillan Publishers Limited* **1**, (2017).

198. Lammers, T., Kiessling, F., Hennink, W. E. & Storm, G. Drug targeting to tumors: Principles, pitfalls and (pre-) clinical progress. *Journal of Controlled Release* **161**, 175–187 (2012).

199. Rosière, R., Amighi, K. & Wauthoz, N. Nanotechnology-Based Targeted Drug Delivery Systems for Lung Cancer. 249–268 (2019) doi:10.1016/B978-0-12-815720-6.00010-1.

200. Hassan, S., Prakasha, G. & Ozturk, B. Evolution and clinical translation of drug delivery nanomaterials. *Elsevier Ltd* (2017) doi:10.1016/j.nantod.2017.06.008.

201. Posgai, R. *et al.* Differential toxicity of silver and titanium dioxide nanoparticles on Drosophila melanogaster development, reproductive effort, and viability: Size, coatings and antioxidants matter. *Chemosphere* **85**, 34–42 (2011).

202. Izci, M., Maksoudian, C., Manshian, B. B. & Soenen, S. J. The Use of Alternative Strategies for Enhanced Nanoparticle Delivery to Solid Tumors. *Chem Rev* **121**, 1746–1803 (2021).

203. Arms, L. *et al.* Advantages and Limitations of Current Techniques for Analyzing the Biodistribution of Nanoparticles. *Frontiers in Pharmacology* **9**, 802 (2018).

204. Ou, Y.-C., Wen, X. & Bardhan, R. Cancer Immunoimaging with Smart Nanoparticles. *Trends Biotechnol* **38**, 388–403 (2020).

205. Sharkey, J. & Lewis, S. Functionalized superparamagnetic iron oxide nanoparticles provide highly efficient iron-labeling in macrophages for magnetic resonance?based detection in vivo. *Elsevier Inc.* **19**, (2017).

206. Heyn, C. *et al.* In vivo magnetic resonance imaging of single cells in mouse brain with optical validation. **55**, (2006).

207. Rosenblum, L. T., Kosaka, N., Mitsunaga, M., Choyke, P. L. & Kobayashi, H. In vivo molecular imaging using nanomaterials: General in vivo characteristics of nano-sized reagents and applications for cancer diagnosis (Review). *Molecular Membrane Biology* **27**, 274–285 (2010).

208. Kirschbaum, K. *et al.* In vivo nanoparticle imaging of innate immune cells can serve as a marker of disease severity in a model of multiple sclerosis. **113**, (2016).

209. Pittet, M. J., Swirski, F. K., Reynolds, F., Josephson, L. & Weissleder, R. Labeling of immune cells for in vivo imaging using magnetofluorescent nanoparticles. **1**, (2006).

210. Jasmin *et al.* Optimized labeling of bone marrow mesenchymal cells with superparamagnetic iron oxide nanoparticles and in vivo visualization by magnetic resonance imaging. *BioMed Central Ltd* **9**, (2011).

211. Williams, M. J. & Corr, S. A. Frontiers of Nanoscience. *Part I: Nanotechnology* **5**, 29–63 (2013).

212. Anani, T., Panizzi, P. & David, A. E. Nanoparticle-based probes to enable noninvasive imaging of proteolytic activity for cancer diagnosis. *Nanomedicine* **11**, 2007–2022 (2016).

213. Laurent, S. & Mahmoudi, M. Superparamagnetic iron oxide nanoparticles: Promises for diagnosis and treatment of cancer. **2**, (2011).

214. Gorbet, M.-J. & Ranjan, A. Cancer immunotherapy with immunoadjuvants, nanoparticles, and checkpoint inhibitors: Recent progress and challenges in treatment and tracking response to immunotherapy. *Pharmacol Therapeut* **207**, 107456 (2020).

215. Lizotte, P. H. *et al.* In situ vaccination with cowpea mosaic virus nanoparticles suppresses metastatic cancer. *Nat Nanotechnol* **11**, 295–303 (2016).

216. Zhao, Y., Zhao, X., Cheng, Y., Guo, X. & Yuan, W. Iron Oxide Nanoparticles-Based Vaccine Delivery for Cancer Treatment. *Molecular pharmaceutics* **15**, 1791–1799 (2018).

217. Sun, Q. *et al.* Nanomedicine and macroscale materials in immuno-oncology. *Chem Soc Rev* **48**, 351–381 (2018).

218. Chakraborty, A., Royce, S. G., Selomulya, C. & Plebanski, M. A novel Approach for Non-Invasive Lung Imaging and Targeting Lung Immune Cells. *Int J Mol Sci* **21**, 1613 (2020).

219. Mukerjee, A., Ranjan, A. P. & Vishwanatha, J. K. Combinatorial Nanoparticles for Cancer Diagnosis and Therapy. *Current Medicinal Chemistry* **19**, 3714–3721 (2012).

220. Smith, B. *et al.* Shape matters: Intravital microscopy reveals surprising geometrical dependence for nanoparticles in tumor models of extravasation. **12**, (2012).

221. Chen, H., Zhang, W., Zhu, G., Xie, J. & Chen, X. Rethinking cancer nanotheranostics. **2**, (2017).

222. Martinez, J., Brown, B. & science …, Q.-N. Multifunctional to multistage delivery systems: The evolution of nanoparticles for biomedical applications. (2012) doi:10.1007/s11434-012-5387-5.

223. Feng, Q. *et al.* Uptake, distribution, clearance, and toxicity of iron oxide nanoparticles with different sizes and coatings. *Scientific reports* **8**, 2082 (2018).

224. Rosen, J. E., Chan, L., Shieh, D.-B. & Gu, F. X. Iron oxide nanoparticles for targeted cancer imaging and diagnostics. *Nanomedicine: Nanotechnology, Biology and Medicine* **8**, 275–290 (2012).

225. Thomas, R., Park, I.-K. & Jeong, Y. Y. Magnetic Iron Oxide Nanoparticles for Multimodal Imaging and Therapy of Cancer. *Int J Mol Sci* **14**, 15910–15930 (2013).

226. Reczyńska, K. *et al.* Superparamagnetic Iron Oxide Nanoparticles Modified with Silica Layers as Potential Agents for Lung Cancer Treatment. *Nanomaterials-basel* **10**, 1076 (2020).

227. Bourquin, J. *et al.* Biodistribution, Clearance, and Long-Term Fate of Clinically Relevant Nanomaterials. *Advanced Materials* **30**, 1704307 (2018).

228. Zanganeh, S. *et al.* Iron oxide nanoparticles inhibit tumour growth by inducing pro-inflammatory macrophage polarization in tumour tissues. *Nature Publishing Group* **11**, (2016).

229. Torrance, J. D. & Bothwell, T. H. A simple technique for measuring storage iron concentrations in formalinised liver samples. *South Afr J Medical Sci* **33**, 9–11 (1968).

230. Pfaffl, M. W. A new mathematical model for relative quantification in real-time RT–PCR. *Nucleic Acids Res* **29**, e45–e45 (2001).

231. Livak, K. J. & Schmittgen, T. D. Analysis of Relative Gene Expression Data Using Real-Time Quantitative PCR and the 2−ΔΔC T Method. *Methods* **25**, 402–408 (2001).

232. Klinker, K. *et al.* Secondary-Structure-Driven Self-Assembly of Reactive Polypept(o)ides: Controlling Size, Shape, and Function of Core Cross-Linked Nanostructures. *Angewandte Chemie International Edition* **56**, 9608–9613 (2017).

233. Bauer, T. A. *et al.* Core Cross-Linked Polymeric Micelles for Specific Iron Delivery: Inducing Sterile Inflammation in Macrophages. *Adv Healthc Mater* 2100385 (2021) doi:10.1002/adhm.202100385.

234. Stuehr, D. J. & Marletta, M. A. Mammalian nitrate biosynthesis: mouse macrophages produce nitrite and nitrate in response to Escherichia coli lipopolysaccharide. *Proc National Acad Sci* **82**, 7738–7742 (1985).

235. Hibbs, J., Taintor, R. & Vavrin, Z. Macrophage cytotoxicity: role for L-arginine deiminase and imino nitrogen oxidation to nitrite. *Science* **235**, 473–476 (1987).

236. Granger, D. L., Hibbs, J. B., Perfect, J. R. & Durack, D. T. Specific amino acid (L-arginine) requirement for the microbiostatic activity of murine macrophages. *J Clin Invest* **81**, 1129–1136 (1988).

237. Mills, C. M1 and M2 Macrophages: Oracles of Health and Disease. *Crit Rev Immunol* **32**, 463–488 (2013).

238. Blondet, N. M., Messner, D. J., Kowdley, K. V. & Murray, K. F. Physiology of the Gastrointestinal Tract. 981–1001 (2018) doi:10.1016/b978-0-12-809954-4.00043-8.

239. Kanter, R. D. *et al.* Drug-metabolizing activity of human and rat liver, lung, kidney and intestine slices. *Xenobiotica* **32**, 349–362 (2008).

240. Bertram, J. S. & Janik, P. Establishment of a cloned line of Lewis lung carcinoma cells adapted to cell culture. *Cancer Lett* **11**, 63–73 (1980).

241. Studies in a Tumor Spectrum III. The Effect of Phosphor amides on the Growth of a Variety of Mouse and Rat Tumors*. (n.d.).

242. Li, X. *et al.* miR-301a promotes lung tumorigenesis by suppressing Runx3. *Mol Cancer* **18**, 99 (2019).

243. Smith, S. M., Wunder, M. B., Norris, D. A. & Shellman, Y. G. A Simple Protocol for Using a LDH-Based Cytotoxicity Assay to Assess the Effects of Death and Growth Inhibition at the Same Time. *Plos One* **6**, e26908 (2011).

244. Inoue, S. & Kawanishi, S. Hydroxyl radical production and human DNA damage induced by ferric nitrilotriacetate and hydrogen peroxide. *Cancer Res* **47**, 6522–7 (1987).

245. Porto, B. N. *et al.* Heme induces neutrophil migration and reactive oxygen species generation through signaling pathways characteristic of chemotactic receptors. **282**, (2007).

246. Neumann, J. *et al.* Nanoscale distribution of TLR4 on primary human macrophages stimulated with LPS and ATI. *Nanoscale* **11**, 9769–9779 (2019).

247. Abboud, S. & Haile, D. J. A Novel Mammalian Iron-regulated Protein Involved in Intracellular Iron Metabolism*. *J Biol Chem* **275**, 19906–19912 (2000).

248. Dhakshinamoorthy, S., Jain, A. K., Bloom, D. A. & Jaiswal, A. K. Bach1 Competes with Nrf2 Leading to Negative Regulation of the Antioxidant Response Element (ARE)-mediated NAD(P)H:Quinone Oxidoreductase 1 Gene Expression and Induction in Response to Antioxidants*. *J Biol Chem* **280**, 16891–16900 (2005).

249. Marro, S. *et al.* Heme controls ferroportin1 (FPN1) transcription involving Bach1, Nrf2 and a MARE/ARE sequence motif at position −7007 of the FPN1 promoter. *Haematologica* **95**, 1261–1268 (2010).

250. Sun, J. *et al.* Hemoprotein Bach1 regulates enhancer availability of heme oxygenase-1 gene. *Embo J* **21**, 5216–5224 (2002).

251. Sudan, K. *et al.* TLR4 activation alters labile heme levels to regulate BACH1 and heme oxygenase-1 expression in macrophages. *Free Radical Bio Med* **137**, 131–142 (2019).

252. Kontoghiorghe, C. N., Kolnagou, A. & Kontoghiorghes, G. J. Antioxidant targeting by deferiprone in diseases related to oxidative damage. *Front Biosci* **19**, 862 (2014).

253. Cai, B. *et al.* Macrophage MerTK Promotes Liver Fibrosis in Nonalcoholic Steatohepatitis. *Cell Metab* **31**, 406-421.e7 (2020).

254. Oldenborg, P.-A. *et al.* Role of CD47 as a Marker of Self on Red Blood Cells. *Science* **288**, 2051–2054 (2000).

255. Olsson, M. & Oldenborg, P. CD47 on experimentally senescent murine RBCs inhibits phagocytosis following Fcγ receptor-mediated but not scavenger receptor-mediated recognition by macrophages. **112**, (2008).

256. Figueiredo, R. T. *et al.* Characterization of heme as activator of toll-like receptor 4. **282**, (2007).

257. Matsunaga, N., Tsuchimori, N., Matsumoto, T. & Ii, M. TAK-242 (resatorvid), a small-molecule inhibitor of Toll-like receptor (TLR) 4 signaling, binds selectively to TLR4 and interferes with interactions between TLR4 and its adaptor molecules. *Mol Pharmacol* **79**, 34–41 (2010).

258. Bhattacharyya, S. *et al.* Pharmacological Inhibition of Toll-Like Receptor-4 Signaling by TAK242 Prevents and Induces Regression of Experimental Organ Fibrosis. *Front Immunol* **9**, 2434 (2018).

259. Schliwa, M. Action of Cytochalasin D on Cytoskeletal Networks. (n.d.) doi:10.1083/jcb.92.1.79.

260. Effects of cytochalasin D and latrunculin B on mechanical properties of cells. (n.d.).

261. Goddette, D. W. & Frieden, C. Actin polymerization. The mechanism of action of cytochalasin D. *J Biol Chem* **261**, 15974–15980 (1986).

262. May, J. A. *et al.* GPIIb-IIIa antagonists cause rapid disaggregation of platelets pre-treated with cytochalasin D. Evidence that the stability of platelet aggregates depends on normal cytoskeletal assembly. *Platelets* **9**, 227–232 (2009).

263. Idrus, F. N. M. *et al.* Differential polarization and the expression of efferocytosis receptor MerTK on M1 and M2 macrophages isolated from coronary artery disease patients. *Bmc Immunol* **22**, 21 (2021).

264. Solanki, S., Dube, P. R., Birnbaumer, L. & Vazquez, G. Reduced Necrosis and Content of Apoptotic M1 Macrophages in Advanced Atherosclerotic Plaques of Mice With Macrophage-Specific Loss of Trpc3. *Sci Rep-uk* **7**, 42526 (2017).

265. T cells. in antigen-specific IL-2 production by human CD28 delivers a costimulatory signal involved. (n.d.).

266. Expression of immunoglobulin-T-cell receptor chimeric molecules. (n.d.).

267. CD28-mediated co-stimulates T prevents of T. (n.d.).

268. Veillette, A. & Chen, J. SIRPα–CD47 Immune Checkpoint Blockade in Anticancer Therapy. *Trends in Immunology* (n.d.) doi:10.1016/j.it.2017.12.005.

269. Lu, Y.-C., Yeh, W.-C. & Ohashi, P. S. LPS/TLR4 signal transduction pathway. *Cytokine* **42**, 145–151 (2008).

270. Janciauskiene, S., Vijayan, V. & Immenschuh, S. TLR4 Signaling by Heme and the Role of Heme-Binding Blood Proteins. *Front Immunol* **11**, 1964 (2020).

271. Bae, Y. S. *et al.* Macrophages Generate Reactive Oxygen Species in Response to Minimally Oxidized Low-Density Lipoprotein. *Circ Res* **104**, 210–218 (2009).

272. Powers, K. A. *et al.* Oxidative stress generated by hemorrhagic shock recruits Toll-like receptor 4 to the plasma membrane in macrophages. *J Exp Medicine* **203**, 1951–1961 (2006).

273. Tolosano, E., Fagoonee, S., Morello, N., Vinchi, F. & Fiorito, V. Heme scavenging and the other facets of hemopexin. *Antioxidants & redox signaling* **12**, 305–20 (2010).

274. Pfeiffer, A. *et al.* Lipopolysaccharide and ceramide docking to CD14 provokes ligand-specific receptor clustering in rafts. *Eur J Immunol* **31**, 3153–3164 (2001).

275. Dutra, F. F. *et al.* Hemolysis-induced lethality involves inflammasome activation by heme. *Proc National Acad Sci* **111**, E4110–E4118 (2014).

276. Soldati, T. & Schliwa, M. Powering membrane traffic in endocytosis and recycling. *Nat Rev Mol Cell Bio* **7**, 897–908 (2006).

277. Elliott, J. A. & Winn, W. C. Treatment of alveolar macrophages with cytochalasin D inhibits uptake and subsequent growth of Legionella pneumophila. *Infect Immun* **51**, 31–36 (1986).

278. Palomba, R. *et al.* Modulating Phagocytic Cell Sequestration by Tailoring Nanoconstruct Softness. *Acs Nano* **12**, 1433–1444 (2018).

279. Shi, T., Denney, L., An, H., Ho, L. & Zheng, Y. Alveolar and lung interstitial macrophages: Definitions, functions, and roles in lung fibrosis. *J Leukocyte Biol* (2020) doi:10.1002/jlb.3ru0720-418r.

280. Joshi, N., Walter, J. M. & Misharin, A. V. Alveolar Macrophages. *Cellular Immunology* (2018) doi:10.1016/j.cellimm.2018.01.005.

281. Barnes, P. J. Alveolar Macrophages as Orchestrators of COPD. *Copd J Chronic Obstr Pulm Dis* **1**, 59–70 (2004).

282. Hussell, T. & Bell, T. J. Alveolar macrophages: plasticity in a tissue-specific context. *Nat Rev Immunol* **14**, 81–93 (2014).

283. Hiraiwa, K. & Eeden, S. F. van. Contribution of Lung Macrophages to the Inflammatory Responses Induced by Exposure to Air Pollutants. *Mediat Inflamm* **2013**, 1–10 (2013).

284. Hoppstädter, J. *et al.* Differential cell reaction upon Toll-like receptor 4 and 9 activation in human alveolar and lung interstitial macrophages. *Respir Res* **11**, 124 (2010).

285. Ferrari-Lacraz, S., Nicod, L. P., Chicheportiche, R., Welgus, H. G. & Dayer, J.-M. Human Lung Tissue Macrophages, but not Alveolar Macrophages, Express Matrix Metalloproteinases after Direct Contact with Activated T Lymphocytes. *Am J Resp Cell Mol* **24**, 442–451 (2001).

286. Brain, J. D. *et al.* Effects of Iron Status on Transpulmonary Transport and Tissue Distribution of Mn and Fe. *Am J Resp Cell Mol* **34**, 330–337 (2006).

287. Park, E.-J. *et al.* Chronic pulmonary accumulation of iron oxide nanoparticles induced Th1-type immune response stimulating the function of antigen-presenting cells. *Environ Res* **143**, 138–147 (2015).

288. Cho, W.-S. *et al.* Pulmonary toxicity and kinetic study of Cy5.5-conjugated superparamagnetic iron oxide nanoparticles by optical imaging. *Toxicology and Applied Pharmacology* **239**, 106–115 (2009).

289. Lay, J. C. *et al.* Cellular and Biochemical Response of the Human Lung after Intrapulmonary Instillation of Ferric Oxide Particles. *American Journal of Respiratory Cell and Molecular Biology* **20**, 631–642 (1999).

290. Park, E.-J. *et al.* Inflammatory responses may be induced by a single intratracheal instillation of iron nanoparticles in mice. *Elsevier Ireland Ltd* **275**, (2010).

291. Ban, M., Langonné, I., Huguet, N. & Goutet, M. Effect of submicron and nano-iron oxide particles on pulmonary immunity in mice. *Toxicol Lett* **210**, 267–275 (2012).

292. Henderson, R. F. Use of bronchoalveolar lavage to detect respiratory tract toxicity of inhaled material. *Exp Toxicol Pathol* **57**, 155–159 (2005).

293. McCracken, J. M. & Allen, L.-A. H. Regulation of Human Neutrophil Apoptosis and Lifespan in Health and Disease. *J Cell Death* **7**, JCD.S11038 (2014).

294. Jacobsen, E. A., Zellner, K. R., Colbert, D., Lee, N. A. & Lee, J. J. Eosinophils Regulate Dendritic Cells and Th2 Pulmonary Immune Responses following Allergen Provocation. *J Immunol* **187**, 6059–6068 (2011).

295. Wang, Z. *et al.* Iron Drives T Helper Cell Pathogenicity by Promoting RNA-Binding Protein PCBP1-Mediated Proinflammatory Cytokine Production. *Immunity* **49**, 80-92.e7 (2018).

296. Wesselius, L. J. *et al.* Alveolar macrophages accumulate iron and ferritin after in vivo exposure to iron or tungsten dusts. *J Lab Clin Med* **127**, 401–409 (1996).

297. Heilig, E. A. *et al.* Manganese and iron transport across pulmonary epithelium. *Am J Physiol-lung C* **290**, L1247–L1259 (2006).

298. Respiratory epithelial cells demonstrate lactoferrin receptors that increase after metal exposure. (n.d.).

299. Pacht, E. R. & Davis, W. B. Role of transferrin and ceruloplasmin in antioxidant activity of lung epithelial lining fluid. *J Appl Physiol* **64**, 2092–2099 (1988).

300. Thompson, A. B., Bohling, T., Payvandi, F. & Rennard, S. I. Lower respiratory tract lactoferrin and lysozyme arise primarily in the airways and are elevated in association with chronic bronchitis. *J Laboratory Clin Medicine* **115**, 148–58 (1990).

301. Ghio, A. J. *et al.* Iron and iron-related proteins in the lower respiratory tract of patients with acute respiratory distress syndrome. *Crit Care Med* **31**, 395–400 (2003).

302. Kim, J. & Wessling-Resnick, M. The Role of Iron Metabolism in Lung Inflammation and Injury. *J Allergy Ther* **01**, 1–6 (2012).

303. Banks, H. T. *et al.* Estimation of Cell Proliferation Dynamics Using CFSE Data. *B Math Biol* **73**, 116–150 (2011).

304. Fiorito, V., Chiabrando, D., Petrillo, S., Bertino, F. & Tolosano, E. The Multifaceted Role of Heme in Cancer. *Frontiers Oncol* **9**, 1540 (2020).

305. Ciccarone, F. *et al.* Aconitase 2 inhibits the proliferation of MCF-7 cells promoting mitochondrial oxidative metabolism and ROS/FoxO1-mediated autophagic response. *Brit J Cancer* **122**, 182–193 (2020).

306. Sun, J. *et al.* Heme regulates the dynamic exchange of Bach1 and NF-E2-related factors in the Maf transcription factor network. *P Natl Acad Sci Usa* **101**, 1461–1466 (2004).

307. Igarashi, K. & Sun, J. The Heme-Bach1 Pathway in the Regulation of Oxidative Stress Response and Erythroid Differentiation. *Antioxid Redox Sign* **8**, 107–118 (2006).

308. Rath, M., Müller, I., Kropf, P., Closs, E. I. & Munder, M. Metabolism via Arginase or Nitric Oxide Synthase: Two Competing Arginine Pathways in Macrophages. *Front Immunol* **5**, 532 (2014).

309. Xu, W. *et al.* STAT-1 and c-Fos interaction in nitric oxide synthase-2 gene activation. *Am J Physiol-lung C* **285**, L137–L148 (2003).

310. Schneider, M. *et al.* CD38 Is Expressed on Inflammatory Cells of the Intestine and Promotes Intestinal Inflammation. *Plos One* **10**, e0126007 (2015).

311. A-Gonzalez, N. *et al.* Phagocytosis imprints heterogeneity in tissue-resident macrophages. *J Exp Med* **214**, 1281–1296 (2017).

312. Desgeorges, T., Caratti, G., Mounier, R., Tuckermann, J. & Chazaud, B. Glucocorticoids Shape Macrophage Phenotype for Tissue Repair. *Front Immunol* **10**, 1591 (2019).

313. Higham, A. *et al.* Effects of corticosteroids on COPD lung macrophage phenotype and function. *Clin Sci* **134**, 751–763 (2020).

314. Yoon, Y.-S. *et al.* PPARγ activation following apoptotic cell instillation promotes resolution of lung inflammation and fibrosis via regulation of efferocytosis and proresolving cytokines. *Mucosal Immunol* **8**, 1031–1046 (2015).

315. Akinrinmade, O. A. *et al.* CD64: An Attractive Immunotherapeutic Target for M1-type Macrophage Mediated Chronic Inflammatory Diseases. *Biomed* **5**, 56 (2017).

316. Dugast, A.-S. *et al.* Decreased Fc receptor expression on innate immune cells is associated with impaired antibody-mediated cellular phagocytic activity in chronically HIV-1 infected individuals. *Virology* **415**, 160–167 (2011).

317. Srivastava, M. *et al.* The TLR4–NOS1–AP1 signaling axis regulates macrophage polarization. *Inflamm Res* **66**, 323–334 (2017).

318. Tan, H.-Y. *et al.* The Reactive Oxygen Species in Macrophage Polarization: Reflecting Its Dual Role in Progression and Treatment of Human Diseases. *Oxid Med Cell Longev* **2016**, 1–16 (2016).

319. Taub, D. D. & Cox, G. W. Murine Th1 and Th2 cell clones differentially regulate macrophage nitric oxide production. *J Leukocyte Biol* **58**, 80–89 (1995).

320. Tyurina, Y. Y. *et al.* Nitrosative Stress Inhibits the Aminophospholipid Translocase Resulting in Phosphatidylserine Externalization and Macrophage Engulfment IMPLICATIONS FOR THE RESOLUTION OF INFLAMMATION. *J Biol Chem* **282**, 8498–8509 (2007).

321. Harada, T. *et al.* Phagocytic Entry of Legionella pneumophila into Macrophages through Phosphatidylinositol 3,4,5-Trisphosphate-Independent Pathway. *Biological Pharm Bulletin* **35**, 1460–1468 (2012).

322. Garvey, E. P. *et al.* 1400W Is a Slow, Tight Binding, and Highly Selective Inhibitor of Inducible Nitric-oxide Synthasein Vitroandin Vivo. *J Biol Chem* **272**, 4959–4963 (1997).

323. Brown, K. L., Christenson, K., Karlsson, A., Dahlgren, C. & Bylund, J. Divergent Effects on Phagocytosis by Macrophage-Derived Oxygen Radicals. *J Innate Immun* **1**, 592–598 (2009).

324. Cunha, C., Gomes, C., Vaz, A. R. & Brites, D. Exploring New Inflammatory Biomarkers and Pathways during LPS-Induced M1 Polarization. *Mediat Inflamm* **2016**, 1–17 (2016).

325. Saha, R. N. & Pahan, K. Regulation of Inducible Nitric Oxide Synthase Gene in Glial Cells. **8**, (2006).

326. Wang, W. *et al.* Targeted metabolomics identifies the cytochrome P450 monooxygenase eicosanoid pathway as a novel therapeutic target of colon tumorigenesis. *Cancer Res* **79**, canres.3221.2018 (2019).

327. Mills, C. D., Lenz, L. L. & Harris, R. A. A breakthrough: Macrophage-directed cancer immunotherapy. **76**, (2016).

328. Pérez-Ruiz, E. *et al.* Cancer immunotherapy resistance based on immune checkpoints inhibitors: targets, biomarkers, and remedies. *Drug Resist Update* **53**, 100718 (2020).

329. Grigore, A., Albulescu, A. & Albulescu, R. Current methods for tumor-associated macrophages investigation. *Journal of Immunoassay and Immunochemistry* 1–17 (2018) doi:10.1080/15321819.2018.1488727.

330. Ridnour, L. A. *et al.* The Biphasic Nature of Nitric Oxide Responses in Tumor Biology. *Antioxid Redox Sign* **8**, 1329–1337 (2006).

331. Miyata, R. & Eeden, S. F. van. The innate and adaptive immune response induced by alveolar macrophages exposed to ambient particulate matter. *Toxicol Appl Pharm* **257**, 209–226 (2011).

332. Bogen, B., Fauskanger, M., Haabeth, O. A. & Tveita, A. CD4+ T cells indirectly kill tumor cells via induction of cytotoxic macrophages in mouse models. *Cancer Immunol Immunother Cii* **68**, 1865–1873 (2019).

333. Porter, M. *et al.* Diesel-Enriched Particulate Matter Functionally Activates Human Dendritic Cells. *Am J Resp Cell Mol* **37**, 706–719 (2007).

334. Li, C., Li, H., Jiang, K., Li, J. & Gai, X. TLR4 signaling pathway in mouse Lewis lung cancer cells promotes the expression of TGF-β1 and IL-10 and tumor cells migration. *Biomed Mater Eng* **24**, 869–875 (2014).

335. Sha, T. *et al.* Therapeutic effects of TAK-242, a novel selective Toll-like receptor 4 signal transduction inhibitor, in mouse endotoxin shock model. *Eur J Pharmacol* **571**, 231–239 (2007).

336. Vinchi, F. *et al.* Hemopexin Therapy Improves Cardiovascular Function by Preventing Heme-Induced Endothelial Toxicity in Mouse Models of Hemolytic Diseases. *Circulation* **127**, 1317–1329 (2013).

337. Zimmermann, M. & Meyer, N. Mammalian Cell Viability, Methods and Protocols. *Methods Mol Biology* **740**, 57–63 (2011).

338. UyBico, S. J. *et al.* Lung Cancer Staging Essentials: The New TNM Staging System and Potential Imaging Pitfalls. *Radiographics* **30**, 1163–1181 (2010).

339. Anfray, C., Ummarino, A., Andón, F. T. & Allavena, P. Current Strategies to Target Tumor-Associated-Macrophages to Improve Anti-Tumor Immune Responses. *Cells* **9**, 46 (2019).

340. Abdelaziz, H. M. *et al.* Inhalable particulate drug delivery systems for lung cancer therapy: Nanoparticles, microparticles, nanocomposites and nanoaggregates. *J Control Release* **269**, 374–392 (2018).

341. Marelli, G., Sica, A., Vannucci, L. & Allavena, P. Inflammation as target in cancer therapy. *Elsevier Ltd* **35**, (2017).

342. Corna, G. *et al.* Polarization dictates iron handling by inflammatory and alternatively activated macrophages. **95**, (n.d.).

343. Agoro, R., Taleb, M., Quesniaux, V. F. & Mura, C. Cell iron status influences macrophage polarization. *PLOS ONE* **13**, e0196921 (2018).

344. Pfefferlé, M. *et al.* Hemolysis transforms liver macrophages into anti-inflammatory erythrophagocytes. *J Clin Invest* (2020) doi:10.1172/jci137282.

345. Daley, J. M., Brancato, S. K., Thomay, A. A., Reichner, J. S. & Albina, J. E. The phenotype of murine wound macrophages. *J Leukocyte Biol* **87**, 59–67 (2010).

346. Nairz, M. *et al.* Iron and innate antimicrobial immunity—Depriving the pathogen, defending the host. *J Trace Elem Med Bio* **48**, 118–133 (2018).

347. Lin, S. *et al.* Heme activates TLR4-mediated inflammatory injury via MyD88/TRIF signaling pathway in intracerebral hemorrhage. **9**, (2012).

348. Belcher, J. D. *et al.* Heme triggers TLR4 signaling leading to endothelial cell activation and vaso-occlusion in murine sickle cell disease Heme triggers TLR4 signaling leading to endothelial cell activation and vaso-occlusion in murine sickle cell disease. **123**, (2014).

349. Haldar, M. *et al.* Heme-mediated SPI-C induction promotes monocyte differentiation into iron-recycling macrophages. **156**, (2014).

350. Behmoaras, J. The versatile biochemistry of iron in macrophage effector functions. *Febs J* (2020) doi:10.1111/febs.15682.

351. Mu, X., Li, Y. & Fan, G.-C. Tissue-Resident Macrophages in the Control of Infection and Resolution of Inflammation. *Shock Augusta Ga* **55**, 14–23 (2021).

352. Movahedi, K. & Ginderachter, J. A. The Ontogeny and Microenvironmental Regulation of Tumor-Associated Macrophages. *Antioxidants & Redox Signaling* (2016) doi:10.1089/ars.2016.6704.

353. Awate, S., Babiuk, L. A. & Mutwiri, G. Mechanisms of Action of Adjuvants. *Frontiers in Immunology* **4**, 114 (2013).

354. Lucas, K. & Maes, M. Role of the Toll Like Receptor (TLR) Radical Cycle in Chronic Inflammation: Possible Treatments Targeting the TLR4 Pathway. *Mol Neurobiol* **48**, 190–204 (2013).

355. Mathieu, C., Rioux, G., Dumas, M.-C. & Leclerc, D. Induction of innate immunity in lungs with virus-like nanoparticles leads to protection against influenza and Streptococcus pneumoniae challenge. *Nanomed Nanotechnol Biology Medicine* **9**, 839–848 (2013).

356. Birgegård, G. *et al.* Cancer-Related Anemia: Pathogenesis, Prevalence and Treatment. *Oncology* **68**, 3–11 (2005).

357. Ludwig, H. *et al.* Iron metabolism and iron supplementation in cancer patients. **127**, (2015).

358. Abdel-Razeq, H. & Hashem, H. Recent Update in the Pathogenesis and Treatment of Chemotherapy and Cancer Induced Anemia. *Crit Rev Oncol Hemat* **145**, 102837 (2019).

359. Snegovoi, A., Larionova, V., Manzyuk, L. & Kononenko, I. Anemias in Oncology: Potential of Maintenance Therapy. *Clin Oncohematology* **9**, 326–335 (2016).

360. Pirker, R. & Filipits, M. Adjuvant Therapy in Patients With Completely Resected Non–small-cell Lung Cancer: Current Status and Perspectives. *Clin Lung Cancer* **20**, 1–6 (2019).

361. Bai, R. *et al.* Neoadjuvant and Adjuvant Immunotherapy: Opening New Horizons for Patients With Early-Stage Non-small Cell Lung Cancer. *Frontiers Oncol* **10**, 575472 (2020).

362. Battiloro, C., Gravara, L. D., Rocco, D. & Gridelli, C. What pharmacotherapeutics should one use for early stage non-small cell lung cancer? *Expert Opin Pharmaco* **19**, 1–4 (2018).

363. Ryu, R. & Ward, K. E. Atezolizumab for the First-Line Treatment of Non-small Cell Lung Cancer (NSCLC): Current Status and Future Prospects. *Frontiers Oncol* **8**, 277 (2018).

364. Brahmer, J. R. *et al.* The Society for Immunotherapy of Cancer consensus statement on immunotherapy for the treatment of non-small cell lung cancer (NSCLC). *J Immunother Cancer* **6**, 75 (2018).

365. Corrales, L. *et al.* Advances in Experimental Medicine and Biology. *Adv Exp Med Biol* **995**, 65–95 (2018).

366. Mills, C. D., Kincaid, K., Alt, J. M., Heilman, M. J. & Hill, A. M. M-1/M-2 Macrophages and the Th1/Th2 Paradigm. *The Journal of Immunology* **164**, 6166–6173 (2000).

367. Zhang, F. *et al.* Genetic programming of macrophages to perform anti-tumor functions using targeted mRNA nanocarriers. *Nat Commun* **10**, 3974 (2019).

368. Kambara, K. *et al.* In Vivo Depletion of CD206+ M2 Macrophages Exaggerates Lung Injury in Endotoxemic Mice. *Am J Pathology* **185**, 162–171 (2015).

369. Arora, S., Dev, K., Agarwal, B., Das, P. & Syed, M. A. Macrophages: Their role, activation and polarization in pulmonary diseases. *Immunobiology* **223**, (n.d.).

370. Huang, W., Chan, M., Chen, M. & Tsai, T. Modulation of macrophage polarization and lung cancer cell stemness by MUC1 and development of a related small-molecule inhibitor pterostilbene. **7**, (2016).

371. Yuan, A. *et al.* Opposite Effects of M1 and M2 Macrophage Subtypes on Lung Cancer Progression. *Nature Publishing Group* **5**, (2015).

372. He, D. *et al.* Single-cell RNA sequencing reveals heterogeneous tumor and immune cell populations in early-stage lung adenocarcinomas harboring EGFR mutations. *Oncogene* 1–14 (2020) doi:10.1038/s41388-020-01528-0.

373. Ma, J. *et al.* The M1 form of tumor-associated macrophages in non-small cell lung cancer is positively associated with survival time. **10**, (2010).

374. Wardrop, S. & Richardson, D. Interferon-γ and lipopolysaccharide regulate the expression of Nramp2 and increase the uptake of iron from low relative molecular mass complexes by macrophages. *European Journal of Biochemistry* **267**, 6586–6593 (2000).

375. Goldstein, E. Z. *et al.* Intraspinal TLR4 activation promotes iron storage but does not protect neurons or oligodendrocytes from progressive iron-mediated damage. *Elsevier* **298**, (2017).